THÈSE

Pour l'obtention du grade de
DOCTEUR DE L'UNIVERSITÉ DE POITIERS
École nationale supérieure d'ingénieurs (Poitiers)
Laboratoire d'informatique et d'automatique pour les systèmes - LIAS (Poitiers)
(Diplôme National - Arrêté du 7 août 2006)

École doctorale : Sciences et ingénierie pour l'information, mathématiques - S2IM (Poitiers)
Secteur de recherche : Automatique, productique

Présentée par :
Ping Dai

Réjection de perturbation sur un système multi-sources
Application à une propulsion hybride

Directeur(s) de Thèse :
Patrick Coirault, Sebastien Cauet

Soutenue le 19 janvier 2015 devant le jury

Jury :

Président	**Xavier Moreau**	Professeur, ENSEIRB, Université de Bordeaux
Rapporteur	**Ahmed El Hajjaji**	Professeur, Université de Picardie, Amiens
Rapporteur	**Malek Ghanes**	Maître de conférences, ENSEA, Cergy-Pontoise
Membre	**Patrick Coirault**	Professeur, Université de Poitiers
Membre	**Sebastien Cauet**	Maître de conférences, LIAS, ENSIP, Université de Poitiers

UNIVERSITÉ DE POITIERS

THÈSE

présentée à
l'Université de Poitiers en vue de l'obtention du

DIPLÔME DE DOCTORAT

SPÉCIALITÉ: AUTOMATIQUE

Présentée par

PING DAI

Réjection de perturbation sur un système multi-sources - Application à une propulsion hybride

Directeur de thèse: Patrick COIRAULT

Co-encadrement: Sébastien CAUET

Soutenue publiquement le lundi 19 janvier 2015

JURY

Rapporteurs :	Ahmed EL HAJJAJI	Professeur des universités Université de Picardie, Amiens
	Malek GHANES	Maître de Conférences HDR ENSEA, Paris
Examinateurs :	Xavier MOREAU	Professeur des universités ENSEIRB, Université de Bordeaux
	Patrick COIRAULT	Professeur des universités Université de Poitiers
	Sébastien CAUET	Maître de Conférences HDR Université de Poitiers

Thèse prépapée au sein du
Laboratoire d'Informatique et d'Automatique pour les Systèmes

Acknowledgments

This thesis is not only a summary of the three-year research in the Laboratoire d'Automatique et d'Informatique (LIAS), but also a milestone in almost a decade of study in the domain of electrical engineering control. I would like to thank my advisor, Professor Patrick COIRAULT, director of the laboratory for offering me such an opportunity to do the project and for welcoming me in the lab. Throughout these three years, he has been providing me academic guidance and professional support and led me to a fresh advanced control field.

I would like to extend the gratitude to my co-supervisor Mr. Sébastien CAUET, Maître de conférence HDR at the University of Poitiers, not only for his continued encouragement, but also for his help and guidance in power electrical domain and in the experimental test bench. His professional qualities have given me a deep impression, and would still be valuable in my future career.

Furthermore, I would like to extend my appreciation to all members of the jury for evaluating my work : Professor Ahmed EL HAJJAJI, Université de Picardie à Amiens, Mr. Malek GHANES, Maître de Conférences HDR à l'ENSEA and Professor Xavier MOREAU, l'université de Bordeaux I. I would like to thank particularly Mr. GHANES for his inspiration which has tremendously pushed forward our study.

In addition, I would also like to express my gratitude to the president of our department Poitou-Charentes for the funding support during these three years.

Moreover, I would like to thank my lab for giving the opportunity of teaching the experiment practical lessons during the last two years, where I got a perfect chance to review, enhance and practice the professional knowledge and accumulate teaching experience. It was my pleasure to play the role of teacher, and I appreciate every moment being with my students.

My thanks and appreciations also extend to each individual in LIAS. Thanks to every colleague in LIAS for giving me enthusiastic concern and help. Especially to Baya, Duong, Farah, Fayçal, Amin for the companion and help all along the three years, and to Lila, Mariem for their help during the short but cherish period together. I offer them all my best wishes in their future.

Finally, I would like to thank my parents, my aunts and my whole family for their endless love and support all along the road. Without them, I will never reach where I am. Also thank you to my dear friends in China, in France and those all over the world for always being there, for all the wonderful time spent together, and for the constant support and encouragement.

Table des matières

Table des figures

Liste des tableaux

Notations et abréviations

Notations	:	
$\mathbb{R}$	:	field of real numbers
$\mathbb{R}^m, \mathbb{R}^n, \mathbb{R}^q$	:	linear space of real vectors of dimension m, n, q
t	:	time, nonnegative real numbers
$\int x$	:	short for $\int_0^t x(s)ds$, time integration
$\frac{d}{dt}x = \dot{x}$	:	time derivative of x
$\frac{\partial x}{\partial \xi}$	:	derivative of $x = f(\xi)$
I	:	identity matrix
$A^\top$	:	the transpose of matrix A
A^{-1}	:	the inverse of matrix A
$sym\{A\}$	:	$sym\{A\} = A + A^\top$ the sum of matrices A and $A^\top$
$\mathcal{L}_s c(\omega)$	:	Lie operation $\mathcal{L}_s c(\omega) = s(\omega)\frac{\partial}{\partial\omega}c(\omega)$
$\mathcal{L}_s^q c(\omega)$	:	Lie operation $\mathcal{L}_s^q c(\omega) = s(\omega)\frac{\partial}{\partial\omega}[\mathcal{L}_s^{q-1}c(\omega)]$
J	:	the mass moment of inertia of the vehicle
ω_m	:	the rotational speed of the vehicle
T_{pmsm}	:	the torque of permanent magnet synchronous machine
T_p	:	the torque generated by the pressure in the cylinder in the combustion process
T_i	:	the torque generated by the oscillating masses and connecting rod
T_l	:	the load torque
i_d,i_q	:	current in the dq reference frame rotating at the same speed of the rotor
p	:	pair of poles of the electric machine
ϕ_m	:	the magnet flux of the electric machine
$S_{1,2,3,4}$	:	controlled switches of the power converters
u, μ	:	duty cycles of the controlled switches (control inputs of the power converters)
L_l, L_2	:	inductances in the power converters
C, C_{sc}	:	capacitance in the DC bus, capacitance in the supercapacitor/ultracapacitor
r	:	inner resistance of battery
R	:	resistance of total loss in the circuit
R_{sc}	:	inner resistance of the supercapacitor/ultracapacitor
$E = V_{bat}$	:	voltage of the battery

V_{dc}	:	voltage on the DC bus
V_{sc}	:	voltage of the supercapacitor/ultracapacitor
I_{L_1}, I_{L_2}	:	currents through the inductors L_1 and L_2
ϕ_{L_l}, ϕ_{L_2}	:	flux in the inductors L_1 and L_2
$q_C, q_{C_{sc}}$	:	charge in the capacitors C and C_{sc}
$I_{ex} = \omega_1$	:	external current of the power converters
$\bar{\omega}_1$	:	constant component of ω_1
$\tilde{\omega}_1$	:	variable component of ω_1
ω	:	exogenerous disterbance
x, x^*	:	state variables of a system, reference of the state variables
u, u^*	:	control input of a system, reference of the control input
Π, Γ	:	matrix mappings from $\{x, u\}$ to $\{x^*, u^*\}$ of linear systems
$\pi(\omega), c(\omega)$	:	mappings from $\{x, u\}$ to $\{x^*, u^*\}$ of nonlinear systems
k_p, k_i	:	proportional gain, integral gain
$\mathcal{V}$	:	magnetic energy in an inductor
$\mathcal{T}$	:	electric energy in a capacitor
$\mathcal{H}$	:	Hamiltonian/energy of a system
$\mathcal{H}_d$	:	desired Hamiltonian/energy of a system
$\nabla\mathcal{H} = \frac{\partial\mathcal{H}(x)}{\partial x}$	:	derivative of $\mathcal{H}$ in terms of x
$\mathcal{J}$	:	interconnection matrix
$\mathcal{J}_d$	:	desired interconnection structure
$\mathcal{R}$	:	damping matrix
$\mathcal{R}_d$	:	desired damping
$\mathcal{R}_a$	:	injected damping $\mathcal{R}_d = \mathcal{R} + \mathcal{R}_a$
Abréviations	:	
AC	:	Alternate Current
DC	:	Direct current
EV	:	Electric Vehicle
HEV	:	Hybrid Electric Vehicle
HESS	:	Hybrid Energy Storage System
ICE	:	Internal Combustion Engine
IDA	:	Interconnection and Damping Assignment
LMI	:	Linear Matrix Inequality
PBC	:	Passivity Based Control
PCH	:	Port-Controlled Hamiltonian
PI	:	Proportional Integral
PMSM	:	Permanent Magnet Synchronous Machine
PWM	:	Pulse-Width Modulation
SMC	:	Sliding Mode Control
SOC	:	State of Charge
SP	:	Singular Perturbation
UC	:	Ultra-Capacitor

General introduction

Context

In the 19th century, petrol or gasoline powered automobiles have gradually replaced steam powered automobiles which have occupied the history for a century. Petrol or gasoline powered internal combustion engine (ICE), being a dominant means of propulsion nowadays, has improved the speed of vehicles dozens or even hundreds of times. Actually, it is not only the vehicle speed that increases, but also the consumption of fossil fuels and exhaust emissions. While we enjoy the convenience brought by automobiles, we are also withstanding the exhaust pollution. In the 20th century, with the increase of the awareness of the protection of non-renewable energy and the air condition, electrical powered automobiles appeared and began to occupy the market today in the 21st century. Hybrid electric vehicles (HEV), being an optimal candidate, significantly reduce the toxic and harmful gas emissions without sacrificing the travelling velocity. It is still fresh in our memory the smog cloud hanging over Paris this March. Even the landmark Eiffel Tower almost disappeared in the smog. The government has taken measures including alternating driving ban to limit the pollution, while HEV is an exception and is not included in the ban. The advantage of HEV is thus evident. In fact, the policy and financial dual support from the government has essentially promoted and advanced the research and the market of HEV.

During all these years in the study of HEV, we have been committed to create a comfortable driving environment with less noise and smoother running. This is achieved via the suppression of the torque ripples generated by the ICE. Instead of utilizing the traditional passive control method with a flywheel, Mohamed NJEH [Nje11] has contributed an active control method to control the torque of the electric machine, a permanent magnet synchronous machine (PMSM), to compensate the ICE torque ripples. The essence of the study is based on the harmonic decomposition. The ripple disturbance is decomposed into different harmonics and then treated in parallel. The torque ripple compensation controller is thus a parallel connection of a series of subcontrollers, with each subcontroller dealing with one main harmonic. The active controller is for the AC-DC converter connecting to the DC bus. Consequently, the torque ripples compensation process results in a transfer of ripple disturbance in the DC bus. This disturbance also needs to be properly dealt with. It is under this circumstance that our study is carried out.

Problem statement

The DC bus voltage is supplied by a battery connecting with a DC-DC converter. The problem left for us is then to deal with the disturbance in the DC bus introduced in the process of torque ripple compensation. The direct damage caused by the disturbance is battery wear. Exposing to such persistent oscillations, batteries, with the property of high energy density but low power density, cannot afford such substantial and frequent power variation cycles, and thus wear down very quickly. Consequently, it is quite necessary to find a solution to reject the disturbance in the DC bus.

Actually, talking about batteries, it is easy to think of ultracapacitors being widely used as a complementary power source in a hybrid battery/ultracapacitor energy storage system. Hybrid energy storage system has been commonly studied in electric vehicles and other applications including renewable energy power generation. In most studies, the application of ultracapacitors in vehicular system is mainly to deal with the transient disturbance, another fact causing battery wear, introduced by the load power demand sudden change during acceleration and deceleration. In contrast with batteries, ultracapacitors, with higher power density, is apt to provide a large amount of energy in a short period and experience frequent and rapid charge discharge cycles. Therefore, battery/ultracapacitor hybrid structure provides a perfect solution to reduce the battery wear if we could force the ultracapacitor to absorb both the transient disturbance and the persistent disturbance. In order to achieve this, it is necessary to design a high-performance control algorithm, and this is the core of our study.

Objectives

Our research object is then a battery/ultracapacitor hybrid energy storage system connecting to the DC bus where there are exogenous transient and persistent disturbances. Our objective is to reject the disturbances in the battery and absorb them in the ultracapacitor. Other accessory control objectives include maintaining a constant DC voltage and compensating the self-discharge of the ultracapacitor to maintain at the nominal state of charge.

From energy management point of view, it requires properly managing the energy allocation in the battery/ultracapacitor system so as to achieve the control objective. Specifically, the task of delivering steady energy in the DC bus is assigned to the battery, while the task of disturbance energy absorption is allocated to the ultracapacitor. From oscillating disturbance rejection point of view, it requires an active controller to turn the ultracapcitor into an active damping.

The battery and the ultracapacitor are connected with a DC-DC converter respectively. For this DC-DC power electrical system, the average model of the whole system is a four-dimensional nonlinear system and is not easy to be linearized, and thus it is not feasible to directly apply classical linear theories. Facing this difficulty, we have explored various nonlinear control theories, from sliding mode control to passivity-based control of Euler-Lagrange systems, and to nonlinear error output regulation, and to the interconnection and damping assignment of Hamiltonian systems. After suffering numerous frustrations, we finally understand deeply the principle of the hybrid energy system and contribute a disturbance rejection control algorithm. The process is progressive, and this is exactly how we organize this dissertation.

Organization of the dissertation

The dissertation is divided into four chapters.

The first chapter presents a state of the art of hybrid energy storage system. In this chapter, we first review the working principles and characteristics of the widely used DC power source and storage devices : fuel cells, batteries and ultracapacitors. Moreover, we summarize different configurations of hybrid storage system and different topologies of DC power converters applied in hybrid storage systems. Furthermore, we present a series of control methods aiming to achieve a proper energy management in hybrid storage systems.

The second chapter elaborates the origin of the sinusoidal persistent disturbance causing battery wear and explores the output regulation theories of linear and nonlinear system. The related theory is then applied to our system. To achieve this, we simplify the problem by considering the battery side converter and the ultracapacitor side converter separately, and apply the output regulation controller to the ultracapacitor side converter, while a passivity-based controller to the battery side converter. Simulation results have shown the effectiveness of the control algorithm. However, separating the battery and the ultracapacitor means that the interactions between them are also ignored. Moreover, the ultracapacitor model used in this chapter is also simplified as an ideal model without considering its self-discharge phenomenon. Consequently, lack of comprehensive consideration, experiments in real-time are not implemented with this control algorithm.

The third chapter presents our contributed disturbance rejection control algorithm. In this chapter, the battery/ultracapacitor hybrid energy storage system is considered as a whole, and the ultracapacitor self-discharge phenomenon is taken into consideration by integrating a resistive loss in the system model. The whole system is therefore a four-dimensional nonlinear Hamiltonian system. However, original method to design the controller of nonlinear Hamiltonian system is not amenable to our system due to the complexities and difficulties of solving partial differential equations. Consequently, we exploit an alternative way. In order to achieve the objective of disturbance absorption in the ultracapacitor, we define a static solution and a dynamic solution. The static solution is the desired equilibrium point of the system when the disturbance doesn't exist, while the dynamic solution is the desired dynamic trajectories of the states when the ultracapacitor absorbs the disturbance. Thus, based on the singular perturbation theory, the system can be considered in two time-scales, a slow one and a fast one, and controlled through a cascade structure. The control objective can then be achieved by driving the system to the desired equilibrium point through the outer slow loop and imposing the desired dynamic through the inner fast loop. Besides, the outer slow loop controller is designed via interconnection and damping assignment, while the inner fast loop is regulated via a simple proportional integral controller. Simulation results are given and show the effectiveness of the cascade control method.

In the fourth chapter, experiments are carried out to further verify the effectiveness of the disturbance rejection control algorithm designed in the third chapter. The communication between the analogue signals of the experimental devices and the digital signals of the control terminal is based on dSPACE hardware and software. A Lithium-Ion battery and an ultracapacitor are connected to the DC bus via a boost converter and a bi-directional DC-DC converter respectively. The disturbances causing battery wear are emulated via an exosystem consisting of a resistive load and an AC power source. Real-time system responses under sinusoidal persistent disturbance, transient disturbance and the combination of both are presented respectively. Under each kind of disturbance, a contrast of system responses with and without the designed disturbance rejection algorithm is given and verifies the effectiveness of the controller.

Chapitre 1

The state of the art of hybrid energy storage system for vehicular application

Sommaire

1.1 Introduction

In today's society, people have gradually realized the importance of environment protection and sustainable development. The combustion of fossil fuels can no longer satisfy the energy demand due to its pollution to the environment and ecology. As alternative energy sources, renewable energy such as wind energy, solar energy and wave's energy etc. are growing rapidly. Moreover, as opposed to traditional energy production that relies on petroleum and natural gas, electrochemical energy production is more environmentally friendly and more sustainable. Electrochemical energy storage and conversion devices include fuel cells, batteries, and electrochemical capacitors. Reducing the consummation of fossil-fuel is an issue requiring the cooperation of not only scientists, but also ecologists, economists and politicians.

In the configuration of vehicles, an energy storage device is necessary. Generally, rechargeable batteries are utilized in vehicles to supply the current to start up and store redundant energy. Fuel cells are widely applied to pure electric vehicles due to its high energy density. Ultracapacitors, or supercapacitors are recently studied as an auxiliary power to capture the instantaneous peak powers. In the configuration of hybrid DC power sources, fuel cells and batteries are often used as primary power source whereas ultracapacitors often serve as auxiliary power source. They are connected in series or in parallel to the DC bus via power converters and supply power to the load (electric motors). Regulation of the DC bus voltage and the energy distribution management becomes a main research issue.

In this chapter, we will first present the working principle and characteristics of different DC power sources : fuel cells, batteries and ultercapacitors. Moreover, we will show some hybrid energy storage system configurations and various DC converter topologies applied in electric vehicles and hybrid vehicles. Finally, we will summarize a series of control technologies aiming to manage the energy distribution for hybrid energy storage systems in order to reduce the stress to the energy storage systems and thus extend their serve cycle. A various control theories to control DC-DC power converters will also be presented.

1.2 Energy storage systems

DC power sources including fuel cells, batteries, and supercapacitors are all electrochemical energy storage and conversion devices. The common features of them is that they all consist of two electrodes and electrolyte solution, and the energy generation happens at the interface of the electrodes and the electrolyte where the electrons and the ions separate and transport in the opposite direction [WB04]. The basic operation mechanism of each system will be presented in the following sections.

In automotive application, fuel cells or batteries generally serve as permanent source providing the required permanent energy to guarantee the system autonomy. Whereas, due to their chemical structures, they cannot totally satisfy the load demand, and thus supercapacitors are introduced to compensate the lacking power at transients and absorb excess power in braking process.

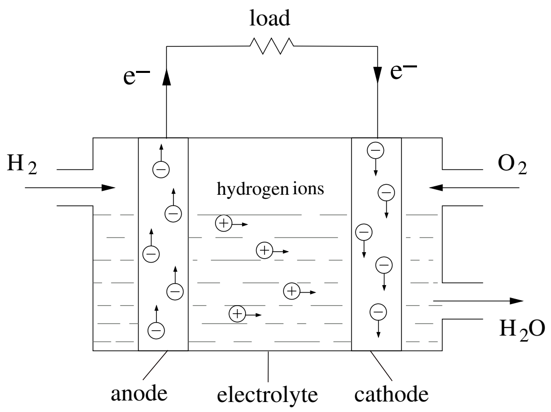

FIGURE 1.1 – Schematic of structure and operation mechanism of fuel cells.

1.2.1 Fuel cells

Fuel cells, as a clean and high-efficiency energy source, are mainly used in electric vehicles, and they are intended to replace traditional combustion engines in automotive field. In fact, these two have a similar operating mechanism, that is they both need external fuels supply. Similar with internal combustion engines, fuel cells supply energy as long as the fuels are supplied. The difference is that the fuels refilled in the tank of fuel cells are hydrogen and oxygen (or air) and that the exhaust is water. Whereas, internal combustion engines consume a large amount of non-renewable energy and generate greenhouse gases and harmful gases.

1.2.1.1 Working principle and characteristics

The hydrogen and hydrocarbon fuels used in fuel cells contain a large amount of energy. This energy is significantly higher than that found in common battery materials [WB04]. Through chemical reaction of hydrogen and oxygen, fuel cells convert the energy into electrical energy. Methanol and natural gas may be used instead of hydrogen gas. In this case, a fuel reformer is necessary to convert the hydrocarbon fuel into hydrogen-rich gas. In this process, quite a little carbon dioxide and nitrogen oxides are generated. In general, this type of chemical reaction produces only water in addition to electricity. Electrical vehicles with fuel cells as propulsion are therefore considered to be the most environmentally friendly vehicles and called “green vehicles".

Figure 1.1 shows a schematic of the structure and operation mechanism of fuel cells. It can be seen from the figure that fuel cells consist of an anode, where hydrogen is oxidized, a cathode, where oxygen is reduced by absorption of the electrons to the anions which react directly with the hydrogen ions to form water, and an electrolyte, where ions movement take places between the two electrodes. The fuels (hydrogen and oxygen) are supplied continuously from an external source, instead of containing within the fuel cell compartment. This feature allows fuels cells to serve longer time than other electrochemical cells as long as the fuels are sufficient, and avoids the charge-discharge cycles.

The principle of chemical reaction is $2H_2 + O_2 \rightarrow 2H_2O$. Fuels refilled in the tank of fuel cells are hydrogen and oxygen (or air). Other fuels like hydrocarbons need to be converted to hydrogen via a reform device. The chemical reactions between the fuels (hydrogen and oxygen) release the energy in the forms of electrical energy and heat.

The earliest fuel cell can be traced back to 1838. German physicist Christian Friedrich Schönbein invented the first fuel cell by inserting two platinum wires in hydrogen and oxygen into hydrochloric acid. Nowadays, in almost 200 years' study, scientists have developed many different structures of fuel cells. According to different types of electrolyte and different operation temperature, fuel cells are classified into the following types : Polymer Electrolyte Membrane Fuel Cell (PEMFC), Alkaline Fuel Cell (AFC), Direct Methanol Fuel Cell (DMFC), Solid Oxide Fuel Cell (SOFC), Molten Carbonate Fuel Cell (MCFC), and Phosphoric Acid Fuel Cell (PAFC) [Nfc]. Among them, the lightweight and compact PEMFC (also called Proton Exchange Membrane Fuel Cell) is the most widely used for automotive applications. A fuel cell stack in automotive application is integrated with several individual fuel cells in order to deliver powerful enough propulsion of vehicles.

1.2.1.2 Advantage and disadvantages

As opposed to internal combustion engines (ICE), other than lower emissions and clean power generation, fuel cells are more efficient in energy conversion. For example, the energy efficiency of traditional internal combustion engine is only about 25%, while PEMFC may reach energy efficiency up to 60%. This efficiency may be increased up to 85-90% if the produced heat can be captured and properly reused [SVP+91]. Moreover, fuel cells can supply continuous energy as long as the reactants are available. Hence, it may serve as energy generator and supply constantly the steady energy to vehicles.

Nowadays, fuel cell power generation systems have become a primary choice for electric vehicles to supply power to electrical machines. Many major manufacturers have invested in the studies of fuel cell vehicles. January 2011, Mercedes-Benz Class B F-CELL fuel cell vehicles, have completed global journey in 125 days ; General Motors Chevrolet Equinox 100 fuel cell vehicles have completed 1.4 million miles in 2010 ; Daimler Motor Company has already announced their project of industrialization of fuel cell cars in 2014 ; Other manufacturers like Toyota, Honda, GM, Mercedes-Benz, Audi, Hyundai etc. have also shown their cutting-edge technology and ambitions in fuel cell vehicles [FCv].

In spite of the aforementioned advantages and despite the advanced technologies, there are still some barriers in using fuel cells. Firstly, the fuel cell research in automotive application is still in the initial stage and is not as well developed as internal combustion engines, which leads to a relatively high cost of fuel cell power system. Secondly, due to its electrochemical characteristics, it is unable to allow bidirection current flow. Current flowing into fuel cells may cause severe damage, and therefore it is unable to capture braking energy during vehicle decelerations. Thirdly, fuel cells have relatively high internal resistance and show slow dynamic response. This results in difficulties during cold start-up. Besides, rapid load power demand during vehicle acceleration may cause fuel starvation phenomenon (drying of the FC membrane) and thus reduce its lifetime.

Consequently, it requires a special design while using fuel cells. Generally, a diode is utilized to avoid the current flowing into the fuel cell. Furthermore, in order to solve the foregoing problems, a hybridization of fuel cells with batteries and/or supercapacitors is often applied. Batteries and/or supercapacitors, working as auxiliary devices, are able to realize braking recovery and supply power during accelerations. Thus, the hybrid power configuration compensates the inadequacies of fuel cells and reduces the overall size and cost as well.

1.2.2 Batteries

There are mainly three classes of batteries : non-rechargeable (primary) batteries, rechargeable (secondary) batteries and specialty batteries [WB04]. As the names suggest, non-rechargeable batteries cannot be recharged and are therefore discarded once they are fully discharged. Rechargeable batteries may recover their original state of charge after discharged, and therefore widely applied in portable electronic devices, such as laptops, mobile phones, cameras, etc. Specialty batteries are not commonly used in daily life. They are specially designed to fulfill some purposes in military or medical applications.

An automotive battery is necessary in traditional vehicles to supply electrical power to the starter motor, the lights, and the ignition system (SLI battery) of a vehicle's engine. Lead-acid type is the most frequently used SLI battery, and provide a relatively low voltage around $12V$. For heavy vehicles, such as tractors or highway trucks equipped with diesel engines, the SLI battery applied is about $24V$. In electric vehicles or hybrid vehicles, batteries serving as a power source of electrical machine are referred to as traction batteries. In parallel hybrid electric vehicles, the electric motor shares the load demand with the engine. According different operating modes, the percentage shared by the electric motor could vary from 0 to 100%. This requires traction batteries to have a relatively high energy storage capacity, so as to perfectly satisfy the load demand.

1.2.2.1 Working principle and characteristics

Batteries convert the self-contained chemical energy into electrical energy on demand. A schematic of the structure and operation mechanism of batteries is depicted in Figure 1.2. As shown in the figure, the basic elements of batteries are : an anode (positive electrode), a cathode (negative electrode), and an electrolyte. The cathode is often made of materials easily loose electrons such as zinc or lithium. While the anode is often made of the ones easily accept electrons such as manganese dioxide or lithium cobalt oxide. The electrolyte provides an environment where the ions transport takes place [WB04]. In the figure, the ions movement between the separated electrolyte is achieved with the help of the bridge.

In 1780, the Italian physician Luigi Galvani noticed that a frog leg, which came into contact with copper and iron, repeatedly shrugged and thought it was an electrical effect. The first working galvanic element and thus the first battery was presented in the form of the voltaic pile in 1800 by Alessandro Volta. A voltaic cell is an electrochemical energy storage means and an energy converter. During discharge, the stored chemical energy is converted into electric energy via electrochemical redox reaction.

Rechargeable batteries can be classified into the following types : lead-acid battery, nickel-cadmium battery, nickel-metal hydride (Ni-MH) battery and lithium-ion (Li-ion) battery. Among them, lead-acid batteries have a relatively high energy storage capacity and low cost, thus occupy a dominant position in the rechargeable market. Nickel-cadmium batteries are relatively old, and have relatively small capacity. They have a memory effect that need to fully discharge before recharging, which makes them inconvenient to users. That is why they are quickly replaced by

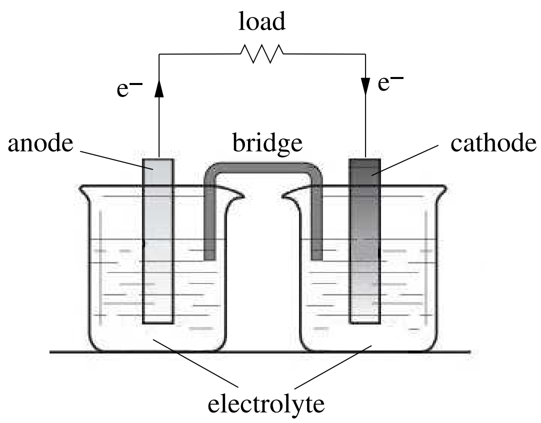

FIGURE 1.2 – Schematic of structure and operation mechanism of batteries

Ni-MH batteries. Ni-MH batteries are a new generation of rechargeable batteries. They have very high energy storage capacities, light weight, and almost no memory effects. They have been applied in hybrid electric vehicles. Li-ion batteries have very good application prospects. They have a high voltage, high capacity, and no memory effect. The self-discharge is only 0.5% - 2% per month, while Ni-MH is around 25%. Li-ion batteries have been used in portable electronic devices. As the production technology becomes increasingly sophisticated, Li-ion batteries are expected to replace Ni-MH and be used as on-board batteries in the near future [Rec].

There are several criteria of choosing battery systems, including self-discharge rate, charge time, energy storage capability, cost and cycle life, etc. Based on an overall consideration, in our study, a $100V$ lithium-ion battery is chosen to supply energy to the electric machine used in our hybrid electric vehicle.

1.2.2.2 Advantage and disadvantages

Battery has relatively high specific energy but relatively low in specific power. The power response is faster than fuel cells, but slower than supercapacitors. Batteries can be used in both electric vehicles and hybrid vehicles. Being different from fuel cells, batteries contain their chemical materials inside, and thus they have a limited lifetime. A automotive SLI battery may last around 6 years. When batteries reach their life limit, it is necessary to well dispose of. Otherwise, the toxic materials in batteries may cause damage to the environment. Hence, battery is one form of electronic waste (e-waste).

Consequently, it is necessary to control battery systems appropriately so as to maximize their lifetime. In hybrid vehicle applications, transient peak power load demand is very likely to reduce batteries lifetime. As a result, it is necessary to limit the battery current slope. To achieve this, a supercapacitor can be added to supply the transient peak power and capture the braking power.

1.2.3 Ultracapacitors

Ultracapacitors, also known as supercapacitors or electric double-layer (EDL) capacitor, are applied in power electronics area. For vehicular application, ultracapacitors serve as braking

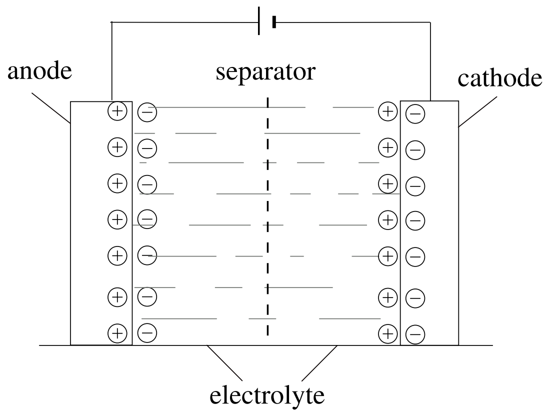

FIGURE 1.3 – Schematic of structure and operation mechanism of supercapacitors

energy recovery and burst-mode power delivery device.

1.2.3.1 Working principle and characteristics

Supercapacitors were first developed by General Electric (GE) engineers in 1950s [JH07]. Supercapacitor is also called ultracapacitor or electric double-layer capacitor (EDLC). Figure 1.3 gives a structure of the principle of supercapacitors. Comparing to capacitors, the anode and cathode of supercapcitors have much higher surface area, and thus can accumulate much more charges at the surfaces. Moreover, the carbon electrodes have high energy storage capacity. Being different from fuel cells and batteries, the energy storage process of supercapacitors is not through chemical reactions, and thus is reversible. As a result, supercapacitors can be repeatedly charged and discharged hundreds of thousands of times.

Supercapacitors exhibit a much longer lifetime than batteries. Generally, supercapacitors do not rely on chemical changes in the electrodes. Their lifetime depends mainly on the rate of evaporation of the liquid electrolyte. This evaporation depends on the temperature. As a result, the higher the temperature is, the faster the evaporation goes, and thus, the shorter the lifetime will be.

1.2.3.2 Advantage and disadvantages

Supercapacitors have a large capacitance density and very small time constants due to their very low internal resistances. Therefore, they have advantages in applications where a large amount of energy in a relatively short period is demanded or where a very high number of charge/discharge cycles is needed. The energy density of Supercapacitors is only about 10% of the same weight batteries, while their power density is about 10 to 100 times greater [KL10]. Ultracapacitors have therefore much faster charge and discharge cycles. They also tolerate many more charge and discharge cycles than batteries. However, ultracapacitors alone cannot supply load power requirement due to its self-discharge property.

Stand-alone fuel cells or stand-alone batteries integrated into an automotive system are not always sufficient to satisfy the load power demands. Due to the foregoing characteristics, ultra-

	Charge time	Discharge Time	Specific energy (Wh/kg)	Specific power (W/kg)	Life Cycle
Batteries	1∼5 hrs	0.3∼3 hrs	10∼100	< 1000	<1000
Ultracapacitors	0.3∼30 s	0.3∼30 s	1∼10	$< 10,000$	$> 500,000$
Capacitors	10^{-3}∼10^{-6}s	10^{-3}∼10^{-6}s	< 0.1	$< 100,000$	$> 500,000$

Table 1.1 – Characteristics of different devices (Source : [Zho06])

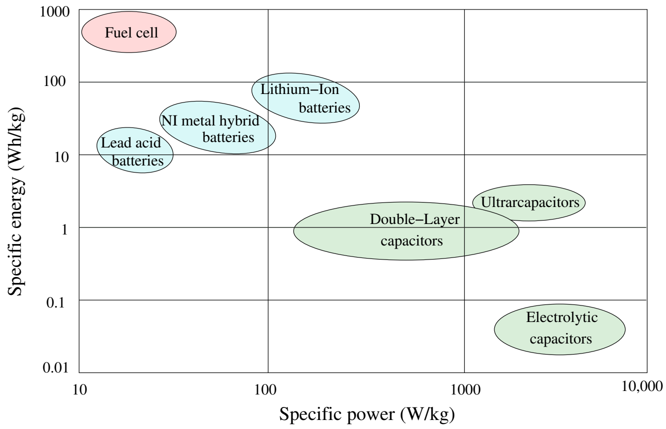

Figure 1.4 – Specific energy and power of different devices (Source : [Zho06])

capacitors are suitable to be a supplement when a rapid load power is required. Ultracapacitors can be used to capture large braking power during deceleration and provide transient peak power demand during acceleration. Integrating ultracapacitors to energy storage systems of EVs and HEVs will help reduce the overall volume and extend the serving life. With proper control strategy, this integration would also improve fuel efficiencies, reduce exhaust emissions, and extend the electric driving ranges.

1.2.4 Comparisons of different devices

Table 1.1 gives a comparison of the characteristics of batteries, ultracapacitors and conventional capacitors in terms of charge/discharge time, specific energy/power, and life cycles. Figure 1.4 gives a comparison of specific energy and specific power of the three energy storage devices. Specific energy (Wh/kg) and specific power (W/kg) are two important indicators of energy storage devices. They describe the energy and power capacities per unit mass of various devices. The indicators are sometimes measured per unit volume, and are referred to as energy density (Wh/L) and power density (W/L).

It can be seen from the figure that the fuel cells have relatively high specific energy but relatively low specific power. On the contrary, the capacitors have high specific power but low specific energy. The property of batteries is between them. Consequently, fuel cells and batteries are often used to supply the main power, while supercapacitors are used to meet the rapid power requirements. The hybridization of different devices improves the overall performance of the system and reduces the overall volume and cost.

1.3 Hybridization of energy storage systems

We have seem from the section above that fuel cells, batteries and ultracapacitors all have their own advantages and disadvantages. Neither one of them can serve all applications by themselves. Hybridization of two or three of the energy storage systems can provide a better performance and meet wider energy requirements. For hybrid vehicles, hybridization of energy storage systems may also contribute to improve fuel efficiency indirectly [KL10].

Instead of using a signal power source, the hybridization of multiple power sources may achieve a compromise between the specific power and the specific energy. Generally, in the configuration of two power sources : we choose one source with high specific energy and another with high specific power. The one with high specific energy supplies the main energy required by the system. While, the other one with high specific power meets the load power demand in a short time. Thus, this configuration can provide rapid and additional power during acceleration when peak load power is required, and achieve a braking power recovery during deceleration. Besides, it has a longer cycle and service life. Moreover, the overall size, volume and cost of the energy storage system can be effectively reduced.

In a hybrid configuration, the role of fuel cells and batteries is generally to supply main power to the load, whereas ultracapacitors deal with the transients and non-stationary fluctuating signals during acceleration and braking. Different topologies of hybrid energy sources have been studied in the literature. This will be presented in the following section.

1.3.1 Configurations of hybrid energy storage system

A hybrid energy storage system is composed of fuel cells stack, battery packs and ultracapacitor modules or any two of them. [WIAT11,TRD09] and [ABH11] give respectively two configurations of hybrid energy storage systems with fuel cell, batteries and ultracapacitors for hybrid electric vehicles. The advantage of three energy storage sources combination is that the battery can be charged by the fuel cell when the load is relatively light.

[WIAT11, TRD09] propose a direct parallel connection of three energy sources. As shown in Figure 1.5, the fuel cell, battery and ultracapacitor are connected to the DC bus via a DC-DC converter respectively. Due to its symmetry and flexibility, it is easy to realize an energy analysis and control. Whereas, the number of the electronic power devices in this topology is more than in other topologies, and thus, this leads to a potential increase of cost. In this configuration, the converters connected to batteries and ultracapacitors are bidirectional converters allowing a current flow in both directions, whereas, the converter connected to the fuel cells is a single direction converter avoiding the current flow into the fuel cells, in order to protect the fuel cells.

Other than a combination of all three energy storage systems, a hybridization of two energy sources is more common. [GFGJ10] researches a fuel cell and batteries combination applied in Metro Centro tramway in Spain. [KP07] has studied fuel cell/battery hybrid vehicles. However, [Gao05] has compared the performance of a fuel cell-battery hybrid system and a fuel cell-ultracapacitor hybrid system and has concluded that the latter, with the existence of ultracapacitors, shows better performance, economizes more fuels, and meet better the load power demand. Similarly, [BK08] has also done a comparative study by building an objective function including performance, fuel economy, and powertrain cost and has indicated that, among fuel

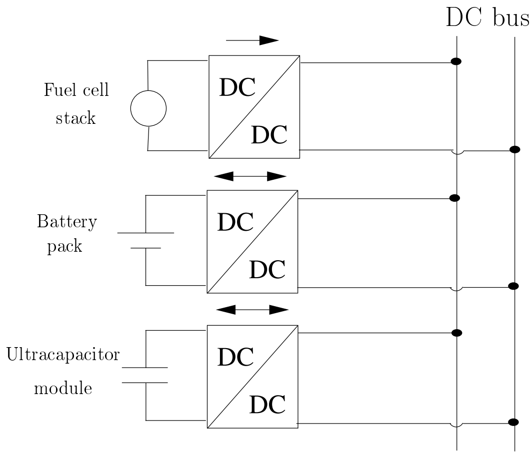

FIGURE 1.5 – Parallel connection of fuel cells, batteries and ultracapacitors

cell-battery, fuel cell-ultracapacitor, and fuel cell-battery-ultracapacitor vehicles, fuel cell-battery hybridization shown the poorest performance.

Compare to the hybridization of fuel cell and battery, the combination of fuel cell/ultracapacitor and battery/ultracapacitor show better performance and are preferred by most researchers. In these two configurations, ultracapacitor effectively complements the common drawbacks of fuel cell and battery, that is, respond for rapid dynamic power demand will cause severe damage to themselves. Thus, in this complement structure, fuel cells or batteries, due to their high specific energy, play a role of supplying continuous steady energy. Whereas, ultracapacitor, due to its high specific power, serves as energy source during accelerations to satisfy the peak power demand, absorbs energy during decelerations and realizes braking energy recovery.

There are several topologies for hybridization of two energy storage systems [LMT13]. Seven different topologies are depicted in Figure 1.6. Here, we consider only the hybridization of batteries and UC. Similar topologies can be extended to the hybridization of any other two energy storage systems.

In Figure 1.6(a), battery pack, paralleled with UC bank is directly linked to the DC bus. The battery charges the UC and supply power to the DC bus. This topology has an advantage of simplicity ; however, it is lack of flexibility since it is difficult to control the current flowing through the battery and the UC, and the voltage on the DC bus is also uncontrollable and always varies with the battery voltage.

To increase the flexibility, DC-DC converters can be applied, Figure 1.6(b, c, d) are three different cascade topologies, also known as series topologies. In Figure 1.6(b), a bidirectional converter is added to connect the UC and the DC bus. In this topology, the DC bus voltage can be boosted to a desired value while it is still difficult to regulate the power in the UC since it operates at the same voltage as the battery. Therefore, the topology is often referred to as a passive cascade structure [KL10]. In Figure 1.6(c) and (d), two converters are applied, and are often referred to as active cascade structure due to their control flexibility. Comparing to (d), (c) may boost the DC voltage to a higher level due to the two converters interfacing between the battery and the DC bus. Therefore, it is possible to choose a smaller size battery to satisfy the same power

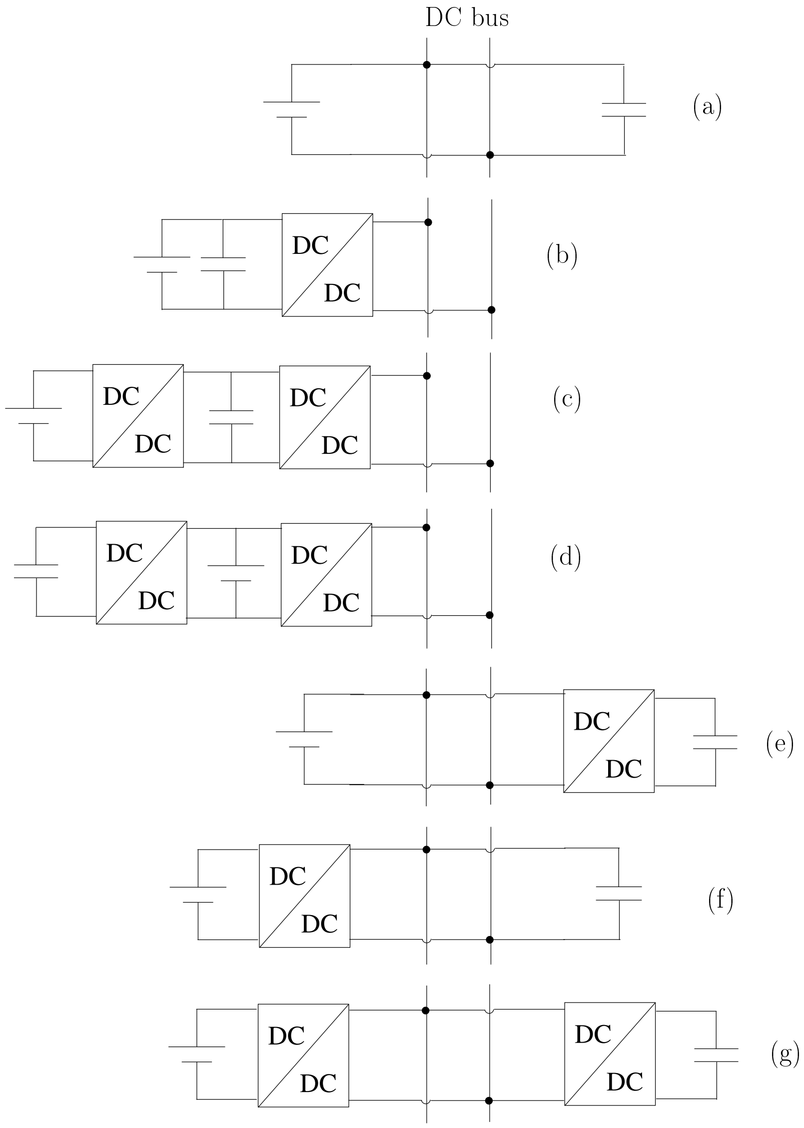

FIGURE 1.6 – Configurations of batteries/UC hybridization

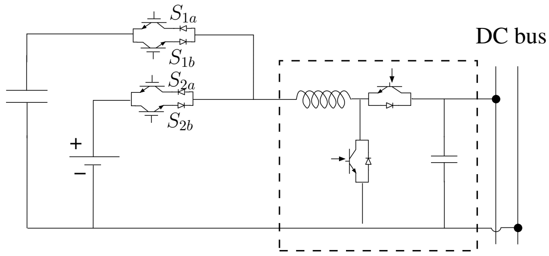

FIGURE 1.7 – Battery and UC sharing one common DC-DC converter

requirement, and thus, reduce the cost.

Other than cascade connections, Figures 1.6(e, f, g) show three different hybrid energy sources topologies with parallel connections. (e) and (f), with only one converter, are more simple but less flexible than (g). In Figure 1.6(e), a DC-DC converter connects the UC to the DC bus, making it possible to control the power in the UC, and the DC bus voltage can be maintained at a certain value without regulation. In Figure 1.6(f), the converter is linked on the battery side, providing a higher and adjustable voltage in the DC bus. However, neither of these two topologies allows achieving an optimum power sharing between the batteries and the UC. To achieve this so as to extend the life cycle of energy sources, the topology 1.6(g) is proposed and is often referred to as an active parallel structure. The two energy sources are connected to the DC bus by a converter respectively. Many researchers have studied this topology and proposed various control strategies.

In order to reduce the cost, size and complexity of control, researchers have proposed other topologies to transform the foregoing topologies. [DC03] has proposed to connect both battery and UC to one common DC-DC converter via two parallel switches, as shown in Figure 1.7. In this configuration, the converter is a two-quadrant DC-DC converter and works in boost mode when energy sources supply the load and works in buck mode for recovering braking energy to recharge the batteries and the UC. The configuration effectively reduces the number of converters. Whereas, it increases the number of switches and thus complicates control strategy.

[CE09] have proposed another topology, as shown in Figure 1.8. Being different from the topology of 1.6(f). A diode is added between the battery and the DC bus. Depending on the load power demand, the diode is reverse biased when the load demand is low and forward biased when the load demand is high. Therefore, the battery can be switched in to supply more power when a high load power is required.

Other than the topologies aforementioned, researchers have also introduced galvanic isolated converter into hybrid energy storage system. This is achieved via replacing the two inductors by a transformer. As shown in Figure 1.9 [OK12], with an integrated magnetic structure, two inductors share one core. This configuration effectively reduces the weight and volume of the system. Moreover, due to the inductor coupling structure, the ripples of the input current and the output voltage can be effectively cancelled, and the system responses to the load transients are much faster [OK12].

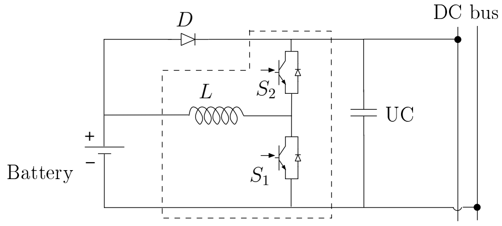

FIGURE 1.8 – Battery and UC hybridization with an additional diode

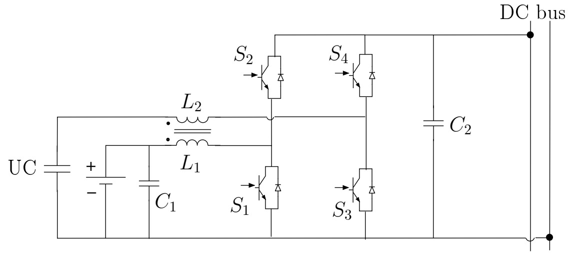

FIGURE 1.9 – Integrated magnetic structure

1.3.2 Configurations of DC-DC converters

In terms of galvanic isolation, DC-DC converters are divided into isolated converters and non-isolated converters. Isolated converter isolates the electrical connection between input and output, and this is achieved by integrating a transformer in the electric circuit. This configuration is based on the users' security consideration. Moreover, it has strong noise and interference blocking capability, thus provides the load with a cleaner DC source which is required by many sensitive loads. Isolated converters have been used in hybrid electric vehicles. An isolated half bridge based DC-DC bidirectional converter is proposed in [HD08] for Plug-in Hybrid Electric Vehicle applications. In the converter, the leakage inductance of the transformer is the primary energy transfer element.

However, the existence of transformer requires a decoupling of the inductance, and thus makes the controller design more complicated. Furthermore, as opposed to common non-isolated DC-DC converters, isolated converters are more bulky, heavier and cost more. Therefore, isolated DC-DC converters are not considered in our study.

For non-isolated converter, as depicted in Figure 1.10, there are three main topologies [SB03]. As shown in Figure 1.10(a), a basic bidirectional converter, works in boost mode when the current flows forwards and works in buck mode when the current flows backwards. This topology is also called half-bridge configuration. A combination of two half-bridge forms a full-bridge buck-boost converter as shown in Figure 1.10(b). In this configuration, the number of active components doubles, but the electrical and thermal stresses of the circuit become lower. Another common configuration is Cuk converter, see Figure 1.10(c). An advantage of Cuk circuit is that the input and output current can be rather smooth without ripples. Therefore, it is quite suitable in fuel cell applications. However, Cuk converter requires more active components than the other two converters and consequently leads to higher conduction loss and larger volume [TT13].

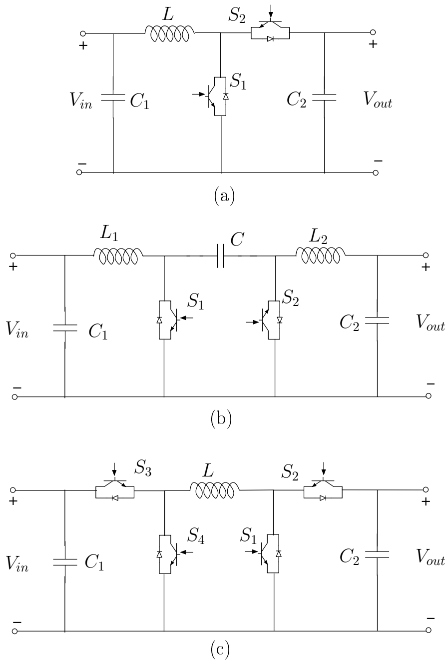

FIGURE 1.10 – Topologies of DC-DC converters

Other DC-DC converter topologies include parallel interleaved structure which is a parallel connection of switching converter with a shared input and output [BDB$^+$14] ; hybrid switched-capacitor bidirectional converter which is a composite of capacitors and switches [PMC12] ; and Z-Source network converter which is a Z-form combination of inductors and capacitors [Pen08]. In our study, a 4-quadrant bidirectional converter, as shown in Figure 1.10(a), is favourable for battery/UC hybrid energy source system in hybrid electric vehicles.

1.4 Control methodologies

In HEVs, in order to exploit the energy storage systems properly so as to extend their lifetimes, increase electric drive range, improve energy efficiency, and economizer fuel consumption, proper energy management for energy storage systems is quite necessary and has attracted the attention of many researchers. Various control strategies are discussed in this section. Rule-based power split control ; cost function optimization ; wavelet-based load sharing algorithm, etc. are proposed considering power distribution between different energy storage systems. Flatness-based control, polynomial (RST) control, PI control, sliding mode control and passivity-based control are also applied considering the converter characteristics.

1.4.1 Energy management

Generally speaking, energy management is to better exploit the hybrid energy storage system to cooperate with vehicles operations. For a batteries/UC hybrid system, in order to satisfy the load

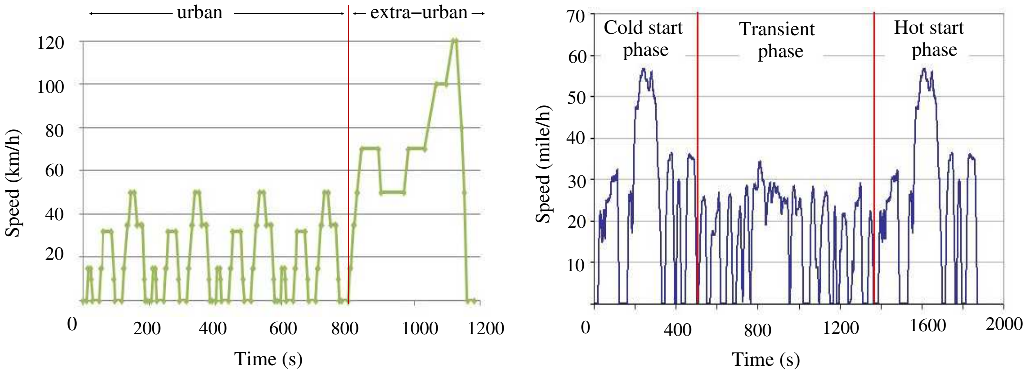

(a) New European Driving Cycle (b) FTP–75

FIGURE 1.11 – Commonly used driving cycles

requirement, batteries need to supply sustainable and steady energy to the electric machine, so as to support continuous propulsion. On the other side, UC needs to be responsible for vehicles starts/stops, acceleration and deceleration. Specifically, UC is in charge of supplying peak power during acceleration and absorbing braking power during deceleration. At the same time, it is important to maintain the state of charge (SOC) in batteries and UC, this is reflected in terms of their terminal voltage. In order to manage the energy distribution of different energy storage and maintain the state of charge, an effective and powerful control strategy is required to achieve a high performance. Over the past few decades, from power splitting strategy to power converter control, researchers have made great efforts to design such a high-performance system.

1.4.1.1 Driving cycle

Driving cycle is an important standard of automobile operation. A driving cycle is a curve describing the vehicle velocity versus time under certain traffic conditions such as highways or urban roads. There are different driving cycles proposed by different organizations. In general, there are three countries generating driving cycles which are Europe (NEDC, ECE15), Japan (10-15 Mode), and United States (FTP, SC03SFTP, UDDS, US06 andLA92) [TT13]. The most commonly used are the EPA Federal Test Procedure (FTP-75), and the New European Driving Cycle (NEDC) describing urban driving conditions. Driving cycle is used as a speed reference in off-line simulation to study the performance of propulsion system and the energy storage system. As shown in Figure 1.11, NEDC is theoretically derived, thus its curve is rather smooth. FTP-75 is measured from a real driving pattern, and thus, it is a non-stationary signal.

1.4.1.2 Control methodologies of energy management

Rule-based control is one of the supervisory control methods of the overall low-level components control. Rule-based control is based on human expertise, intuition and heuristic [TT13]. The rules are designed to share the load demanded power between primary and auxiliary energy sources. The controller can be achieved through fuzzy logic control. Rule-based controller is favourable due to its simplicity and possibility to implement onboard for real-time control. However, it requires a relatively large amount of calibration effort when applied on-line.

Another supervisory control method is optimization approach, which is realized through optimizing an objective function. Optimization approach, which is generally exploited to maximize the efficiency on the powertrain and minimize the losses, can be extended to manage the energy distribution for hybrid energy system. Optimization approach includes linear programming, dynamic programming (DP), stochastic DP, etc. Such an approach is based on a priori knowledge of the power demands over a driving cycle, and thus the results are not necessarily optimal when it is implemented on-line.

[SSL14] presents a comparison of a predictive controller, a dynamic programming algorithm, and a rule-based strategy for vehicular batteries/UC hybrid system. Referring to the study, all the three methods effectively reduce battery wear, and thus extend its lifetime. Moreover, the designed dynamic programming algorithm shows the best performance among these three methods.

The main idea of energy management for hybrid energy system is that the auxiliary energy source UC should capture the dynamic components of the load current while the primary energy source operates at a steady current level. Then the objective is to get the current reference for UC. Generally, this can be simply obtained by passing the load current through a high-pass filter. The filtered high frequency current is then the current reference for UC. However, simple filters may lead to a delay and thus the UC may not absorb the peak power promptly. [AS10] proposes a low-phase-shift filter to reduce the phase shift introduced by the filter.

[UA08] proposes a wavelet-base power sharing algorithm for fuel cell/UC hybrid vehicular power system. The authors utilize ADVISOR, an effective analysis tool for vehicle simulation, to get a required power demand profile corresponding to the vehicle driving cycle, and then apply wavelet transforms to the profile to filter the transient sharp peak power demands. The obtained peak power demand is then chosen as the power reference for UC.

[PPMT08, PPMTD11] propose a flatness-based control for energy management of fuel cell/UC hybrid power source. The paper proves that the nonlinear differential equations describing hybrid energy storage system have flatness property. Hence, all states and inputs of the system can be explicitly expressed in terms of the flat output and a finite number of its derivatives. The considered output of the system is the energy stored in the DC-bus capacitor. The system is controlled by planning the desired reference trajectories on the flat output space, and implement state feedback regulators to force the states to follow their references.

1.4.2 Power converter control

If we could say that energy management is a top-level control, then the power converter control could be referred to as a low-level control. Energy management is achieved through power converter control. Top-level control alone is not enough, it gives only an general overview. The study of power converters is relatively developed. Various control theory methods have been proposed by researchers.

1.4.2.1 Linear control

[WIAT11] applies traditional PI controllers to control each power converter connecting the energy storage system to the DC bus. As shown in Figure 1.12, power converter output voltage

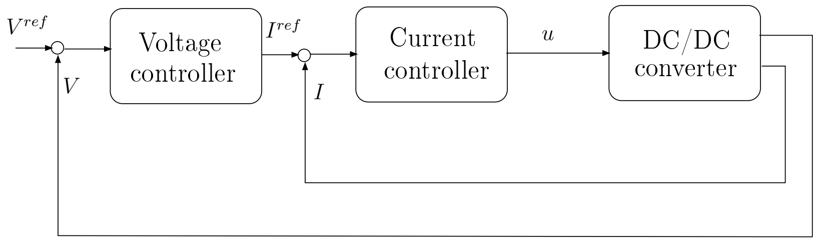

Figure 1.12 – Cascade control structure for power converters

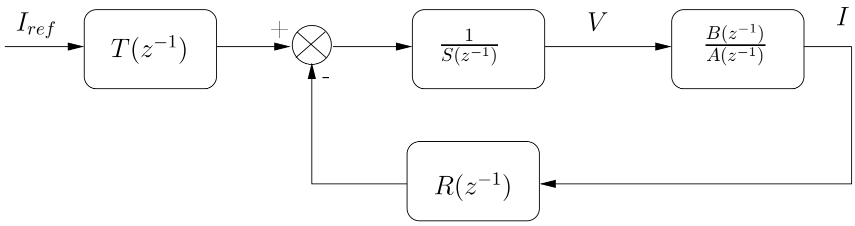

Figure 1.13 – RST converter control structure

can be regulated through a cascade structure with a current inner loop and a voltage outer loop. The current and voltage controllers can be simply realized with a proportional term and an integral term.

[CGG+10, CDG12] propose a polynomial control strategy, also known as RST digital control, for voltage and current management of battery/UC system. The principal control structure is presented in Figure 1.13. The key point of the control strategy is to determinate $R(z), S(z)$ and $T(z)$ polynomials. Where, $R(z), S(z)$ are deduced from Diophantine equation. This algorithm is robust and easy to implement in a microcontroller.

1.4.2.2 Sliding mode control

Other than Pulse-width modulation (PWM) control and peak current mode control, sliding mode control gives another method to control power electric switches. Being different from other controllers, sliding mode controller doesn't give a continuous duty cycle signal for switches but a discontinuous control signal which can be directly used to control switches. Consequently, this property leads to a stiff pushing motion to the system and results in chatting problem. The basic idea of sliding mode control is to find the sliding surface (see Figure 1.14) and force the system to move along the surface until reaching the equilibrium point. The sliding mode along the sliding surface $s = 0$ is exist only when the condition $s\dot{s} < 0$ is satisfied [UGS99].

For power converter control, sliding mode control is often utilized to control an inner current loop in a cascade control structure to converge the current to its reference [UGS99]. [ABDM07] has proposed to apply sliding mode controller to energy management of fuel cell/batteries/UC hybrid energy storage system. A cascade control configuration with voltage control as outer loop and current control as inner loop is applied. The sliding controller is used to control the fuel cell

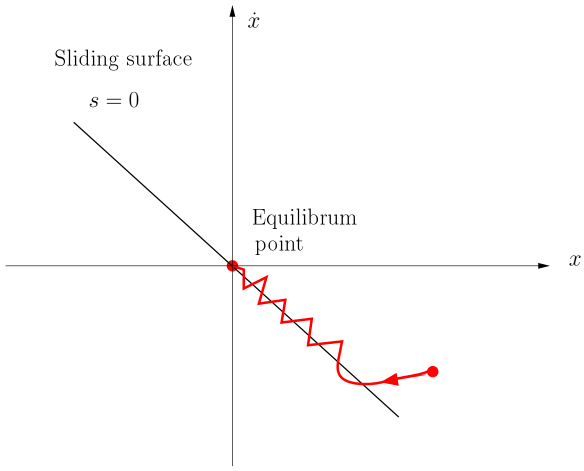

FIGURE 1.14 – Sliding surface and the system movement

converter current and the UC converter current. The outer voltage loop is controlled by a PI linear controller.

In [DCC13b], the sliding mode controller is applied to a supercapacitor connected DC-DC converter to absorb the current disturbance in the DC bus. The sliding surface is the error difference between the current and its reference. The current reference is not a simple nominal value, but a varying manifold aiming to absorb the current disturbance. The disturbance absorption objective is easily achieved with sliding mode control. More details can be find in the reference.

1.4.2.3 Passivity based control

Passivity-based control, first proposed by Ortega at the end of 20th century, dealing with system total energy, is a quite powerful nonlinear control method. Consider a system with states $x \in \mathbb{R}^n$ input $u \in \mathbb{R}^m$ and output $y \in \mathbb{R}^m$, if there exists a non-negative storage function $H(x)$ which can be written in the following form, then the system is said to be passive.

$$H[x(t)] - H[x(0)] \leq \int_0^t u^\top(s)y(s)ds \tag{1.1}$$

The inequality can be rewritten as :

$$\underbrace{H[x(t)] - H[x(0)]}_{\text{stored energy}} = \underbrace{\int_0^t u^\top(s)y(s)ds}_{\text{supplied energy}} - \underbrace{d(t)}_{\text{dissipated energy}} \tag{1.2}$$

Where, the left side of the equation represents the energy stored in the system, and the integral term on the right side is the energy supplied to the system, and $d(t) \geq 0$ is the dissipated energy of the system.

Let the control input $u(x) = \beta(x(t)) + v(t)$, and make the following assumption :

$$-\int_0^t \beta^\top(x(s))ds = H_a(x(t)) + n_0 \tag{1.3}$$

Where, n_0 is a constant of integration $n_0 = H_a(x(0))$. Substitute u into (1.2), and after some manipulation, we may get :

$$H_d(x(t)) - H_d(x(0)) = \int_0^t v(s)^\top (y(s))ds - d(t) \tag{1.4}$$

with energy function $H_d(x(t)) = H(x(t)) + H_a(x(t))$ being closed-loop energy. It can be seen from (1.4) that with the new control input $v(t)$, the closed-loop system is still passive. Moreover, if $H_d(x)$ has a strict (local) minimum at x^*, then x^* is an equilibrium point, and $H_d(x)$ decreases while x converges to x^* asymptotically. This is the principle of PBC.

Passivity based control is designed via interconnection and damping assignment, based on an Euler- Lagrange model or a Hamiltonian model [OvdSME02]. Passivity-based controllers have been studied to control a boost type and a buck-boost type DC-DC converter in [SRO95]. It has been proved that an output voltage direct control leads to an unstable controller, and thus, the controller is based on an indirect current control. PBC has also been studied in hybrid energy storage systems. [ABH$^+$10] applies PBC to a DC-DC converter cascade configuration for fuel cell/UC hybrid energy source. The system is written as a port-controller Hamiltonian system, and the controller is designed by preserving the system passivity.

1.5 Conclusions

In this chapter, we have summarized the principles and characteristics of fuel cells, batteries and UC, and analyzed their roles in EVs and HEVs. Fuel cells and batteries, due to their high energy density, are often used to supply steady energy to the load. Fuel cells, primary energy source, are often applied in electrical vehicles. Batteries work as primary sources mainly in HEVs. UC, due to its high power density, is exploited to capture the braking power and supplies instantaneous peak power demand. Hybridization of two or three of them provides a better energy storage system. Moreover, we have shown different hybridization structures and various topologies of DC-DC converters in vehicular applications. Among them, a parallel batteries/UC configuration with bidirectional DC-DC converters is chosen in our study due to its flexibility. Furthermore, in order to control hybrid energy storage systems, and properly manage the energy distribution between energy storage systems, a series of control strategies and control theory methods have been briefly presented. However, all these researches aim to deal with instantaneous peak power. In our study, we will focus not only on instantaneous peak power but also on sinusoidal disturbances introduced by ICE torque ripple compensation, and this will be elaborated in the following chapter.

Chapitre 2

Disturbance rejection theory and application

Sommaire

2.1 Introduction

In this chapter we will discuss two types of disturbances : transient and persistent disturbances. Both kinds of disturbances exist in hybrid electric vehicles. Transient disturbances are mainly caused by the instantaneous change in power demand, while the persistent disturbances are originated from the reciprocating motion of the piston in internal combustion engine. In our study, we focus mainly on the influence to DC electrical part. The influence of the disturbances to DC electrical part will be further explained, and the electrical model will also be built in this chapter.

For the past many years, to suppress and attenuate persistent disturbances, researchers have made great efforts and resumed a large amount of theories. In 1970s, Francis and Wonham have studied disturbance rejection for linear time-invariant and finite-dimensional systems and proposed the internal model principle which defines the feedback controller structure. Under the inspiration of Francis and Wonham, Byrnes, and Isidori have extended the theories to nonlinear systems and published their contributions in 1990s. Afterwards, an increasing number of researchers get interested in the related study. It is worth mentioning that Van der shaft has applied and extended some related theories to a typical class of system, port-controlled Hamiltonian system. In this chapter, we will review the main contributions of the predecessors on disturbance rejection for linear and nonlinear systems and then we attempt to solve our problem in hybrid electric vehicles with some related theories.

For our problem, the system is a non-linear system and specifically a port-controlled Hamiltonian system. However, the aforementioned theories cannot be applied in a direct manner. The problem remains complex, yet it is undeniable that the attempt to apply the related theories provides a clue to solve our problem and widen the horizon.

2.2 Disturbances in electrical part of HEVs

A hybrid electrical vehicle consists of an internal combustion engine and an electric machine. Referring to [Nje11], there exist several interconnections between the engine and the electric machine, such as series, parallel and hybrid connection. In our study, we concern the HEV with the ICE connected in parallel to a PMSM, providing propulsion to the load vehicle. As shown in Figure 2.1, for the mechanical part, the ICE and the PMSM are connected in parallel and deliver propulsion to the load. For the electrical part, a hybrid energy storage system (batteries and ultracapacitors) supplies power to the PMSM interfacing DC-DC converters and a DC-AC converter. The presence of the DC-DC converters makes the whole system more flexible and easier to control.

2.2.1 Mechanical equations

The influence of the vehicle speed to electrical DC part can be seen from mechanical and electrical equations. For sake of simplicity, neglecting the influence of the connection belt, the mechanical equation on the shaft can be written as :

$$J\dot{\omega}_m = (T_p + T_i) - T_{pmsm} - T_l \tag{2.1}$$

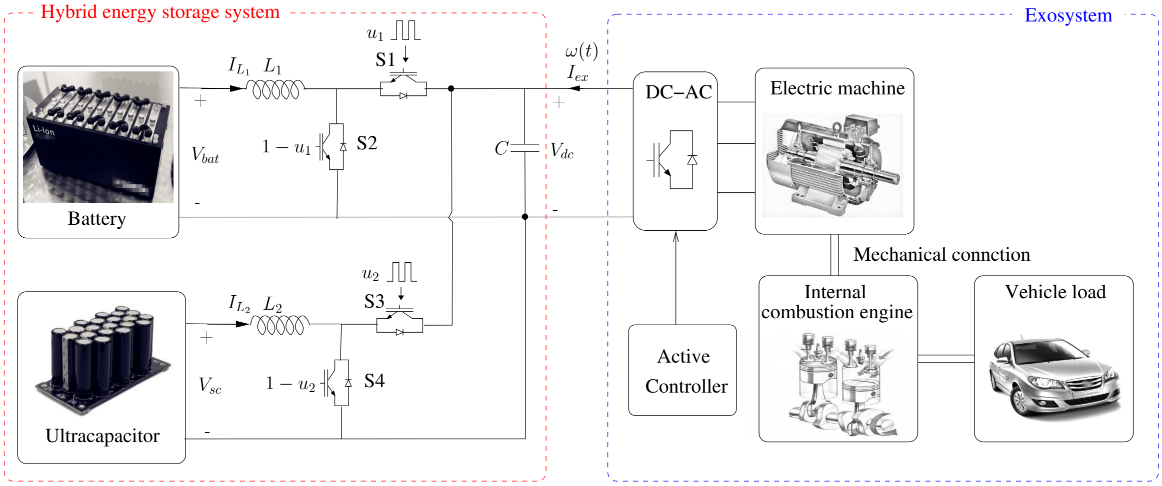

FIGURE 2.1 – Battery/Ultracapacitor hybrid energy storage system in hybrid electric vehicles

where, J is the mass moment of inertia, ω_m is the rotational speed, T_{pmsm} is the PMSM torque, T_p is the torque generated by the pressure in the cylinder in the combustion process, T_i is the torque generated by the oscillating masses and connecting rod, T_l is the load torque.

Equation (2.1) shows the relation between torques and the rotational speed. It can be seen that the control of the variation of the speed can be achieved through torque control. When a vehicle is running steadily, it is desired that the vehicle runs as smooth as possible, as a result, in order to obtain a constant speed, the torques need to satisfy the following equation :

$$T_{pmsm} = (T_p + T_i) - T_l \tag{2.2}$$

It is well known that the torque on the shaft generated by the ICE is due to the movement of pistons in the cylinders, which leads to ripples on the torque. Mechanical and chemical researchers have attempted to solve the problem in their domains. Traditionally, a flywheel is added to smooth the rotational speed by increasing the inertia, and the speed gets smoother as the size of the flywheel increases. However, the size of flywheel cannot increase infinitely because large flywheel increases the weight of vehicles and makes it difficult to spin up. Consequently, we attempt to solve the problem of torque ripples in electrical domain. [NCCM11] does a contribution and proposes several control algorithms to control the DC-AC converter. Through the designed controllers, the PMSM generates torque ripples that compensate the ones generated by the ICE, which achieves an "active flywheel". Herein, we consider only the DC-DC converters with the same objective that is to control the torque of the PMSM, so as to compensate the torque ripples generated by the ICE.

2.2.2 Electrical equations

Consider a dynamic model of PMSM expressed in the dq reference frame rotating at the same speed as the rotor. Set the d axis current i_d to 0, then the torque generated by the PMSM T_{pmsm}

is proportional to the q axis current i_q :

$$T_{pmsm} = \frac{3}{2} p \phi_m i_q \tag{2.3}$$

where, p is the number of pair poles and ϕ_m is the magnet flux of the PMSM rotor. Thereby, the PMSM torque control can be achieved via the control of the current i_q.

As shown in Figure 2.1, the power of the PMSM is supplied by the hybrid energy storage system through DC-DC converters and a DC-AC converter. From energy conservation point of view, neglecting the losses in the circuit, the power on the DC bus ($V_{dc}I_{dc}$) equals to the PMSM power (P_{pmsm}). This is equivalent to :

$$V_{dc}I_{dc} = P_{pmsm} = T_{pmsm}\omega_m = \frac{3}{2} p \omega_m \phi_m i_q \tag{2.4}$$

Therefore, the power in the DC bus is related to the PMSM power. If we suppose that the voltage on the DC bus is constant, then the current in the DC bus varies as P_{pmsm} varies.

2.2.3 Current disturbances in DC bus

The mechanical and electrical relations can be seen from the equations above. As aforementioned, in order to achieve a smooth rotational speed, the torque T_{pmsm} is required to compensate the torque ripples generated by the ICE. In other words, the ripples are thus introduced in the PMSM torque. Referring to equation (2.3), these ripples, being regarded as persistent disturbances, are transferred to the current i_q, and then transferred to the DC bus, and thus leads to persistent disturbances in the DC bus.

It is not difficult to understand that the phenomenon of ripple torque gets more obvious as the rotational speed reduces, and the ripple disturbances are quasi-periodical. Reference [NCCM11] presents a frequency analysis of rotational speed signal for a single-cylinder diesel engine under low rotational speed. Referring to this analysis, the speed signal is composed of a constant component and different sinusoidal harmonics that are multiples of the $7.5Hz$ which corresponds to the fundamental of a low rotational speed $900rpm(94.2rad/s)$.

Other than the persistent disturbances in the DC bus due to the torque ripple compensation when vehicles run smoothly, there exists another type of disturbance. During acceleration or deceleration, when the PMSM works in motor mode and large power is demanded instantaneously, or when the PMSM switches to generator mode and the power is fed back, the variation of P_{pmsm} can be regarded as a step signal and thus introduces a step variation (in other words, transient disturbance) in the DC bus.

Without loss of generality, both transient disturbances and persistent disturbances in the DC bus are considered in our study. The disturbances in the DC bus can be considered as an exogenous influence generated by an exogenous system. The exogenous influence to the DC bus can be described as an external current ω. It can be decomposed into a constant component and a variable component, i.e.,$\omega = \bar{\omega} + \tilde{\omega}$, where, $\bar{\omega}$ represents the constant component and $\tilde{\omega}$ represents the variable component, which is the disturbance that we want to rejected.

Mathematically, disturbances $\tilde{\omega}$ could take the following two forms :

— Persistent disturbance $\omega(t)$, is a periodical disturbance, and defined as $\omega(kT) = \omega((k+1)T)$, for all non-negative integers k, and T is the period of the signal ;

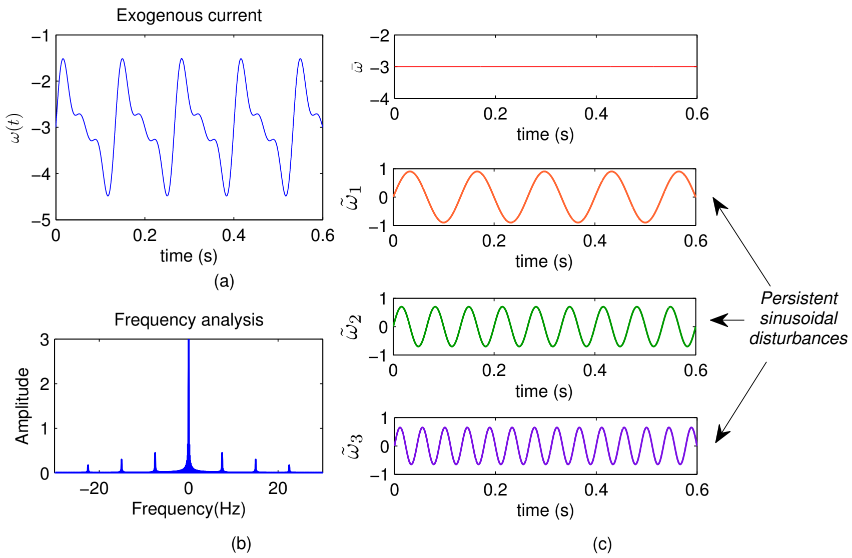

FIGURE 2.2 – Persistent disturbance and harmonic decomposition

— Transient disturbance $\omega(t)$, defined as $\omega(t_1) = \omega(t_1 + T)$ in the time interval $[t_1; t_1 + T]$, with $T \geq 0$.

Figure 2.2 and Figure 2.3 give an example of persistent disturbances and transient disturbances respectively. Based on the harmonic decomposition method (a recurrence least squares algorithm with a forgetting factor) used in reference [NCCM11], the external current can be decomposed into a constant component and different harmonic components. This is to say, $\omega = \bar{\omega} + \tilde{\omega}_1 + \tilde{\omega}_2 + \tilde{\omega}_3 + \cdots$, where, $\tilde{\omega}_i$ $(i = 1, 2, 3, \cdots)$ are sinusoidal component with different frequencies. Herein, for sake of simplicity, we take only one harmonic $\tilde{\omega}_1$ into consideration. Same principles can be extended to other harmonics. The controller dealing with the persistent disturbance can be constructed by a combination of the subcontrollers dealing with each harmonic. Moreover, when $\bar{\omega} < 0$, it corresponds to the PMSM working in motor mode. Likewise, when $\bar{\omega} > 0$, it corresponds to the PMSM working in generator mode.

2.2.4 Control objectives

Now that we have introduced the origins and the mathematical expressions of the two types of disturbances, it is obvious that the control objective is to achieve disturbance rejection. The idea of disturbance rejection is to reject the disturbances in the battery by absorbing them via the ultracapacitor. This is actually reflected in the construction of an "active damping".

Specifically, if the battery is the only power source to feed the PMSM, then the disturbances in the DC bus may be transferred totally to the battery and result in an oscillating or a step current in the battery, which will cause severe damage to the battery and reduce its lifetime. Therefore, it is necessary to design an “active damping" which gives an effect that reduces the amplitude of oscillations and the rapid variations in the battery. Taking this into consideration, the ultracapacitor is utilized to play the role of “active damping". It is connected to the DC bus through another DC-DC converter and aims to absorb the disturbances through an effective

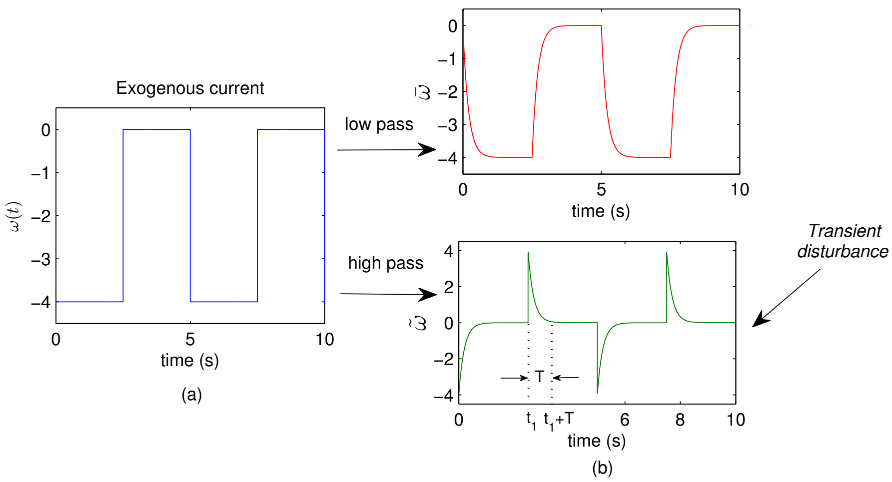

FIGURE 2.3 – Transient disturbance and filtered signals

high-performance controller. The controller needs to be well-designed and this is a main task of our study.

The control objective for the DC-DC converters is clear. In summary, the control of the hybrid energy storage system aims to maintain a constant voltage in the DC bus ; moreover and most importantly, to absorb the transient and persistent disturbances by the ultracapacitor ; meanwhile to maintain the voltage of the ultracapacitor around its nominal value.

2.3 Disturbance rejection theories

Figure 2.4 gives the configuration of a plant with exogenous disturbances generated by an exosystem. The disturbance rejection problem can be expressed as to find an error output feedback controller to drive the error output to zero as time goes to infinity.

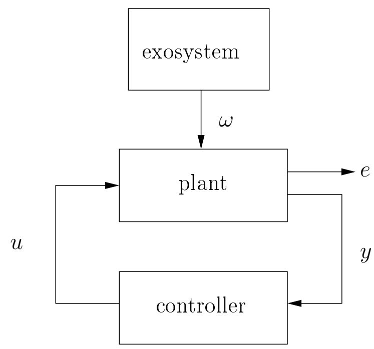

FIGURE 2.4 – System with exogenous disturbances

As aforementioned, in our study, we consider transient disturbances and persistent disturbances. Here, we consider persistent disturbances first. Persistent disturbances are quasi-periodical disturbances, so can be considered as the output of the following linear exosystem :

$$\dot{\omega} = s(\omega) = S\omega \tag{2.5}$$

with

$$S = \begin{pmatrix} 0 & & & & & & & \\ & 0 & \alpha_1 & & & & & \\ & -\alpha_1 & 0 & & & & & \\ & & & 0 & \alpha_2 & & & \\ & & & -\alpha_2 & 0 & & & \\ & & & & & \ddots & & \\ & & & & & & 0 & \alpha_k \\ & & & & & & -\alpha_k & 0 \end{pmatrix}, \alpha_{1,2,\cdots,k} \neq 0$$

Thus, ω corresponds to sinusoidal signals, and $\alpha_i (i = 1, 2, \cdots, k)$ corresponds to the frequency of each sinusoidal element. However, the information of phase is not included in this representation.

The plant in Figure 2.4 could be linear or non-linear. Researchers have made great effort for linear and non-linear output regulation problem for decades. We will resume the main contributions and important results in this section and attempt to apply them to our problem.

2.3.1 Linear systems

Early in 1970s, Francis and Wonham have studied output regulation for linear time-invariant and finite-dimensional systems, this problem is concerned with designing a control law for a plant such that the output of the plant asymptotically tracks a class of reference inputs and rejects a class of disturbances. Moreover, they have studied the situation when certain plant parameters vary, which is referred to as structurally stable output regulation [FSW74, FW76].

A main contribution of Francis and Wonham is the internal model principle which claims that a controlled system is structurally stable only if the controller utilizes feedback of the regulated variables and incorporates in the feedback path a suitably reduplicated model of the dynamic structure of the exogenous signals [FW76]. The principle gives an important overview of the control law. Another contribution of Francis and Wonham is a series of Sylvester equations which are named as regulator equations. They have proved that the solvability of regulator equations is a necessary condition for the solvability of a structurally stable output regulation problem for linear systems.

Consider a linear plant and an exosystem in state space representation :

$$\begin{aligned} \dot{x} &= Ax + Bu + E_w\omega \\ y &= C_y x + D_{yu}u + D_{yw}\omega \\ e &= C_e x + D_{eu}u + D_{ew}\omega \\ \dot{\omega} &= S\omega \end{aligned} \tag{2.6}$$

The equations describe a plant with state $x \in \mathbb{R}^n$, control input $u \in \mathbb{R}^m$, measurable output $y \in \mathbb{R}^p$ and error output $e \in \mathbb{R}^q$. The exosystem with state $\omega \in \mathbb{R}^s$ generates exogenous input to the plant. It can be seen that when $E_w = 0$ and $D_{yw} = 0$, and let $-D_{ew}\omega$ be a reference, the problem becomes a classical *reference tracking problem*, what the exosystem generates is only the reference, and what the controller needs to do is only to track the reference. However, when $E_w \neq 0$ and $D_{yw} \neq 0$, the system becomes more complex, and represents a system with exogenous disturbances. The control objective is to achieve disturbance rejection.

It is necessary to make the following three assumptions :

— A1 : The pair (A, B) is stabilizable.
— A2 : The pair (C_y, A) is detectable.
— A3 : All the eigenvalues of matrix S are ≥ 0 (S is anti-Hurwitz-stable).

2.3.1.1 Regulator equations

Lemma 2.3.1. *Assumptions A1 and A2 hold, the output regulation problem for linear system 2.6 has a solution if there exist matrices* Π *and* Γ *such that the following Sylvester equations are satisfied.*

$$\begin{aligned} \Pi S &= A\Pi + B\Gamma + E_w \\ 0 &= C_e\Pi + D_{eu}\Gamma + D_{ew} \end{aligned} \tag{2.7}$$

The existence of Π and Γ satisfying the regulator equations (2.7) is a necessary condition for the solvability of output regulation problem for linear system. As a matter of fact, $\Pi\omega$ and $\Gamma\omega$ provide a mapping for the state x and the input u respectively to reach their desired equilibrium. Therefore, the existence of the matrices Π and Γ implies the existence of such mappings or such paths to the desired equilibrium.

2.3.1.2 Feedback controllers

State feedback

When $y = x$, which means that all states are measurable, the regulator is a state feedback controller :

$$u = Fx + (\Gamma - F\Pi)\omega \tag{2.8}$$

where, F is an arbitrary matrix such that all the eigenvalues of $A + BF$ have negative real parts.

This can be easily proved by variable replacement. Replacing x by $\tilde{x} = x - \Pi\omega$, we obtain :

$$\begin{aligned} \dot{\tilde{x}} &= (A + BF)\tilde{x} \\ e &= (C_e + D_{eu}F)\tilde{x} + (C_e\Pi + D_{eu}\Gamma + D_{ew})\omega \end{aligned} \tag{2.9}$$

When $C_e\Pi + D_{eu}\Gamma + D_{ew} = 0$, we have $lim_{t\to\infty}e(t) = 0$. The stability is guaranteed by the stability of $A + BF$. It can be seen that the variable replacement actually transform x to $\tilde{x}$ through mapping $\Pi\omega$, where the error output converges to zero.

Output feedback

More general cases when $y \neq x$, the regulator is an observer based controller and has the following form :

$$\begin{aligned} \begin{pmatrix} \dot{\hat{x}} \\ \dot{\hat{\omega}} \end{pmatrix} &= \begin{pmatrix} A & E_\omega \\ 0 & S \end{pmatrix} \begin{pmatrix} \hat{x} \\ \hat{\omega} \end{pmatrix} + \begin{pmatrix} B \\ 0 \end{pmatrix} u + \begin{pmatrix} K_A \\ K_S \end{pmatrix} \left[\begin{pmatrix} C_y & D_{yw} \end{pmatrix} \begin{pmatrix} \hat{x} \\ \hat{\omega} \end{pmatrix} - y \right] \\ u &= \begin{pmatrix} F & (\Gamma - F\Pi) \end{pmatrix} \begin{pmatrix} \hat{x} \\ \hat{\omega} \end{pmatrix} \end{aligned} \tag{2.10}$$

where, K_A, K_S and F are matrices such that all the eigenvalues of matrices

$$A + BF \quad \textit{and} \quad \begin{pmatrix} A + K_A C_y & E_w + K_A D_{yw} \\ K_S C_y & S + K_S D_{yw} \end{pmatrix}$$

have negative real parts.

Take $v = \begin{pmatrix} v_1 \\ v_2 \end{pmatrix} = \begin{pmatrix} \hat{x} \\ \hat{\omega} \end{pmatrix}$, then the control algorithm (2.10) can be written in a general form as follow :

$$\begin{cases} \dot{v} = A_c v + B_c y \\ u = C_c v + D_c y \end{cases} \tag{2.11}$$

with

$$\begin{aligned} A_c &= \begin{pmatrix} A + K_A C_y + BF & E_w + K_A D_{yw} + B(\Gamma - F\Pi) \\ K_S C_y & S + K_S D_{yw} \end{pmatrix} \\ B_c &= -\begin{pmatrix} K_A \\ K_S \end{pmatrix} \\ C_c &= \begin{pmatrix} F & \Gamma - F\Pi \end{pmatrix} \\ D_c &= 0 \end{aligned}$$

It is worth mentioning that the control algorithm (2.11) can be deduced from a designed system (2.12) with no constraint, then the control algorithm to this auxiliary system is equivalent to the output feedback controller of system (2.6) [SSS03] :

$$\begin{aligned} \dot{\bar{x}} &= \bar{A}\bar{x} + \bar{B}\bar{u} \\ \bar{y} &= \bar{C}_y \bar{x} \end{aligned} \tag{2.12}$$

with

$$\bar{A} = \begin{pmatrix} A & -B\Gamma \\ 0 & S \end{pmatrix} \quad \bar{B} = \begin{pmatrix} 0 & B \\ I & 0 \end{pmatrix} \quad \bar{C}_y = \begin{pmatrix} C_y & D_{yw} + C_y\Pi \end{pmatrix}$$

The control algorithm to the auxiliary system is :

$$\begin{cases} \dot{\varsigma} = \bar{A}_c \varsigma + \bar{B}_c \bar{y} \\ u = \bar{C}_c \varsigma + \bar{D}_c \bar{y} \end{cases} \tag{2.13}$$

with

$$\begin{aligned} \bar{A}_c &= \begin{pmatrix} S + \bar{D}_{c_1}(D_{yw} + C_y\Pi) & \bar{C}_{c_1} \\ \bar{B}_{c_1}(D_{yw} + C_y\Pi) & \bar{A}_c \end{pmatrix} \\ \bar{B}_c &= -\begin{pmatrix} \bar{D}_{c_1} \\ \bar{D}_{c_2} \end{pmatrix} \\ \bar{C}_c &= \begin{pmatrix} -\Gamma + \bar{D}_{c_2}(D_{yw} + C_y\Pi) & \bar{C}_{c_2} \end{pmatrix} \\ \bar{D}_c &= \bar{D}_{c_2} \end{aligned}$$

The control algorithm (2.13) can be explicitly rewritten as :

$$\begin{aligned} \dot{\varsigma}_1 &= S\varsigma_1 + \bar{C}_{c,1}\varsigma_2 + \bar{D}_{c,1}\bar{y} \\ \dot{\varsigma}_2 &= \bar{A}_c\varsigma_2 + \bar{B}_c\bar{y} \\ u &= \underbrace{-\Gamma\varsigma_1}_{u_1} + \underbrace{\bar{C}_{c,2}\varsigma_2 + \bar{D}_{c,2}\bar{y}}_{u_2} \end{aligned} \tag{2.14}$$

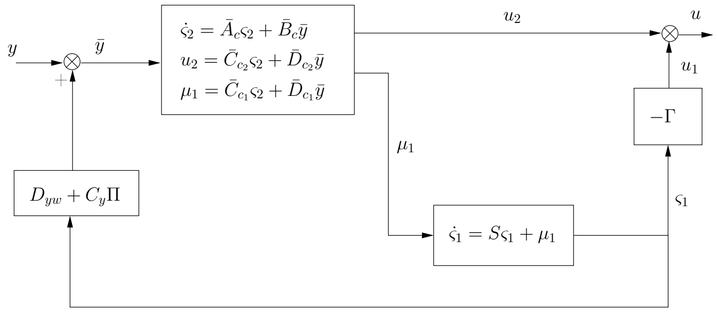

FIGURE 2.5 – Output regulator for linear systems

where, $\bar{y} = (y + (D_{yw} + C_y\Gamma))\varsigma_1$. The output feedback controller can be depicted in Figure 2.5. It can be seen from the figure that the controller is the sum of two subcontrollers.

2.3.2 Nonlinear systems

In 1990s, Isidoris et al. have extended the linear output regulation theories to nonlinear systems and published their studies [BPI97, IB90, BPIK97]. Huang have done some further contributions afterwards [HL93, Hua01]. In this section, we resume the main results of error output regulation for nonlinear systems with exogenous disturbances in contract with linear systems. Consider the state space representation of a nonlinear system with exogenous disturbances :

$$\begin{aligned} \dot{x} &= f(x, u, \omega) \\ \dot{\omega} &= s(\omega) \\ e &= h(x, \omega) \end{aligned} \tag{2.15}$$

where, system state $x \in \mathbb{R}^n$, control input $u \in \mathbb{R}^m$, and error output $e \in \mathbb{R}^q$. The exosystem with state $\omega \in \mathbb{R}^s$ generates exogenous input to the plant. The objective is to find an error output feedback regulator to drive the error output to zero as time converges to infinity.

Similar with linear systems, the related theories are based on the following hypotheses :

- H1. $\dot{x} = f(x, u, 0)$ is locally exponentially stabilizable at equilibrium point.
- H2. $\dot{x} = f(x, 0, \omega)$ is locally exponentially detectable at equilibrium point.
- H3. The Jacobin matrix $S = \frac{\partial s}{\partial \omega}(0)$ has all eigenvalues on the imaginary axis.

2.3.2.1 Regulator equations

One of the main contributions of Isidoris et al. is that they found the Sylvester equations for non-linear systems corresponding to the regulator equations (2.7) for linear systems, and proved that, under the three hypotheses aforementioned, the solvability of the Sylvester equations is one of the necessary conditions for the existence of controller for nonlinear systems. Mathematically represented as :

Lemma 2.3.2. *The nonlinear output regulation problem is solvable if there exist mappings* $x = \pi(\omega)$ *and* $u = c(\omega)$*, satisfying the following regulator equations :*

$$\begin{aligned} \frac{\partial \pi}{\partial \omega} s(\omega) &= f(\pi(\omega), c(\omega), \omega) \\ 0 &= h(\pi(\omega), \omega) \end{aligned} \tag{2.16}$$

The regulator equations (2.16) express the property that the mapping $x = \pi(\omega)$ provides a desired invariant manifold on which the error is zero, and the mapping $u = c(\omega)$ drives the plant to this manifold. The existence of the mappings $x = \pi(\omega)$ and $u = c(\omega)$ implies the existence of this desired manifold and the existence of the path from the plant to this manifold. Therefore, it is a necessary condition for the solvability of a non-linear error output regulation problem.

2.3.2.2 Linear controllers

If the regulator equations are satisfied, then there exists a controller in the following general form :

$$\begin{aligned} \dot{\xi} &= \varphi(\xi) \\ u &= \gamma(\xi) \end{aligned} \tag{2.17}$$

Now we are on the point to define the specific form of the controller. Generally, the controller could be linear or nonlinear. Due to the complexity and diversity of nonlinear systems, it is rather difficult to describe the form of a nonlinear controller. Furthermore, taking into account the closed-loop stability, despite the Lyapunov stability theory, it remains difficult to exam the stability of a close loop interconnecting a non-linear plant and a non-linear controller. Therefore, Isidoris et al. consider the linearization of the plant, and attempt to design a linear controller to solve the problem. The linearization of the plant leads to the following matrices :

$$A = \left[\frac{\partial f}{\partial x}\right]_{(0,0,0)}, \quad B = \left[\frac{\partial f}{\partial u}\right]_{(0,0,0)}, \quad C = \left[\frac{\partial h}{\partial x}\right]_{(0,0)}.$$

Isidoris et al. also give conditions of the existence of linear controllers, as described in the following proposition.

Proposition 2.3.3. *The assumptions* H_1 *and* H_2 *hold. The output regulator for nonlinear system* (2.15) *can be a linear controller if there exist mappings* $x = \pi(\omega)$ *and* $u = c(\omega)$*, with* $\pi(0) = 0$ *and* $c(0) = 0$*, satisfying the regulator equations* (2.16) *with* $c(\omega)$ *such that, for some set of* q *real numbers* $a_0, a_1, \cdots, a_{q-1}$*,*

$$\mathcal{L}_s^q c(\omega) = a_0 c(\omega) + a_1 \mathcal{L}_s c(\omega) + \cdots + a_{q-1} \mathcal{L}_s^{q-1} c(\omega) \tag{2.18}$$

and moreover the matrix

$$\begin{pmatrix} A - \lambda I & B \\ C & 0 \end{pmatrix}$$

is nonsingular for every λ *that is a root of the polynomial*

$$p(\lambda) = a_0 + a_1 \lambda + \cdots + a_{q-1} \lambda^{q-1} - \lambda^q \tag{2.19}$$

having non-negative real part.

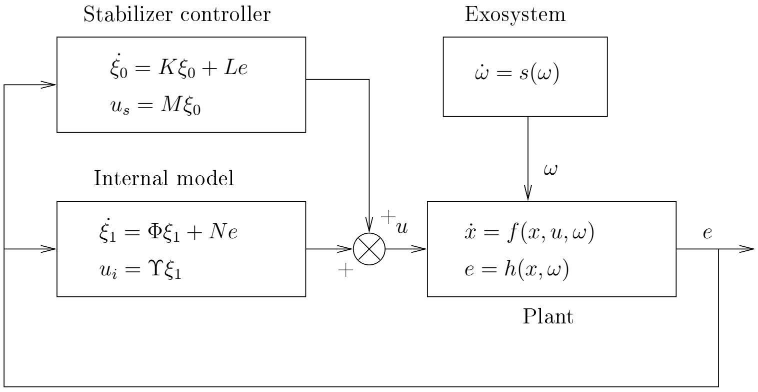

Figure 2.6 – Structure of the controlled system for nonlinear case

In the terminology of [BPIK97], the condition (2.18) indicates that the system $\{W, s, c\}$ is *immersed* into a linear system (2.20). In other terms, there exists a linear system (2.20) that generates the same response output as $c(\omega)$.

$$\begin{cases} \dot{\xi} = \Phi\xi \\ u = \Upsilon\xi \end{cases} \tag{2.20}$$

with

$$\Phi = \begin{pmatrix} 0 & 1 & 0 & 0 & \cdots & 0 & 0 \\ 0 & 0 & 1 & 0 & \cdots & 0 & 0 \\ \vdots & \vdots & \vdots & \vdots & \ddots & \vdots & \vdots \\ 0 & 0 & 0 & 0 & \cdots & 0 & 1 \\ 0 & a_1 & 0 & a_3 & \cdots & a_{r-2} & 0 \end{pmatrix}$$

$$\Upsilon = \begin{pmatrix} 1 & 0 & 0 & \cdots & 0 \end{pmatrix}$$

Furthermore, the proposition (2.3.3) gives an abstract condition under which the system $\{W, s, c\}$ is immersed into a linear system. A particular case yet a concrete example is when the mapping $c(\omega)$, which satisfies the regulator equation (2.16), is a polynomial in ω. It can be easily verified that a polynomial $c(\omega)$ fulfills the condition (2.18). Consequently, if there exists a mapping $c(\omega)$ that is a polynomial in ω, then it is immersed into a linear system driving the plant to the desired invariant manifold on which the error is zero. This is to say that it is possible to find a linear controller to solve the non-linear error output regulation problem. The controller (2.17) may have the following form :

$$\begin{cases} \dot{\xi}_0 = K\xi_0 + Le \\ \dot{\xi}_1 = \Phi\xi_1 + Ne \\ u = M\xi_0 + \Upsilon\xi_1 \end{cases} \tag{2.21}$$

Figure 2.6 gives a structure of the whole system interconnecting the plant, the exosystem and the error output feedback controller. It can be seen that the controller consists of two subcontrollers. One subcontroller is :

$$\begin{cases} \dot{\xi}_0 = K\xi_0 + Le \\ u_s = M\xi_0 \end{cases} \tag{2.22}$$

and the other subcontroller is :

$$\begin{cases} \dot{\xi}_1 = \Phi\xi_1 + Ne \\ u_i = \Upsilon\xi_1 \end{cases} \tag{2.23}$$

The subcontroller (2.23) is to generate a desired manifold, which is referred to as an internal model, while the subcontroller (2.22) is to stabilize the interconnection of the plant and the internal model.

2.3.2.3 System stability

The matrices in the controller K, M, L, N are chosen to stabilize the matrix (2.24) which characterizes the closed-loop system. The controlled system is asymptotically stable when the matrix (2.24) has all eigenvalues with negative real part.

$$\begin{pmatrix} A & BM & B\Upsilon \\ LC & K & 0 \\ NC & 0 & \Phi \end{pmatrix} \tag{2.24}$$

2.3.3 Hamiltonian systems

In the last section, we resume the theories of error output regulation for non-linear plant with exogenous disturbances. Isidoris et al. introduce linear controllers to solve the problem, and verify the system stability based on system linearization. Van der Schaft et al. have extended the theories to port-controlled Hamiltonian systems and have proved that for a class of Hamiltonian systems, it is possible to design an error output regulator as a Hamiltonian system and guarantee the whole stability by fulfilling the LaSalle's invariant principle [GvdS03]. Some related studies are presented in this section.

Consider a port-controlled Hamiltonian system with exogenous disturbances described by :

$$\begin{cases} \dot{x} = f(x,u,\omega) = [\mathcal{J}(x,\omega) - \mathcal{R}(x,\omega)]\dfrac{\partial\mathcal{H}(x,\omega)}{\partial x} + g(x,\omega)u \\ e = h(x,\omega) \quad = g^\top(x,\omega)\dfrac{\partial\mathcal{H}(x,\omega)}{\partial x} \\ \dot{\omega} = s(\omega) \end{cases} \tag{2.25}$$

where, $H = \frac{1}{2}x^\top x$. Notice that the port-controlled Hamiltonian system (2.25) has a special form. That is, the input and the output are conjugated variables, in the sense that their duality product defines the power flows exchanged with the environment of the system, such as, the currents and voltages in electrical circuits.

As described in the section of nonlinear system, the solvability of the regulator equations is a necessary condition for the existence of error output feedback controller. Proposition 2.3.4 presents all necessary conditions for the existence of such a controller and claims that under these conditions, it is possible to design the internal model of the controller as a port-controlled Hamiltonian system instead of a linear system.

Proposition 2.3.4. *The assumptions A_1 and A_2 hold, it is possible to design an internal model unit as a port-controlled Hamiltonian system to solve the error output regulation problem for system* (2.25) *if there exist mappings $x = \pi(\omega)$ and $u = c(\omega)$, with $\pi(0) = 0$ and $c(0) = 0$, satisfying the regular equations* (2.16)*, and $c(\omega)$ a polynomial of ω.*

2.3.3.1 Hamiltonian system controller

Through some linear transformation, it can be deduced that the linear system (2.20) is immersed into (equivalent to) another linear system :

$$\begin{cases} \dot{z} = \Psi z \\ u = \Lambda z \end{cases} \tag{2.26}$$

with $r = 2n_k + 1$ and,

$$\Psi = \begin{pmatrix} 0 & \hat{\omega}_1 & & & & & \\ -\hat{\omega}_1 & 0 & & & & & \\ & & 0 & \hat{\omega}_2 & & & \\ & & -\hat{\omega}_2 & 0 & & & \\ & & & & \ddots & & \\ & & & & & 0 & \hat{\omega}_{n_k} \\ & & & & & -\hat{\omega}_{n_k} & 0 \end{pmatrix}$$

$$\Lambda = \begin{pmatrix} 1 & 0 & 1 & 0 & \cdots & 1 & 0 \end{pmatrix}^\top$$

through linear transformation $z = T\xi$

$$T^{-1} = \begin{pmatrix} \Lambda & \Lambda\Psi & \Lambda\Psi^2 & \cdots & \Lambda\Psi^{r-1} \end{pmatrix}^\top$$

Therefore, the immersed system (2.26) can be written in the following form :

$$\begin{aligned} \dot{z} &= \mathcal{J}_i \frac{\partial \mathcal{H}_i}{\partial z} \\ u &= \Lambda \frac{\partial \mathcal{H}_i}{\partial z} \end{aligned}$$

with $\mathcal{J}_i = \Psi$ and $H_i = \frac{1}{2} z^\top z$. Thus, the internal model (2.23) can be written as a port-controller Hamiltonian system :

$$\begin{aligned} \dot{z} &= \mathcal{J}_i \frac{\partial \mathcal{H}_i}{\partial z} + g_i e \\ u_i &= g_i^\top \frac{\partial \mathcal{H}_i}{\partial z} \end{aligned} \tag{2.27}$$

with $g_i = \Lambda^\top$.

As presented before, an error output feedback controller consists of an internal model and a stabilizer. Now that we have already the internal model, we have only the stabilizer is to determine. As a matter of fact, due to the conjugated structure of Hamiltonian system (2.25), the stabilizer u_s can simply be :

$$u_s = -e \tag{2.28}$$

This can be verified through the examination of the closed-loop system stability.

2.3.3.2 System stability

The closed-loop system interconnecting the plant, the exosystem and the error output feedback controller can be written in port-controlled Hamiltonian form :

$$\begin{pmatrix} \dot{x} \\ \dot{z} \\ \dot{\omega} \end{pmatrix} = \left[\begin{pmatrix} \mathcal{J}(x,\omega) & g(x,\omega)g_i^\top & 0 \\ -g_i g(x,\omega)^\top & \mathcal{J}_i & 0 \\ 0 & 0 & S \end{pmatrix} - \begin{pmatrix} \mathcal{R}(x,\omega) & 0 & 0 \\ 0 & 0 & 0 \\ 0 & 0 & 0 \end{pmatrix} \right] \begin{pmatrix} \frac{\partial \mathcal{H}}{\partial x} \\ \frac{\partial \mathcal{H}_i}{\partial z} \\ \frac{\partial \mathcal{H}_w}{\partial \omega} \end{pmatrix} + \begin{pmatrix} g(x,\omega) \\ 0 \\ 0 \end{pmatrix} u_s \tag{2.29}$$

It can be verified that the total Hamiltonian $\mathcal{H}_{tot}$ and its first order derivative fulfill the Lyaponov energy theory.

$$\begin{aligned} \mathcal{H}_{tot} &= \mathcal{H} + \mathcal{H}_i + \mathcal{H}_w = \mathcal{H} + \frac{1}{2} z^\top z + \frac{1}{2} \omega^\top \omega \geq 0 \\ \dot{\mathcal{H}}_{tot} &= -y^2 - \frac{\partial^\top \mathcal{H}}{\partial x} \mathcal{R}(x,\omega) \frac{\partial \mathcal{H}}{\partial x} \leq 0 \end{aligned} \tag{2.30}$$

Therefore, the designed internal model and the stabilizer controller solve the error output regulation problem for Hamiltonian system (2.25). However, the designed controller can only be applied to Hamiltonian systems with special conjugated structure as described before. It is easy to see that the stabilizer becomes much more complex to determine without this particularity. Therefore, the controller cannot be applied to other Hamiltonian systems straightforwardly, and the error output regulation problem for nonlinear systems with exogenous disturbances remains open to researchers.

2.4 Theory application

Now that we have summarized the related theories about output regulation for linear and nonlinear systems with exogenous disturbances, we attempt to apply the theory to our problem. As mentioned in section 2.2, the disturbance to the paralleled DC-DC converters is considered as an exogenous current input ω. The objective is to control the two DC-DC converters to maintain a constant DC voltage and more importantly, to absorb the disturbances by the ultracapacitor.

Consider the topology in Figure 2.7. The hybrid energy storage devices are connected through two DC-DC converters in parallel. The battery is supposed to maintain the voltage in the DC bus, and the ultracapacitor is expected to absorb the disturbances. As a result, it is possible to consider them separately. In this way, the multi-input multi-output system is simplified into two single-input single-output systems. Specifically, we separate the system into a battery side converter with constant external current and an ultracapacitor side converter with exogenous persistent disturbance.

The controller for the battery side converter can actually be solved with classic passivity-based control method. While the problem for the ultracapacitor side converter with exogenous persistent disturbance can be regarded as an output regulation problem for a nonlinear system with an exogenous disturbance. Therefore, the aforementioned theories can be applied. In this section, we first present the design of the battery side controller based on passivity-based control, and then elaborate the output regulator design for the ultracapacitor side converter. The simulation results are given and prove the effectiveness of the controllers.

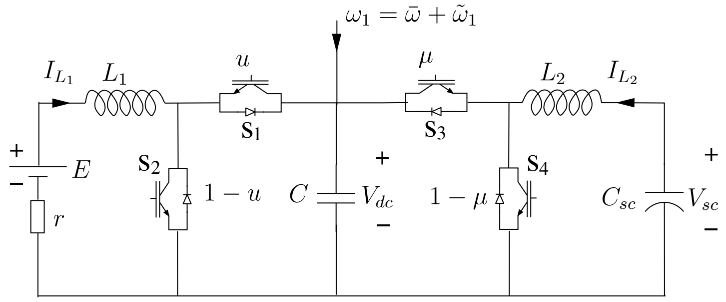

FIGURE 2.7 – Considered topology of the hybrid energy storage system

2.4.1 Battery side converter

The average model of the DC-DC converter can be written with Euler-Lagrange approach as the following form :

$$\begin{aligned} L_1\dot{I}_{L_1} + uV_{dc} + rI_{L_1} &= E \\ C\dot{V}_{dc} - uI_{L_1} &= \bar{\omega} \end{aligned} \tag{2.31}$$

where, I_{L_1} is the current flowing through the inductor L_1, V_{dc} is the output capacitor voltage, r is the battery inner resistor and u is the duty cycle of control input signal for the switch.

For classical boost circuit topology, direct output voltage control is not feasible since the zero dynamics of the system corresponding to the output voltage is unstable. The voltage regulation is therefore implemented through indirect current control [OPNSR98]. Fortunately, for the topology shown in Figure 2.7, the zero dynamic analysis associated to the output voltage is stable under certain conditions, and thus it is possible to directly control the output voltage, i.e., the DC bus voltage. Combine equation (2.31) by eliminating I_{L_1}, one may get the following input-output differential equation :

$$C\ddot{V}_{dc} - [-\frac{1}{u}(\dot{u} - u\frac{r}{L_1})(\bar{\omega} - C\dot{V}_{dc}) + u\frac{E}{L_1} - u^2\frac{V_{dc}}{L_1}] = \dot{\bar{\omega}} \tag{2.32}$$

Let $\ddot{V}_{dc} = \dot{V}_{dc} = 0$ to obtain the zero dynamic at the desired equilibrium point $V_{dc} = V_{dc}^*$:

$$\dot{u} = -\frac{u}{L_1\bar{\omega}}[u^2V_{dc}^* - uE - (r\bar{\omega} + L_1\dot{\bar{\omega}})] \tag{2.33}$$

The equilibrium points for the above zero dynamics expression are :

$$u = 0 \quad ; \quad u = \frac{1}{2V_{dc}^*}\left[E \pm \sqrt{E^2 + 4V_{dc}^*(r\bar{\omega} + L_1\dot{\bar{\omega}})}\right]$$

Among them, $u = \frac{1}{2V_{dc}^*}\left[E + \sqrt{E^2 + 4V_{dc}^*(r\bar{\omega} + L_1\dot{\bar{\omega}})}\right]$ is the only point which has physical significance. As long as the stability of this equilibrium point is guaranteed, the voltage regulation can be achieved through direct control. A phase-plane diagram of equation (2.33) is drawn in Figure 2.8.

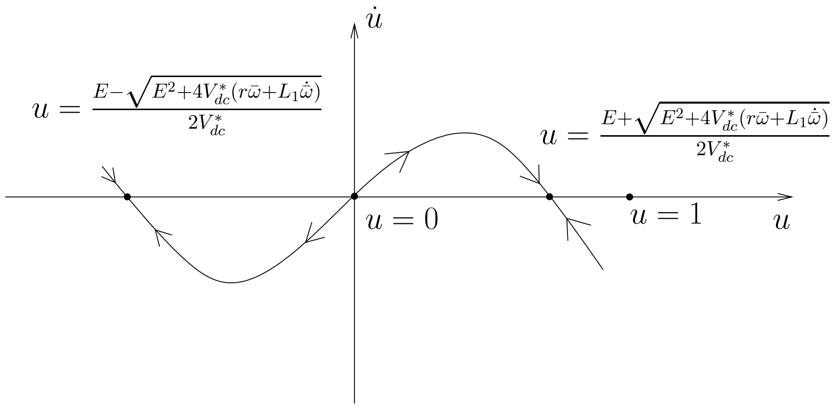

FIGURE 2.8 – Zero dynamic corresponding to the output voltage

As the arrows illustrate in the figure, while $\dot{u} < 0$, u decreases ; while $\dot{u} > 0$, u increases. Hence, the equilibrium point is locally stable. However, this phase-plane is true only under one condition, that is, the denominator of equation (2.33) remains positive. It can be seen that the denominator does not affect the value of the equilibrium points, but only affects the "dynamic process". So it is reasonable to add a positive parameter b ($b > 0$) in the denominator to avoid it being zero or negative. Thus, a direct output voltage regulation can be applied.

2.4.1.1 Passivity based control law

Rewrite the average model (2.31) as the following matrix form :

$$\mathcal{D}\dot{x} + \mathcal{J}(u)x + \mathcal{R}x = \mathcal{E} \tag{2.34}$$

$$\mathcal{D} = \begin{pmatrix} L_1 & 0 \\ 0 & C \end{pmatrix} ; \mathcal{J}(u) = \begin{pmatrix} 0 & u \\ -u & 0 \end{pmatrix} ; \mathcal{R} = \begin{pmatrix} r & 0 \\ 0 & 0 \end{pmatrix} ;$$

$$x = \begin{pmatrix} I_{L_1} \\ V_c \end{pmatrix} ; \mathcal{E} = \begin{pmatrix} E \\ \bar{\omega} \end{pmatrix}$$

The controller can be deduced from a copy of the system with additional damping [OvdSME02] :

$$\mathcal{D}\dot{x}_d + \mathcal{J}(u)x_d + \mathcal{R}x_d = \mathcal{E} + \mathcal{R}_1\tilde{x} \tag{2.35}$$

where, $\mathcal{R}_1 = diag\{0, \rho\}$ is the damping injection term, $\rho > 0$, and x_d is an auxiliary vector corresponding to a "desired" value for x, and $\tilde{x} = x - x_d$ is the error between the state variable and the desired value. The idea is to have the error dynamics :

$$\mathcal{D}\dot{\tilde{x}} + \mathcal{J}(u)\tilde{x} + \mathcal{R}_d\tilde{x} = 0 \tag{2.36}$$

with $\mathcal{R}_d = \mathcal{R} + \mathcal{R}_1 = diag\{r, \rho\}$ be exponentially convergent, i.e., $\tilde{x} \to 0$, with the desired storage function :

$$H_d(\tilde{x}) = \frac{1}{2}L_1\tilde{x_1}^2 + \frac{1}{2}C\tilde{x_2}^2 = \frac{1}{2}\tilde{x}^T\mathcal{D}\tilde{x} \tag{2.37}$$

Set $x_{2d} = V_{dc}^*$ and after some algebraic operations, one may find the following control algorithm :

$$\dot{u} = u\frac{-V_{dc}^* u^2 + Eu + r\mathcal{M} + L_1[\frac{\rho}{C}(\bar{\omega} + ux_1) + \dot{\bar{\omega}}]}{L_1\mathcal{M}} \tag{2.38}$$

where, $\mathcal{M} = a_1(x_2 - V_{dc}^*) + \bar{\omega}$.

In order to guarantee the stability of the controller, as explained in the previous section, a positive parameter b is added in the denominator to avoid being divided by zero or a negative value, which yields the following controller :

$$\dot{u} = u\frac{-V_{dc}^* u^2 + Eu + r\mathcal{M} + L_1[\frac{\rho}{C}(\bar{\omega} + ux_1) + \dot{\bar{\omega}}]}{b + L_1\mathcal{M}} \tag{2.39}$$

where, $\bar{\omega}$ is considered as the constant part of the external current, and thus $\dot{\bar{\omega}} = 0$.

2.4.1.2 Stability analysis

To verify the system stability analysis, choose the closed-loop storage function (2.37) as Lyapunov function, and its derivative is :

$$\dot{H}_d(\tilde{x}) = \tilde{x}\mathcal{D}\dot{\tilde{x}} = \tilde{x}(-\mathcal{J}(u)\tilde{x} - \mathcal{R}_d\tilde{x}) = -\tilde{x}\mathcal{R}_d\tilde{x} \tag{2.40}$$

It can be seen that $H_d(\tilde{x}) > 0$ and $\dot{H}_d(\tilde{x}) < 0$ for $\forall x \neq x_d$, and $H_d = \dot{H}_d = 0$ only for $x = x_d$. Consequently, the closed-loop system is Lyapunov asymptotically stable.

2.4.2 Ultracapacitor side converter

The role of the ultracapacitor sider converter can be described as an “active damping". The control objective of this converter is to absorb the persistent disturbance. For sake of simplicity, we consider only a main harmonic component of the disturbance with frequency ω_0. Thus, the exogenous current disturbance can be written as :

$$\begin{pmatrix} \dot{\omega}_1 \\ \dot{\omega}_2 \end{pmatrix} = \begin{pmatrix} 0 & -\omega_0 \\ \omega_0 & 0 \end{pmatrix} \begin{pmatrix} \omega_1 \\ \omega_2 \end{pmatrix} \tag{2.41}$$

where, $\omega \in W \subset \mathbb{R}^2$.

The average model of the converter can be written as state space representation :

$$C\dot{V}_{dc} = \omega_1 + \mu I_{L_2} \tag{2.42a}$$
$$L_2\dot{I}_{L_2} = V_{sc} - \mu V_{dc} \tag{2.42b}$$
$$C_{sc}\dot{V}_{sc} = -I_{L_2} \tag{2.42c}$$

where, V_{sc} is the ultracapacitor voltage and μ is the duty cycle of control input signal for the switch. The control objective is to maintain V_{dc} as a constant, this is equivalent to : $\mu I_{L_2} = -\omega_1$. However, this simple expression cannot be directly taken as a control objective since there exists the product of the system input and a state variable. Hence, it is necessary to develop an expression which does not contain the control input and may also express the control objective.

Multiply I_{L_2} at both sides of (2.42b), substitute with (2.42a) and (2.42c) and after some manipulations, one may get, at steady states :

$$L_2 I_{L_2} \dot{I}_{L_2} + C_{sc} V_{sc} \dot{V}_{sc} = \omega_1 V_{dc}^* \tag{2.43}$$

This is equivalent to :

$$\frac{d}{dt}(\frac{1}{2} L_2 I_{L_2}^2) + \frac{d}{dt}(\frac{1}{2} C_{sc} V_{sc}^2) = \frac{d}{dt}(\frac{\omega_2}{\omega_0}) V_{dc}^* \tag{2.44}$$

Consequently,

$$\frac{1}{2} L_2 I_{L_2}^2 + \frac{1}{2} C_{sc} V_{sc}^2 = \frac{\omega_2}{\omega_0} V_{dc}^* + a \tag{2.45}$$

where, a is a constant and $a = \frac{1}{2} C_{sc} \bar{V}_{sc}^2$ ($\bar{V}_{sc}$ is the initial voltage of the ultracapacitor, and this will be given a physical explanation below). Thus, the control objective can be achieved through regulating the error output :

$$e = h(x) = \left(\frac{1}{2} L_2 I_{L_2}^2 + \frac{1}{2} C_{sc} V_{sc}^2\right) - \left(\frac{\omega_2}{\omega_0} V_{dc}^* + \frac{1}{2} C_{sc} \bar{V}_{sc}^2\right) \tag{2.46}$$

Equation (2.45) may also be directly deduced from energy conservation point of view. The "kinetic energy" stored in the inductor is $\frac{1}{2} L_2 I_{L_2}^2$, while the "potential energy" stored in the ultracapacitor is $\frac{1}{2} C_{sc} V_{sc}^2$. Thus, the total energy stored in the converter is the sum of the "kinetic energy" and the "potential energy". On the other side, the disturbance energy which needs to be absorbed is $\int_0^t V_{dc}^* \omega_1(t) dt$. Consider that the control objective is to absorb the disturbance by the converter, in other words, the energy stored in the converter should be equal to the disturbance energy, which is corresponding to equation (2.45). Then, the constant a can be understood as the initial energy stored in the ultracapacitor.

So far, we have known the plant (2.42), error output (2.46), and the exosystem (2.41). The next step is to find an error output regulator which asymptotically drives the system to the desired manifold where the error converges to zero.

2.4.2.1 Desired manifold

We represent the states on the desired manifold as $\pi(\omega) = [V_{dc}^* \ I_{L_2}^* \ V_{sc}^*]^\top$, and the path which drives the plant to the manifold as $c(\omega) = \mu^*$. These variables are functions of ω, and thus the trajectory of them is not a point, but actually a limit cycle.

Set $e = 0$ in equation (2.46) to get the expression of $I_{L_2}^*$ and V_{sc}^* :

$$\frac{1}{2} L_2 {I_{L_2}^*}^2 + \frac{1}{2} C_{sc} {V_{sc}^*}^2 = \frac{\omega_2}{\omega_0} V_{dc}^* + \frac{1}{2} C_{sc} \bar{V}_{sc}^2 \tag{2.47}$$

Consider the general case when the amplitude of the harmonic disturbance is not extremely large, then the right side of equation (2.47) remains non-negative. This requires that the disturbance ω satisfies :

$$\frac{\omega_2}{\omega_0} \geq -\frac{C_{sc} \bar{V_{sc}}^2}{2 V_{dc}^*}$$

Then equation (2.47) is actually an expression of ellipses, which indicates that the trajectory of $I_{L_2}^*$ and V_{sc}^* forms a limit cycle at steady states. Rewrite it in standard ellipse form :

$$\begin{pmatrix} I_{L_2}^* & V_{sc}^* \end{pmatrix} \mathbf{M} \begin{pmatrix} I_{L_2}^* \\ V_{sc}^* \end{pmatrix} = 1 \tag{2.48}$$

where,

$$\mathbf{M} = \begin{pmatrix} \frac{L_2}{2\frac{\omega_2}{\omega_0}V_{dc}^* + C_{sc}\bar{V}_{sc}^2} & 0 \\ 0 & \frac{C_{sc}}{2\frac{\omega_2}{\omega_0}V_{dc}^* + C_{sc}\bar{V}_{sc}^2} \end{pmatrix}$$

Notice that equation (2.48) describes not a static ellipse but a dynamic one, a dynamic ellipse formed by the movement of two vectors. To be more specific, the two vectors ($I_{L_2}^*$ and V_{sc}^*) move respectively along their axis, and the trajectory of the composite vector forms an ellipse. Thus, the trajectory of V_{sc}^* can be written in the following form :

$$V_{sc}^* = \left(\frac{C_{sc}}{2\frac{\omega_2}{\omega_0}V_{dc}^* + C_{sc}\bar{V}_{sc}^2}\right)^{-\frac{1}{2}} = \bar{V}_{sc}(\underbrace{2\frac{\omega_2}{\omega_0}\frac{V_{dc}^*}{C_{sc}\bar{V}_{sc}^2}}_{2y(\omega)} + 1)^{\frac{1}{2}} \tag{2.49}$$

From physical significance, it can be seen that $2y(\omega)$ is a sinusoidal signal and its amplitude

$$|2y(\omega)| < 1.$$

Thereby, it is possible to use the binominal series [1] to expand the expression (2.49) as a power series. The sum of the first 3 terms of the binomial series is :

$$(2y(\omega) + 1)^{\frac{1}{2}} \approx 1 + y(\omega) - \frac{1}{2}y(\omega)^2 \tag{2.50}$$

Then, one may get the reference of ultracapacitor voltage as follow :

$$V_{sc}^* = \pi_1(\omega) \approx \bar{V}_{sc}(1 + y(\omega) - \frac{1}{2}y(\omega)^2) \tag{2.51}$$

Thus, the trajectory of $I_{L_2}*$ is obtained by substituting (2.51) into (2.42c) :

$$I_{L_2}* = \pi_2(\omega) = -C_{sc}\dot{V}_{sc}^* \tag{2.52}$$

The desired trajectory of the control input μ^* is also a function of ω, and may be deduced from equation (2.42) :

$$\mu^* = \frac{V_{sc}^*}{V_{dc}^*} + L_2 C_{sc}\frac{\ddot{V}_{sc}^*}{V_{dc}^*} \tag{2.53}$$

Substitute equations (2.51) into (2.53) :

$$\mu^* = c(\omega) = \bar{\mu} + a_1\omega_1 + a_2\omega_2 + a_3\omega_1\omega_2 + a_4\omega_1^2 + a_5\omega_2^2 \tag{2.54}$$

1. The binomial series is explicitly written as :

$$(1 + x)^p = \sum_{n=0}^{\infty} \binom{p}{n} x^n = 1 + px + \frac{p(p-1)}{2!}x^2 + \cdots$$

where, $\binom{p}{n} = \frac{p!}{n!(p-n)!}$. When $|x| < 1$, the series converges absolutely for any complex number p.

with constants $\bar{\mu}, a_i (i = 1, 2 \cdots 5)$

$$\begin{aligned}
\bar{\mu} &= \bar{V}_{sc}/V_{dc}^* \\
a_1 &= 0 \\
a_2 &= \tfrac{1}{V_{sc}}(\tfrac{1}{\omega_0 C_{sc}} - L_2\omega_0) \\
a_3 &= 0 \\
a_4 &= -L_2\tfrac{V_{dc}^*}{C_{sc}V_{sc}^3} \\
a_5 &= -\tfrac{V_{dc}^*}{C_{sc}V_{sc}^3}(\tfrac{1}{2\omega_0^2 C_{sc}} - L_2)
\end{aligned}$$

2.4.2.2 Internal model design

As shown in the control structure (Figure 2.6), at ideal steady state ($e = 0$), the internal model is to generate the control input driving the plate to generate the desired response. Based on proposition 2.3.3, we may calculate :

$$\begin{aligned}
\xi_1 &= c(\omega) \\
&= a_0 + a_1\omega_1 + a_2\omega_2 + a_3\omega_1\omega_2 + a_4\omega_1^2 + a_5\omega_2^2 \\
\xi_2 &= \mathcal{L}_s c(\omega) \\
&= -\omega_0[a_1\omega_2 - a_2\omega_1 - a_3\omega_1^2 + a_3\omega_2^2 + 2(a_4 - a_5)\omega_1\omega_2] \\
\xi_3 &= \mathcal{L}_s^2 c(\omega) \\
&= -\omega_0^2[a_1\omega_1 + a_2\omega_2 + 2(a_4 - a_5)\omega_1^2 - 2(a_4 - a_5)\omega_2^2 + 4a_3\omega_1\omega_2] \\
\xi_4 &= \mathcal{L}_s^3 c(\omega) \\
&= \omega_0^3[a_1\omega_2 - a_2\omega_1 - 4a_3\omega_1^2 + 4a_3\omega_2^2 + 8(a_4 - a_5)\omega_1\omega_2] \\
\xi_5 &= \mathcal{L}_s^4 c(\omega) \\
&= \omega_0^4[a_1\omega_1 + a_2\omega_2 + 8(a_4 - a_5)\omega_1^2 - 8(a_4 - a_5)\omega_2^2 + 16a_3\omega_1\omega_2] \\
\xi_6 &= \mathcal{L}_s^5 c(\omega) \\
&= -\omega_0^5[a_1\omega_2 - a_2\omega_1 - 16a_3\omega_1^2 + 16a_3\omega_2^2 + 32(a_4 - a_5)\omega_1\omega_2]
\end{aligned}$$

After some iterative computation, it can be deduced that :

$$\mathcal{L}_s^5 c(\omega) = -4\omega_0^4\mathcal{L}_s c(\omega) - 5\omega_0^2\mathcal{L}_s^3 c(\omega) \tag{2.55}$$

As a result, the autonomous system $\{W, s, c\}$ is immersed into a five-dimension linear system :

$$\begin{aligned}
\dot{\xi} &= \Phi\xi = \begin{pmatrix} 0 & 1 & 0 & 0 & 0 \\ 0 & 0 & 1 & 0 & 0 \\ 0 & 0 & 0 & 1 & 0 \\ 0 & 0 & 0 & 0 & 1 \\ 0 & -4\omega_0^4 & 0 & -5\omega_0^2 & 0 \end{pmatrix}\xi \\
\mu^* &= \Upsilon\xi = \begin{pmatrix} 1 & 0 & 0 & 0 & 0 \end{pmatrix}\xi
\end{aligned} \tag{2.56}$$

through the immersion mapping :

$$\tau(\omega) = \begin{pmatrix} c(\omega) \\ \mathcal{L}_s c(\omega) \\ \mathcal{L}_s^2 c(\omega) \\ \mathcal{L}_s^3 c(\omega) \\ \mathcal{L}_s^4 c(\omega) \end{pmatrix}$$

This is to say that the mapping $c(\omega)$ (2.54) is equivalent to the linear system (2.56) via mapping $\tau(\omega)$. So we have found the matrices Φ and Υ in the internal model in Figure 2.6.

2.4.2.3 Stabilizer controller design

As shown in the control structure (Figure 2.6), the stabilizer controller is used to stabilize the interconnection of the internal model and the plant. The linear controllers allow to exam the local stability via eigenvalues of matrices. We study the operating point $(V_{dc} = V_{dc}^*, I_{L_2} = 0, V_{sc} = \bar{V}_{sc})$ and set matrices :

$$\begin{aligned} A &= \left[\frac{\partial f}{\partial x}\right]_{(V_{dc}^*;0;\bar{V}_{sc})} = \begin{pmatrix} 0 & \frac{\bar{\mu}}{C} & 0 \\ -\frac{\bar{\mu}}{L_2} & 0 & \frac{1}{L_2} \\ 0 & -\frac{1}{C_{sc}} & 0 \end{pmatrix} \\ B &= \left[\frac{\partial f}{\partial \mu}\right]_{(V_{dc}^*;0;\bar{V}_{sc})} = \begin{pmatrix} 0 & -\frac{V_{dc}^*}{L_2} & 0 \end{pmatrix}^\top \\ C &= \left[\frac{\partial h}{\partial x}\right]_{(V_{dc}^*;0;\bar{V}_{sc})} = \begin{pmatrix} 0 & 0 & C_{sc}\bar{V}_{sc} \end{pmatrix} \end{aligned}$$

The whole system is exponentially stable if the matrix (2.24) which characterizes the closed-loop system has all eigenvalues with negative real part. Based on this principle, parameters K, L, M and matrix N can be found with the help of linear matrix inequality (LMI) program.

We first search for a matrix N such that the matrix :

$$\tilde{A} = \begin{pmatrix} A & B\Upsilon \\ NC & \Phi \end{pmatrix}$$

is stable.

This is equivalent to require :

$$\begin{aligned} X^\top &= X > 0 \\ \tilde{A}^\top X + X\tilde{A} &< 0 \end{aligned} \tag{2.57}$$

This can be written as :

$$\begin{aligned} (I \quad \tilde{A}^\top) \begin{pmatrix} 0 & X \\ X & 0 \end{pmatrix} \begin{pmatrix} I \\ \tilde{A} \end{pmatrix} &< 0 \\ (I \quad -I)(-X \quad X) \begin{pmatrix} I \\ -I \end{pmatrix} &= -2X < 0 \end{aligned} \tag{2.58}$$

Calling upon the lemma of simplification of matrices. The inequalities are equivalent to :

$$\begin{aligned} \begin{pmatrix} 0 & X \\ X & 0 \end{pmatrix} + sym\left\{ \begin{pmatrix} \tilde{A}^\top \\ -I \end{pmatrix} G(I\ I) \right\} &< 0 \\ X &> 0 \end{aligned} \tag{2.59}$$

The first inequality can be explicitly written as :

$$\begin{pmatrix} 0 & X \\ X & 0 \end{pmatrix} + \begin{pmatrix} \tilde{A}^\top G + G^\top \tilde{A} & \tilde{A}^\top G - G^\top \\ G^\top \tilde{A} - G & -G - G^\top \end{pmatrix} < 0 \tag{2.60}$$

Notice that

$$\tilde{A}^\top = \underbrace{\begin{pmatrix} A^\top & 0 \\ \Upsilon^\top B^\top & \Phi^\top \end{pmatrix}}_{\bar{A}^\top} + \underbrace{\begin{pmatrix} C^\top & 0 \\ 0 & 0 \end{pmatrix}}_{\bar{C}^\top} \underbrace{\begin{pmatrix} 0 & N^\top \\ 0 & 0 \end{pmatrix}}_{\bar{K}^\top}$$

We take

$$G = \begin{pmatrix} G_1 & G_2 \\ G_3 & G_4 \end{pmatrix}$$

and impose $G_3 = 0$, $Z = N^\top G_4$, and $X = \begin{pmatrix} X_1 & X_3 \\ X_3^\top & X_2 \end{pmatrix}$. Thus, the inequality becomes :

$$\begin{gathered} \begin{pmatrix} 0 & 0 & X_1 & X_3 \\ 0 & 0 & X_3^\top & X_2 \\ X_1 & X_3^\top & 0 & 0 \\ X_3 & X_2 & 0 & 0 \end{pmatrix} + \left(\begin{matrix} G_1^\top A + A^\top G_1 & A^\top G_2 + C^\top Z + G_1^\top B\Upsilon \\ \Upsilon^\top B^\top G_1 + G_2^\top A + Z^\top C & G_2^\top B\Upsilon + G_4^\top \Phi + \Phi^\top G_4 + \Upsilon^\top B^\top G_2 \\ G_1^\top A - G_1 & G_1^\top B\Upsilon - G_2 \\ G_2^\top A + Z^\top C & G_2^\top B\Upsilon + G_4^\top \Phi - G_4 \end{matrix} \right. \\ \left. \begin{matrix} A^\top G_1 - G_1^\top & A^\top G_2 + C^\top Z \\ \Upsilon^\top B G_1 - G_2 \top & \Upsilon^\top B^\top G_2 + \Phi^\top G_4 - G_4^\top \\ -G_1 - G_1^\top & -G_2 \\ -G_2^\top & -G_4 - G_4^\top \end{matrix} \right) < 0 \end{gathered} \tag{2.61}$$

Solving the equalities with program in MATLAB gives the matrix N. Likewise, the parameters K, L, M can be found to make the closed-loop matrix (2.24) be stable. For instance, for the given system parameters : L_1=2.5mH L_2=2.5mH C=440μF C_{sc}=3.25F V_{dc}^*=600V $\bar{V}_{sc}$=100V

We may find the following controller parameters :

$$\begin{aligned} K &= -0.5; \\ M &= 190433/2112; \\ L &= 1/72360000; \\ N &= \begin{pmatrix} 0 & 0 & 0 & 0.001 & 0 \end{pmatrix}^\top . \end{aligned}$$

Calculating the eigenvalues of matrix (2.24) gives $eig = \{\pm 94.24i, \pm 47.12i, -0.13 \pm 18.32i, 0, 0\}$.

2.4.3 Simulation and results

Now that we have considered the Battery side converter and the ultracapacitor side converter separately and designed the controller for each side respectively, we need to combine them together so as to further verify the control performance. The combined system are tested under MATLAB/Simulink environment. Simulation runs with the hybrid DC source model shown in Figure 2.7. Set the initial voltage of the supercapaciter as $\bar{V}_{sc} = 100V$ and the nominal DC voltage is given as $V_{dc}^{*} = 600V$. The external current is set as $I_{ex} = -2 + 5sin(2\pi ft + \frac{\pi}{2})$. The other system parameters are given in the appendix. The PBC is applied to the battery side converter. For the ultracapacitor side converter, in order to clearly observe the effect of the regulator, an open loop control input $\mu = 1/6$ is first applied. Then, at time $t = 5s$, the output regulator is switched in to obtain a contrast of the system responses under different controllers.

As shown in Figure 2.9, the simulation results are rather satisfying. As long as the error output regulator is added, the oscillations in I_{L1} and V_{dc} attenuate remarkably. On the other side, the oscillation is absorbed by the supercapaciter, which leads to an increase of the amplitude of I_{L_2} and V_{sc}. The error output signal is presented in Figure 2.10. It can be seen that at time $t = 5s$, the error output signal tends to converge to zero. The control inputs are given in Figure 2.11. It can be seen from the figure that when $t > 5s$, the control input for the ultracapacitor side converter is a sinusoidal signal. In Figure 2.12, the trajectory of states of each converter is given respectively. It can be seen that the trajectory of the ultracapacitor side converter forms a desired limit cycle, while the the trajectory of the battery side converter converges to a desired equilibrium point. It has also been verified that the output regulator is robust with respect to the system parameters.

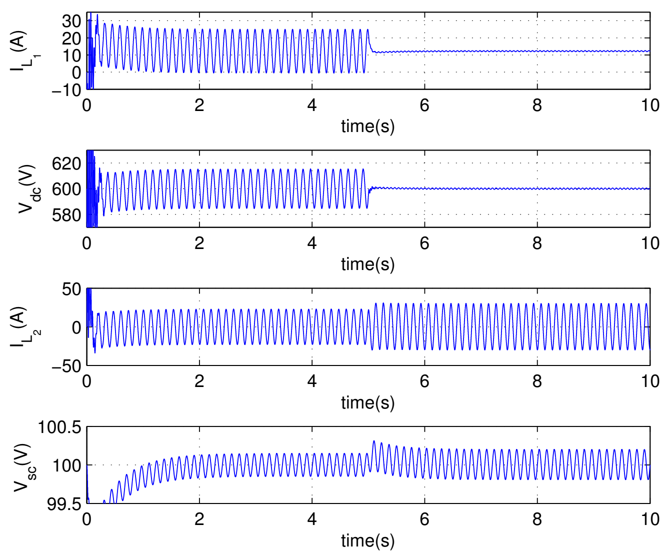

FIGURE 2.9 – Simulation results

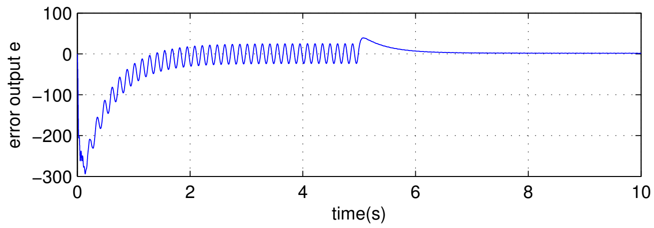

FIGURE 2.10 – Error output of the ultracapacitor side converter

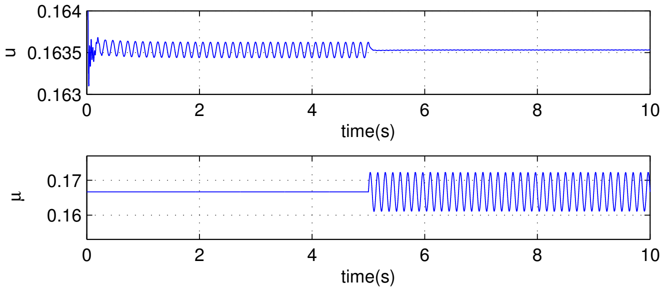

FIGURE 2.11 – Duty cycles of the control signals of the converters

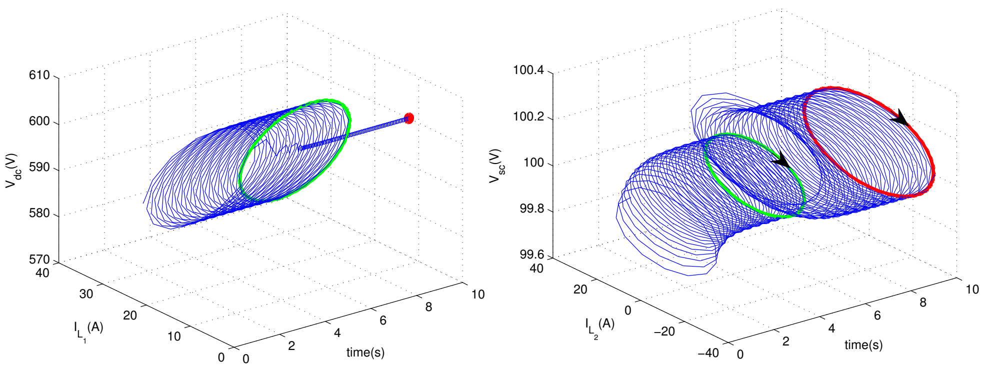

FIGURE 2.12 – Trajectory evolution for battery side converter (left : from a large closed trajectory to a desired equilibrium point) and trajectory evolution for ultracapacitor side converter (right : from a small closed trajectory to a desired limit cycle)

2.5 Conclusions

In this chapter, we have analyzed the battery/ultracapacitor hybrid energy storage system in hybrid electric vehicles. In previous studies, the PMSM is controlled to compensate the torque ripples generated by the internal combustion engine. During this process, the influence to the hybrid energy storage system is concerned as exogenous current disturbances. In order to reject the disturbances, we attempt to apply an output regulation theory. The output regulation theory for nonlinear systems is extended from the theories for linear systems. We have summarized the main results of the related theories and applied to solve our problem. The disturbance rejection task is assigned to the ultracapacitor, and the battery is expected to maintain the DC voltage. Therefore, a classical passivity-based controller is designed for the battery side converter, while the ultracapacitor side converter is developed based on the elaborated output regulation theory. The simulation results have shown the effectiveness of the controllers. However, there still exist some drawbacks of the control algorithms. First of all, due to the limit of the control method, we have only take the sinusoidal disturbance into consideration. The control stabilizer is not easy to apply in the case of transient disturbance. Besides, in the theoretical analysis, the system reaches a local critical stability, because there are eigenvalues of the closed-loop characterized matrix on the imaginary axis. This is not ideal in reality. Furthermore, we solve the problem by separating the battery side and the ultracapacitor side converters and considering them independently. This is actually based on the assumption that the battery alone is able to supply a constant DC voltage. However, this is not always the case. Moreover, in our system model, we consider the ultracapacitor as an ideal capacitor without considering the losses, which is not comprehensive neither. Consequently, in the next chapter, we will consider the paralleled battery/ultracapacitor system as a whole and take the self-discharge of the ultracapacitor into consideration, and we will develop controllers for the disturbed system with another advanced control strategy.

Chapitre 3

Hybrid battery/ultracapacitor control structure design

Sommaire

3.1 Introduction

In the last chapter, we have summarized the control objective of the hybrid energy storage system. The main target is to control the ultracapacitor to absorb the current disturbances in the DC bus introduced in the process of torque ripples compensation. This is equivalent to design an "active damping" which attenuates the amplitude of oscillations. Based on this idea, we have considered the ultracapacitor side converter separately and considered the external current as an exogenous signal generated by an exosystem. We have solved the problem via a designed error output feedback regulator. The error output regulation theories for linear and nonlinear and PCH systems as well have been reviewed in the last chapter. However, due to some drawbacks of the control method, it is not advantageous to apply the designed controller in the reality.

In this chapter, we take the whole hybrid energy storage system into consideration and analyze the rate of motion of different variables and design a cascade control structure. The whole system is therefore a four-dimensional nonlinear PCH system. We will review in the following sections the classical PCH models and divide the models into control-affine and control-nonaffine PCH systems. Moreover, we will review the most prevailing control method for PCH system, that is interconnection and damping assignment passivity based control. The control method aims to preserve the Hamiltonian form of the system and requires the system designer to redesign the interconnection matrix and damping matrix, and meanwhile preserve the system passivity. Finding such a controller for control-affine PCH systems is relatively simple. Usually, it is enough to solve some analytical equations. However, the problem for control-nonaffine PCH systems is much more complex, usually we need to solve several partial differential equations. The problem gets more complex when the system order increases and the number of partial differential equations increases.

Our studied system is identified as a control-nonaffine PCH system. Due to the complexity and difficulty of solving such a problem with traditional method that solves partial differential equations, we attempt to transform the system into a degenerated system where the system order is less than the original one. This is based on the singular perturbation theory (Kokotovic 1986, Khalil 1996). And thus, the system is separated into a fast system and a slow system. On the other hand, our control objective is to maintain a constant voltage in the DC bus and absorb the exogenous perturbed current by the ultracapacitor while maintaining its voltage oscillating around a given value. We may first consider the system without the exogenous current and define the solution as a static solution, and then we consider the perturbed system and define the solution as a dynamic solution. Then, the essence of our control method is, through a cascade control structure, to drive the slow system to the static solution and impose the fast system converge to the dynamic solution. The simulation results will be presented at the end of the chapter to verify the effectiveness of the control algorithm.

3.2 System Modeling

Herein, we take the system losses and the ultracapacitor inner resistor into consideration. The new system model is given in Figure 3.1.

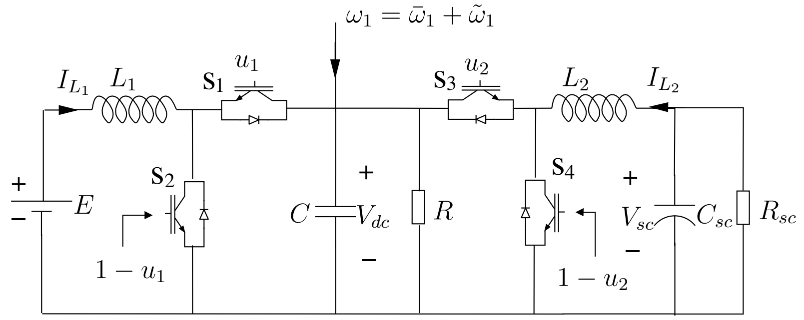

FIGURE 3.1 – Topology of electrical DC part

3.2.1 Average model

From Kirchoff's law, the average model of the power converters can be written as the following form :

$$\begin{cases} L_1 \dot{I}_{L_1} = E - u_1 V_{dc} \\ L_2 \dot{I}_{L_2} = V_{sc} - u_2 V_{dc} \\ C\dot{V}_{dc} = I_{ex} - \dfrac{V_{dc}}{R} + u_1 I_{L_1} + u_2 I_{L_2} \\ C_{sc}\dot{V}_{sc} = -I_{L_2} - \dfrac{V_{sc}}{R_{sc}} \end{cases} \tag{3.1}$$

where, I_{L_1} and I_{L_2} are respectively the currents going through the inductors L_1 and L_2 ; V_{dc} is the DC bus voltage and V_{sc} is the supercapacitor voltage. $u_1, u_2 \in [0, 1]$ are the duty cycles of the control input signals for switches S1 and S3 respectively. S1 and S2 are complementary switches, S3 and S4 are likewise. The resistor R_{sc} is introduced to represent the self-discharging in the ultracapacitor, and the resistor R is introduced to represent the rest total loss in the circuit. $I_{ex} = \omega_1$ is the exogenous current.

By defining $x = \begin{bmatrix} L_1 I_{L_1} & L_2 I_{L_2} & CV_{dc} & C_{sc}V_{sc} \end{bmatrix}^\top$, the average model can be rewritten in the following form :

$$\dot{x}_1 = E - u_1 \frac{x_3}{C} \tag{3.2a}$$

$$\dot{x}_2 = -u_2 \frac{x_3}{C} + \frac{x_4}{C_{sc}} \tag{3.2b}$$

$$\dot{x}_3 = \omega_1 - \frac{x_3}{RC} + u_1 \frac{x_1}{L_1} + u_2 \frac{x_2}{L_2} \tag{3.2c}$$

$$\dot{x}_4 = -\frac{x_2}{L_2} - \frac{x_4}{R_{sc}C_{sc}} \tag{3.2d}$$

3.2.2 Hamiltonian modeling

As a matter of fact, Hamiltonian modeling is mainly applied in mechanical systems [OPNSR98]. In electrical domain, Hamiltonian modeling cannot cover all electrical systems, but can be extended to power electronic circuits, and build a port-controlled Hamiltonian (PCH) model. Each electrical element in the circuit is considered as an electrical port. The current through the port is represented as a flow f, and the voltage as an effort e correspondingly. In a RLC circuit,the flow f_r and the effort e_r for a resistor is given by $e_r = Rf_r$. The flow f_l and the effort e_l for a inductor is given by $f_l = \phi_l/L; e_l = \dot{\phi}_l$ (ϕ_l is the flux). The flow f_c and the effort e_c for a capacitor is given by $f_c = \dot{q}_c; e_c = \dot{q}_c/C$ (q_c is the charge). Thus, the magnetic energy in an inductor is identified as $\mathcal{V} = \phi_l/2L$, and the electric energy in a capacitor is then $\mathcal{T} = q_c^2/2C$. The Hamiltonian refers to the total energy of the system. Thus, in a LC circuit, the Hamiltonian is the sum the electric energy and the magnetic energy $\mathcal{H} = \mathcal{V} + \mathcal{T} = \phi_l^2/2L + q_c^2/2C$, and thus is a quadratic function.

The Hamiltonian modeling approach considers the energy conserving LC network and writes the relation between the LC ports and other ports in the circuit. Consider our electric power system shown in Figure 3.1, the Hamiltonian is the total energy of the LC network :

$$\mathcal{H} = \mathcal{V} + \mathcal{T} = \frac{1}{2L_1}\phi_{L_l}^2 + \frac{1}{2L_2}\phi_{L_2}^2 + \frac{1}{2C}q_C^2 + \frac{1}{2C_{sc}}q_{C_{sc}}^2$$

The relation between the LC ports and the other ports can be written as :

$$\begin{aligned}
\begin{pmatrix} \dot{\phi}_{L_l} \\ \dot{\phi}_{L_2} \\ \dot{q}_C \\ \dot{q}_{C_{sc}} \end{pmatrix} &= \begin{pmatrix} 0 & 0 & -1 & 0 \\ 0 & 0 & -1 & 1 \\ 1 & 1 & 0 & 0 \\ 0 & -1 & 0 & 0 \end{pmatrix} \begin{pmatrix} \frac{\phi_{L_l}}{L_1} \\ \frac{\phi_{L_2}}{L_2} \\ \frac{q_C}{C} \\ \frac{q_{C_{sc}}}{C_{sc}} \end{pmatrix} + \begin{pmatrix} E \\ 0 \\ \omega_1 \\ 0 \end{pmatrix} \\
&+ \begin{pmatrix} 0 \\ 0 \\ -1 \\ 0 \end{pmatrix} (-f_{S_1}) + \begin{pmatrix} -1 \\ 0 \\ 0 \\ 0 \end{pmatrix} (-e_{S_3}) + \begin{pmatrix} 0 \\ 0 \\ -1 \\ 0 \end{pmatrix} (-f_R) \\
&+ \begin{pmatrix} 0 \\ 0 \\ -1 \\ 0 \end{pmatrix} (-f_{S_2}) + \begin{pmatrix} 0 \\ -1 \\ 0 \\ 0 \end{pmatrix} (-e_{S_4}) + \begin{pmatrix} 0 \\ 0 \\ 0 \\ -1 \end{pmatrix} (-f_{R_{sc}})
\end{aligned}$$

The flow and the effort variables satisfy the following relations :

$$\begin{aligned}
f_{S_1} &= u_1\frac{\phi_{L_l}}{L_1}; \quad e_{S_3} = u_1\frac{q_C}{C}; \\
f_{S_2} &= u_2\frac{\phi_{L_2}}{L_2}; \quad e_{S_4} = u_2\frac{q_C}{C}; \\
f_R &= \frac{q_C}{CR}; \quad f_{R_{sc}} = \frac{q_{C_{sc}}}{C_{sc}R_{sc}}.
\end{aligned}$$

Setting the state coordinate $x = (\phi_{L_l}\ \phi_{L_2}\ q_C\ q_{C_{sc}})^\top$, then the gradient of the Hamiltonian is :

$$\frac{\partial \mathcal{H}(x)}{\partial x} = \begin{pmatrix} \frac{\phi_{L_l}}{L_1} & \frac{\phi_{L_2}}{L_2} & \frac{q_C}{C} & \frac{q_{C_{sc}}}{C_{sc}} \end{pmatrix}^\top$$

Therefore, the Hamiltonian model of our system can be rewritten in the following form :

$$\dot{x} = [\mathcal{J}(u) - \mathcal{R}]\frac{\partial \mathcal{H}(x)}{\partial x} + g(\omega) \tag{3.3}$$

with

$$\mathcal{J}(u) = \begin{pmatrix} 0 & 0 & -u_1 & 0 \\ 0 & 0 & -u_2 & 1 \\ u_1 & u_2 & 0 & 0 \\ 0 & -1 & 0 & 0 \end{pmatrix} \quad \mathcal{R} = \begin{pmatrix} 0 & 0 & 0 & 0 \\ 0 & 0 & 0 & 0 \\ 0 & 0 & \frac{1}{R} & 0 \\ 0 & 0 & 0 & \frac{1}{R_{sc}} \end{pmatrix}$$

$$g(\omega) = \begin{pmatrix} E & 0 & \omega_1 & 0 \end{pmatrix}^\top$$

$$\mathcal{H}(x) = \frac{1}{2} x^\top Q x \quad ; \quad Q = \begin{pmatrix} \frac{1}{L_1} & 0 & 0 & 0 \\ 0 & \frac{1}{L_2} & 0 & 0 \\ 0 & 0 & \frac{1}{C} & 0 \\ 0 & 0 & 0 & \frac{1}{C_{sc}} \end{pmatrix}$$

where, $\mathcal{J}(u) = -\mathcal{J}(u)^\top$ and $\mathcal{R} = \mathcal{R}^\top \geq 0$. $\mathcal{H}(x)$ is a quadratic function of x. It can be seen that the Hamiltonian model (3.3) is equivalent to the average model (3.2).

3.3 Control strategies

3.3.1 Port-controlled Hamiltonian systems

We remind here the general form of a PCH system [SS99] is represented as :

$$\dot{x} = [\mathcal{J}(x) - \mathcal{R}(x)] \frac{\partial \mathcal{H}(x)}{\partial x} + g(x)u \tag{3.4}$$

where, the state variable $x \in \mathbb{R}^n$, and the input $u \in \mathbb{R}^m (m < n)$. The matrix $\mathcal{J}(x) = -\mathcal{J}(x)^\top$ is skew-symmetric reflecting the interconnections of the system states. The matrix $\mathcal{R}(x) = \mathcal{R}(x)^\top \geq 0$ represents the intrinsic system damping. $\mathcal{H}(x)$ is the total energy of the system. It can be seen that the control input appears linearly with respect to the states. Hence, we may define the system having this form a *control-affine PCH system*. This form is applicable for most mechanical systems. However, for electrical systems, it is not always the case.

It can be seen that in our system (3.3) the control input is included in the matrix $\mathcal{J}(u)$. In other words, the control action has an effect in the interconnection structure. As a matter of fact, this is a common form for switch-included power electric systems where the duty cycles of the PWM driving the switches decide the ratio of the currents (and voltages) before and after the switches [OvdSME02]. Hence, we may call the systems having the following form :

$$\dot{x} = [\mathcal{J}(x, u) - \mathcal{R}(x)] \frac{\partial \mathcal{H}(x)}{\partial x} + g(x, u) \tag{3.5}$$

a *control-nonaffine PCH system*, where the control input is included in the interconnection structure $\mathcal{J}(x, u)$, and $\mathcal{J}(x, u) = -\mathcal{J}(x, u)^\top$. Being different from control-affine PCH system where the control input is excluded from the interconnection structure, the dual relation of the control inputs and the states makes the system more complex. Even so, this form is more general and applicable for more systems. Finding a stable controller for such a system has attracted numerous reserchers in the related domain.

3.3.2 Passivity-based control

A quite powerful technique being applied to design effective and robust controllers for PCH systems is interconnection and damping assignment passivity-based control (IDA-PBC) [OGC04]. It aims to conserve the system passivity through interconnection and damping assignment.

Consider a PCH system (3.4) or (3.5). We suppose that there exist an energy function $\mathcal{H}_d$ and matrices, $\mathcal{J}_d$ ($\mathcal{J}_d = -\mathcal{J}_d^\top$), $\mathcal{R}_d$ ($\mathcal{R}_d = \mathcal{R}_d^\top$), and the control input $u = \beta(x)$ such that the closed-loop system with control input preserves PCH structure and takes the following form :

$$\dot{x} = [\mathcal{J}_d(x) - \mathcal{R}_d(x)] \frac{\partial \mathcal{H}_d(x)}{\partial x} \tag{3.6}$$

where, $\mathcal{H}_d(x)$ is the closed-loop energy having a strict (local) minimum at the desired equilibrium point $x^* \in \mathbb{R}^n$.

Then we have

$$\dot{\mathcal{H}}_d = -\frac{\partial \mathcal{H}_d(x)}{\partial x} \mathcal{R}_d \frac{\partial \mathcal{H}_d(x)}{\partial x} \leq 0 \tag{3.7}$$

We choose $\mathcal{H}_d$ as a Lyapunov function, then we obtain immediately the asymptotic stability of the closed-loop system by calling upon Lasalle's invariance principle.

This concept of IDA-PBC provides an effective approach to find the control input and meanwhile guarantees the system stability. It is relatively easy to find such a controller for a control-affine system (3.4). Generally, we may assign a desired interconnection structure $\mathcal{J}_d(x)$ and inject a damping in the damping matrix $\mathcal{R}_d(x)$. Thus, the control input $\beta(x)$ may be obtained by solving algebraic equation as follow :

$$\beta(x) = \left[g(x)^\top g(x)\right]^{-1} g(x)^\top \left[(\mathcal{J}_d(x) - \mathcal{R}_d) \frac{\partial \mathcal{H}_d(x)}{\partial x} - (\mathcal{J}(x) - \mathcal{R}) \frac{\partial \mathcal{H}(x)}{\partial x}\right] \tag{3.8}$$

However, finding such a controller for a control-nonaffine system (3.5) is much more complex. It is not possible to find $\beta(x)$ via solving algebraic equations. A classical procedure is to set a vector function $K(x)$ [OvdSME02] :

$$K(x) = \frac{\partial \mathcal{H}_a(x)}{\partial x}$$

with $\mathcal{H}_a(x) = \mathcal{H}_d(x) - \mathcal{H}(x)$ and thus from (3.5) and (3.6), we obtain :

$$[\mathcal{J}_d(x, \beta(x)) - \mathcal{R}_d(x)]\, K(x) = -\left[(\mathcal{J}_a(x) - \mathcal{R}_a(x)) \frac{\partial \mathcal{H}(x)}{\partial x}\right] + g(x, \beta(x))$$

where, $\mathcal{J}_a(x) = \mathcal{J}_d(x, \beta(x)) - \mathcal{J}(x)$ and $\mathcal{R}_a = \mathcal{R}_d(x) - \mathcal{R}(x)$.

Referring to the poincare Lemme, $K(x)$ is the gradient of a scalar function if and only if

$$\frac{\partial K}{\partial x}(x) = \left[\frac{\partial K}{\partial x}(x)\right]^\top$$

Thus, we obtain a series of partial differential equations (PDE). Solving these equations provides a way to find the control input. However, it is rather difficult to solve these PDE and to find an analytical solution, especially when the system is a high dimensional system.

Therefore, we propose to simplify our studied system by reducing the system order. This can be achieved through singular perturbation theories [KG02].

3.3.3 Singular perturbation theories

We consider the so-called standard singular perturbation model [KG02] :

$$\begin{aligned} \dot{x} &= f(t, x, z, \varepsilon) \\ \varepsilon \dot{z} &= g(t, x, z, \varepsilon) \end{aligned} \tag{3.9}$$

where, $x \in \mathbb{R}^n$ and $z \in \mathbb{R}^m$. Setting $\varepsilon = 0$ causes a fundamental and abrupt change in the dynamics properties of the system, as the second differential equation degenerates into an algebraic equation :

$$0 = g(t, x, z, 0) \tag{3.10}$$

Thus, the singular perturbation causes a discontinuity in the system solutions. The essence of the singular perturbation method is a multi-time-scale approach that analyses the system in separate time scales. The small positive parameter ε may be a homogeneously small time constant. Thus, the second differential equation tends towards its static solution in a very rapid rate, and the static solution is the solution of the algebraic equation (3.10).

In the solutions of equation (3.10), if there exist $k (k \geq 1)$ real roots :

$$z = h_i(t, x) \quad i = 1, 2, \cdots, k \tag{3.11}$$

then, it is assured that corresponding to each root of (3.10) the original $n + m$ dimensional system can be reduced into a n dimensional system via injecting the roots (3.11) into the first differential equation of (3.9). Thus the reduced model is written as :

$$\dot{x} = f(t, x, h(t, x), 0) \tag{3.12}$$

For each stable root of (3.10), calling upon the Tychonoff's theorem, the solutions of the original system (3.9) approaches the ones of the reduced system (3.12). The reduced model (3.12) is also known as a slow model, in contrast to the second differential equation which converges rapidly to its static solution.

3.4 Controller design

3.4.1 Static and dynamic solutions

We remind here that our control objective is to maintain a constant voltage in the DC bus. This corresponds to a constant x_3 at steady state. On the other hand, we aim to absorb the disturbances by the ultracapacitor and maintain its voltage oscillating around a certain value. We first disregard the current disturbances and consider the case when there is no external disturbance (model (3.2) with $\omega_1 = \bar{\omega}_1$). We define the solutions of this problem as *static solutions*, represented as $\bar{x}$, where, $\bar{x}_3$ and $\bar{x}_4$ are known references which correspond to the desired DC voltage and the ultracapacitor voltage. Moreover we represent the error between the state variables and the static solutions as $\tilde{x}$. By letting $\dot{x} = 0$, we may obtain the static solutions as follows :

$$\begin{aligned} \bar{x}_1 &= \frac{L_1}{E}\left(\frac{\bar{x}_3^2}{RC^2} - \frac{\bar{x}_3}{C}\bar{\omega}_1 + \frac{\bar{x}_4^2}{R_{sc}C_{sc}^2}\right) \\ \bar{x}_2 &= -\frac{L_2}{R_{sc}C_{sc}}\bar{x}_4 \end{aligned} \tag{3.13}$$

The control inputs generate the system response $\bar{x}$ is :

$$\begin{aligned} \bar{u}_1 &= \frac{C}{\bar{x}_3}E \\ \bar{u}_2 &= \frac{C}{C_{sc}}\frac{\bar{x}_4}{\bar{x}_3} \end{aligned} \tag{3.14}$$

Now, we take the external disturbance into consideration. We first consider a typical fixed-frequency sinusoidal disturbance, and then we may extend the design idea and the control method to the general cases where the external perturbed current is either persistent or transient. At steady state, we aim to have a constant DC voltage and a smooth battery current, while absorbing the disturbance by the ultracapacitor side converter. We define the solutions that achieve the control objective as *dynamic solutions* and represent the desired trajectories of state variables as x^*. Now that the perturbed current is a periodical sinusoidal signal, then, this means that we want x_1^* and x_3^* to be constant, whereas x_2^* and x_4^* to form a periodic orbit. In order to achieve a stable orbit, x_2^* and x_4^* are supposed to form a stable limit cycle at steady states. Therefore, let the desired trajectories $x_1^* = \bar{x}_1$, $x_3^* = \bar{x}_3$ and $x_2^* = \bar{x}_2 + \hat{x}_2$, $x_4^* = \bar{x}_4 + \hat{x}_4$, where, $\hat{x}_3$ and $\hat{x}_4$ are limit cycles around zero, which represent the differences between the desired trajectories and the mean values.

Herein, for sake of clarity, we list the foregoing various symbols with their representations as follows :

x	state variables ;
$\bar{x}$	static solutions of the average model, equilibrium point ;
$\tilde{x}$	static errors, $\tilde{x} = x - \bar{x}$;
x^*	dynamic solutions, desired trajectories of state variables ;
$\hat{x}$	limit cycles, $\hat{x} = x^* - \bar{x}$.

If we could drive the system to the equilibrium point and then force it to operate along the desired trajectory, then we could achieve our control objective. There remains two key points to consider : how to force the system to operate as we want and what are the desired trajectories. The first point is achieved through a cascade control structure and will be elaborated in the next section. For the second point, it is easy to find the static solutions where the system alone is not perturbed, it is simply an equilibrium point. When the system is perturbed, we want the desired trajectories (x_3^* and x_4^*) to be periodical signals. We may conceptually identify them as limit cycles, but it is not easy to write it in analytical forms. Therefore, similar with the procedure in the last chapter, we consider from an energy point of view and write an approximation form of the desired trajectories. In the control structure, the desired trajectory is generated from an isolated block named internal model. The algorithm in the internal model will also be presented in the following section.

3.4.2 Cascade control structure

The control idea is based on the decomposition of the system into a slow model and a fast model. The essence is to force an outer slow loop to maintain the system operating around the equilibrium point and impose the dynamic to the system through an inner fast loop, so as to drive the system operating along the desired trajectory. The control structure of the power converters is shown in Figure 3.2.

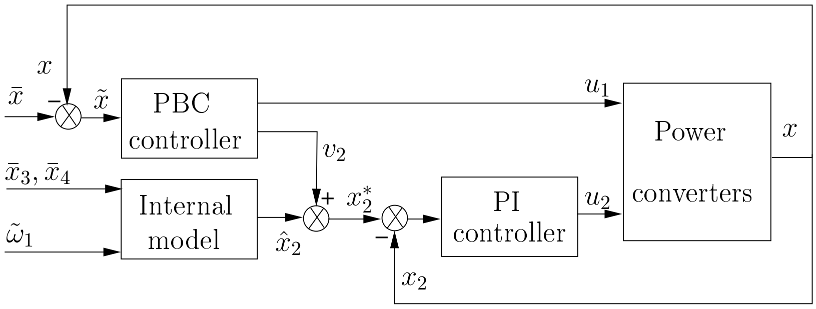

FIGURE 3.2 – Control structure of the power converters

The ultracapacitor side current feedback control (corresponding to x_2 control) is chosen as the inner fast loop. This is bases on the following two considerations. On one hand, since the control objective is to absorb the fast high frequency disturbance by the ultracapacitor side converter, the motion rates of the current and the voltage on the ultracapacitor side are supposed to be much faster than the ones on the battery side. On the other hand, for the ultracapacitor side converter, due to the different time scales between the ultracapacitor voltage and the inductor current, the motion rate of the current is much faster than the motion rate of the voltage.

Therefore, based on the singular perturbation theory, the control problem can be solved by using a cascaded control structure with two control loops : an inner fast control loop and an outer slow control loop.

3.4.2.1 Inner fast loop

To control x_2, the inner fast PI controller can be simply designed as follow [1] :

$$u_2 = k_p(x_2^* - x_2) + k_i \int (x_2^* - x_2) \tag{3.15}$$

where, k_p and k_i are the gains of the proportional term and the integral term.

1. We remark here : $\int x$ is short for $\int_0^t x(s)ds$

3.4.2.2 Outer slow loop

We rewrite the system model (3.2) :

$$\begin{aligned}
\dot{x}_1 &= E - u_1\frac{x_3}{C} \\
\dot{x}_3 &= \omega_1 - \frac{x_3}{RC} + u_1\frac{x_1}{L_1} + u_2\frac{x_2}{L_2} \\
\dot{x}_4 &= -\frac{x_2}{L_2} - \frac{x_4}{R_{sc}C_{sc}} \\
\dot{x}_2 &= -u_2\frac{x_3}{C} + \frac{x_4}{C_{sc}}
\end{aligned} \tag{3.16}$$

Setting $\dot{x}_2 = 0$, we obtain

$$u_2 = \frac{C}{C_{sc}}\frac{x_4}{x_3} \tag{3.17}$$

This implies that after transient, the current is supposed to converge to its static reference, i.e., $x_2 \to \bar{x}_2$, and the control input u_2 is (3.17). The reduced model can then be deduced by substituting (3.17) into equations (3.16), and replacing the state x_2 by v_2.

$$\begin{aligned}
\dot{x}_1 &= E - u_1\frac{x_3}{C} \\
\dot{x}_3 &= \omega_1 - \frac{\tilde{x}_3}{RC} - \frac{\bar{x}_3}{RC} + u_1\frac{x_1}{L_1} + \frac{Cx_4}{C_{sc}x_3}\frac{v_2}{L_2} \\
\dot{x}_4 &= -\frac{v_2}{L_2} - \frac{x_4}{R_{sc}C_{sc}}
\end{aligned} \tag{3.18}$$

Thus, the original four-dimensional system is degenerated into a three-dimensional slow model. This model holds as long as the dynamics of the outer loop is slower than the internal dynamics of the current loop (3.15). With this model, we aim to design an outer slow loop which drives the system to the equilibrium point. Therefore, we consider the Hamiltonian form of the slow model in terms of the error dynamic, and design a controller through interconnection and damping assignment.

The reduced model (3.18) can be written in terms of error dynamics :

$$\begin{aligned}
\dot{\tilde{x}}_1 &= E - u_1\frac{x_3}{C} \\
\dot{\tilde{x}}_3 &= -\frac{\tilde{x}_3}{RC} + \bar{\omega}_1 - \frac{\bar{x}_3}{RC} + u_1\frac{x_1}{L_1} + \frac{Cx_4}{C_{sc}x_3}\frac{v_2}{L_2} \\
\dot{\tilde{x}}_4 &= -\frac{\tilde{x}_4}{R_{sc}C_{sc}} - \frac{v_2}{L_2} - \frac{\bar{x}_4}{R_{sc}C_{sc}}
\end{aligned} \tag{3.19}$$

Thus, we obtain a new PCH system :

$$\dot{\tilde{x}} = (\mathcal{J} - \mathcal{R})\frac{\partial \mathcal{H}}{\partial \tilde{x}} + g(x, u) \tag{3.20}$$

with

$$\mathcal{J} = \begin{pmatrix} 0 & 0 & 0 \\ 0 & 0 & 0 \\ 0 & 0 & 0 \end{pmatrix} \quad \mathcal{R} = \begin{pmatrix} 0 & 0 & 0 \\ 0 & \frac{1}{R} & 0 \\ 0 & 0 & \frac{1}{R_{sc}} \end{pmatrix}$$

$$g(x,u) = \begin{pmatrix} E - u_1 \frac{x_3}{C} \\ \bar{\omega}_1 - \frac{\bar{x}_3}{RC} + u_1 \frac{x_1}{L_1} + \frac{Cx_4}{C_{sc}x_3} \frac{v_2}{L_2} \\ -\frac{v_2}{L_2} - \frac{\bar{x}_4}{R_{sc}C_{sc}} \end{pmatrix}$$

$$\mathcal{H}(\tilde{x}) = \frac{1}{2L_1}\tilde{x}_1^2 + \frac{1}{2C}\tilde{x}_3^2 + \frac{1}{2C_{sc}}\tilde{x}_4^2$$

The desired error dynamic in terms of the desired storage function $\mathcal{H}_d$ is [OGC04] :

$$\dot{\tilde{x}} = (\mathcal{J}_d - \mathcal{R}_d) \frac{\partial \mathcal{H}_d}{\partial \tilde{x}} \tag{3.21}$$

where,

$$\mathcal{H}_d = \frac{1}{2L_1}\tilde{x}_1^2 + \frac{1}{2C}\tilde{x}_3^2 + \frac{1}{2C_{sc}}\tilde{x}_4^2, \tag{3.22}$$

J_d is a skew-symmetry matrix ($J_d^\top = -J_d$) and R_d is a positive semi-definiteness matrix. We define the matrices J_d and R_d as the following forms :

$$\mathcal{J}_d = \begin{pmatrix} 0 & j_1 & j_2 \\ -j_1 & 0 & j_3 \\ -j_2 & -j_3 & 0 \end{pmatrix} \quad , \quad \mathcal{R}_d = \begin{pmatrix} r_1 & 0 & 0 \\ 0 & r_2 & 0 \\ 0 & 0 & r_3 \end{pmatrix} .$$

The main idea is to design the interconnection matrix $\mathcal{J}_d$ and the damping matrix $\mathcal{R}_d$, such that the dynamic error model (3.19) can be written in the desired error form (3.21). Matching the two models leads to the following equations :

$$\begin{aligned} E - u_1 \frac{x_3}{C} &= -r_1 \frac{\tilde{x}_1}{L_1} + j_1 \frac{\tilde{x}_3}{C} + j_2 \frac{\tilde{x}_4}{C_{sc}} \\ \bar{\omega}_1 - \frac{\bar{x}_3}{RC} + u_1 \frac{x_1}{L_1} + \frac{Cx_4}{C_{sc}x_3} \frac{v_2}{L_2} &= -j_1 \frac{\tilde{x}_1}{L_1} + (\frac{1}{R} - r_2) \frac{\tilde{x}_3}{C} + j_3 \frac{\tilde{x}_4}{C_{sc}} \\ \frac{v_2}{L_2} + \frac{\bar{x}_4}{R_{sc}C_{sc}} &= j_2 \frac{\tilde{x}_1}{L_1} + j_3 \frac{\tilde{x}_3}{C} + (r_3 - \frac{1}{R_{sc}}) \frac{\tilde{x}_4}{C_{sc}} \end{aligned}$$

If we could find the coefficients j_i $(i = 1, 2, 3)$ and r_i $(i = 1, 2, 3)$ satisfying the matching equations above, then the system converges asymptotically to the equilibrium point. Choose $\mathcal{H}_d$ as a Lyapunov function, then

$$\dot{\mathcal{H}}_d(\tilde{x}) = -[\frac{\partial \mathcal{H}_d}{\partial x}]^\top \mathcal{R}_d \frac{\partial \mathcal{H}_d}{\partial x} \leq 0$$

Calling upon the La Salle's invariance principle, the asymptotic stability of the closed-loop system is satisfied.

We may deduce from the matching equations that :

$$\begin{aligned} u_1 &= \frac{CE}{max\{x_3, x_{3min}\}} + \frac{C}{max\{x_3, x_{3min}\}} \left[r_1 \frac{\tilde{x}_1}{L_1} - j_1 \frac{\tilde{x}_2}{C} - j_2 \frac{\tilde{x}_4}{C_{sc}} \right] \\ v_2 &= -L_2 \frac{\bar{x}_4}{R_{sc}C_{sc}} + L_2 \left[j_2 \frac{\tilde{x}_1}{L_1} + j_3 \frac{\tilde{x}_2}{C} + (r_3 - \frac{1}{R_{sc}}) \frac{\tilde{x}_4}{C_{sc}} \right] \end{aligned} \tag{3.23}$$

Herein, considering of the system security, we add x_{3min} corresponding to the minimum value of the DC bus voltage which needs to be defined. If the DC bus voltage reduces below this value, then the algorithm can no longer to used so as to avoid the overflow of u_1. Choosing $r_1 = \frac{1}{2R_{sc}}$; $r_2 = \frac{1}{R} - \frac{1}{2R_{sc}}$; $r_3 = \frac{1}{2R_{sc}}$ and $j_1 = -r_3$; $j_2 = r_1$; $j_3 = r_3$, which satisfy the first and the third matching equations, we obtain the following non-linear control algorithm :

$$\begin{aligned} u_1 &= \frac{CE}{max\{x_3, x_{3min}\}} + \frac{C}{max\{x_3, x_{3min}\}}\tilde{v} \\ v_2 &= -\frac{L_2\bar{x}_4}{R_{sc}C_{sc}} + L_2\tilde{v} \end{aligned} \tag{3.24}$$

with

$$\tilde{v} = r_1\frac{\tilde{x}_1}{L_1} - j_1\frac{\tilde{x}_3}{C} - j_2\frac{\tilde{x}_4}{C_{sc}}$$

It can be seen from the structure of the controllers (3.24) that they are the sum of two parts. The first part is associated to the desired open-loop duty cycle, while the second part is proportional-like error feed-back control. If we could find the coefficients such that the second matching equation is satisfied and that the controllers show good dynamic performance, then we may fix the controllers. However, from physical consideration and experimental analysis, due to the inherent relation between the coefficients and the system nature damping, it is not easy to find such controllers because the coefficients cannot be large enough to guarantee a good dynamic performance.

Therefore, we consider to add some integral terms to improve the dynamic performance. With regard to this, we introduce new states $\int\tilde{x}_1, \int\tilde{x}_3, \int\tilde{x}_4$. Then, the new system is written as :

$$\begin{pmatrix} \dot{\tilde{x}} \\ \int\dot{\tilde{x}} \end{pmatrix} = \begin{pmatrix} -R & 0_{3\times3} \\ -D & 0_{3\times3} \end{pmatrix} \nabla\mathcal{H} + \begin{pmatrix} g(\tilde{x},\bar{x})v \\ 0_{3\times1} \end{pmatrix} \tag{3.25}$$

with

$$R = \begin{pmatrix} 0 & 0 & 0 \\ 0 & \frac{1}{R} & 0 \\ 0 & 0 & \frac{1}{R_{sc}} \end{pmatrix} \quad D = \begin{pmatrix} L_1 & 0 & 0 \\ 0 & C & 0 \\ 0 & 0 & C_{sc} \end{pmatrix}$$

$$g(\tilde{x},\bar{x})v = \begin{pmatrix} E - u_1\frac{x_3}{C} \\ \bar{\omega}_1 - \frac{\bar{x}_3}{RC} + u_1\frac{x_1}{L_1} + \frac{Cx_4}{C_{sc}x_3}\frac{v_2}{L_2} \\ -\frac{v_2}{L_2} - \frac{\bar{x}_4}{R_{sc}C_{sc}} \end{pmatrix}$$

$$\mathcal{H}(\tilde{x}) = \frac{1}{2L_1}\tilde{x}_1^2 + \frac{1}{2C}\tilde{x}_3^2 + \frac{1}{2C_{sc}}\tilde{x}_4^2 + \frac{1}{2L_1}(\int\tilde{x}_1)^2 + \frac{1}{2C}(\int\tilde{x}_3)^2 + \frac{1}{2C_{sc}}(\int\tilde{x}_4)^2$$

Similarly, we want that the desired error dynamics be written in terms of the desired Hamiltonian form :

$$\begin{pmatrix} \dot{\tilde{x}} \\ \int\dot{\tilde{x}} \end{pmatrix} = (\mathcal{J}_d - \mathcal{R}_d)\frac{\partial\mathcal{H}_d}{\partial\tilde{x}} \tag{3.26}$$

with $\mathcal{J}_d = -\mathcal{J}_d^\top$ and $\mathcal{R}_d$ being positive definite matrix. Thus, we explicitly write the matrices with coefficients $j_i(i=1,2,3)$, $r_i(i=1,2,3)$ and $c_i(i=1,2,\cdots,6)$ as follows :

$$\mathcal{J}_d = \left(\begin{array}{ccc|ccc} 0 & j_1 & j_2 & 0 & 0 & 0 \\ -j_1 & 0 & j_3 & 0 & 0 & 0 \\ -j_2 & -j_3 & 0 & 0 & 0 & 0 \\ \hline 0 & 0 & 0 & 0 & 0 & 0 \\ 0 & 0 & 0 & 0 & 0 & 0 \\ 0 & 0 & 0 & 0 & 0 & 0 \end{array}\right)$$

$$\mathcal{R}_d = \left(\begin{array}{ccc|ccc} r_1 & 0 & 0 & c_1 & c_2 & c_3 \\ 0 & r_2 & 0 & c_2 & c_4 & c_5 \\ 0 & 0 & r_3 & c_3 & c_5 & c_6 \\ \hline -L_1 & 0 & 0 & 0 & 0 & 0 \\ 0 & -C & 0 & 0 & 0 & 0 \\ 0 & 0 & -C_{sc} & 0 & 0 & 0 \end{array}\right)$$

Matching the system (3.25) and (3.26) leads to the following controller form :

$$\begin{aligned} u_1 &= \frac{CE}{max\{x_3, x_{3min}\}} + \frac{C}{max\{x_3, x_{3min}\}}\left[r_1\frac{\tilde{x}_1}{L_1} - j_1\frac{\tilde{x}_3}{C} - j_2\frac{\tilde{x}_4}{C_{sc}} + c_1\int\frac{\tilde{x}_1}{L_1} + c_2\int\frac{\tilde{x}_3}{C} + c_3\int\frac{\tilde{x}_4}{C_{sc}}\right] \\ v_2 &= -L_2\frac{\bar{x}_4}{R_{sc}C_{sc}} + L_2\left[j_2\frac{\tilde{x}_1}{L_1} + j_3\frac{\tilde{x}_3}{C} + (r_3 - \frac{1}{R_{sc}})\frac{\tilde{x}_4}{C_{sc}} + c_3\int\frac{\tilde{x}_1}{L_1} + c_5\int\frac{\tilde{x}_3}{C} + c_6\int\frac{\tilde{x}_4}{C_{sc}}\right] \end{aligned} \tag{3.27}$$

By writing the desired error dynamic as the form (3.26), we loose the property that the damping matrix R_d has and only has positive values on the diagonal. Consequently, it becomes complex to determine the sign of the derivative of the Hamiltonian (3.28).

$$\dot{\mathcal{H}}_d(\tilde{x}) = \left(\frac{\partial\mathcal{H}_d}{\partial\tilde{x}}\right)^\top\dot{\tilde{x}} = \left(\frac{\partial\mathcal{H}_d}{\partial\tilde{x}}\right)^\top(\mathcal{J}_d - \mathcal{R}_d)\frac{\partial\mathcal{H}_d}{\partial\tilde{x}} = -\left(\frac{\partial\mathcal{H}_d}{\partial\tilde{x}}\right)^\top\mathcal{R}_d\frac{\partial\mathcal{H}_d}{\partial\tilde{x}} \tag{3.28}$$

Hence, we cannot exam the closed-loop stability through Lyapunov method and guarantee the asymptotic stability via LaSalle's invariance principle. Alternatively, we notice that the desired error dynamic (3.26) is also a linear system. Therefore, the stability of the closed-loop system can be verified through classical linear theories. Rewrite (3.26) as a standard linear form :

$$\dot{\tilde{x}} = A\tilde{x} \tag{3.29}$$

with

$$A = \left(\begin{array}{ccc|ccc} -\frac{r_1}{L_1} & \frac{j_1}{C} & \frac{j_2}{C_{sc}} & -\frac{c_1}{L_1} & -\frac{c_2}{C} & -\frac{c_3}{C_{sc}} \\ -\frac{j_1}{L_1} & -\frac{r_2}{C} & \frac{j_3}{C_{sc}} & -\frac{c_2}{L_1} & -\frac{c_4}{C} & -\frac{c_5}{C_{sc}} \\ -\frac{j_2}{L_1} & -\frac{j_3}{C} & -\frac{r_3}{C_{sc}} & -\frac{c_3}{L_1} & -\frac{c_5}{C} & -\frac{c_6}{C_{sc}} \\ \hline 1 & 0 & 0 & 0 & 0 & 0 \\ 0 & 1 & 0 & 0 & 0 & 0 \\ 0 & 0 & 1 & 0 & 0 & 0 \end{array}\right)$$

being the characterized matrix of closed-loop system. Hence, if we could find the coefficients $j_i(i=1,2,3)$, $r_i(i=1,2,3)$ and $c_i(i=1,2,\cdots,6)$ making all the eigenvalues of matrix A located on the left side of the complex plan, then the closed-loop stability can be guaranteed.

In order to find the coefficients, we analyze the desired error dynamic (3.26) in frequency domain. After Laplace transformation, (3.26) becomes :

$$\begin{aligned}
(L_1 s^2 + r_1 s + c_1)\tilde{x}_1 &= L_1(-\frac{c_2}{C} + \frac{j_1}{C}s)\tilde{x}_3 + L_1(-\frac{c_3}{C_{sc}} + \frac{j_2}{C_{sc}}s)\tilde{x}_4 \\
(Cs^2 + r_2 s + c_4)\tilde{x}_3 &= C(-\frac{c_2}{L_1} - \frac{j_1}{L_1}s)\tilde{x}_1 + C(-\frac{c_5}{C_{sc}} + \frac{j_3}{C_{sc}}s)\tilde{x}_4 \\
(C_{sc}s^2 + r_3 s + c_6)\tilde{x}_4 &= C_{sc}(-\frac{c_3}{L_1} + \frac{j_2}{L_1}s)\tilde{x}_1 + C_{sc}(-\frac{c_5}{C} - \frac{j_3}{C}s)\tilde{x}_3
\end{aligned} \tag{3.30}$$

Thus, we obtain a series of transfer functions of multi-variable systems. For each input and output, it is a second order system with a zero. We may therefore, define the coefficients based on the physical consideration and the response characteristics of second order systems. Specifically, we may determinate the coefficients in the denominator by locating the poles, which gives the pairs $(r_1, c_1), (r_2, c_4), (r_3, c_6)$, and then, we choose proper gains and zeros, which gives the coefficients in the nominator c_2, c_3, c_5 and j_1, j_2, j_3.

Consider a second order system in series with a proportional and derivative term :

$$H(s) = \frac{\omega_n^2(\tau s + 1)}{s^2 + 2\xi\omega_n s + \omega_n^2} \tag{3.31}$$

where, the damping ratio ξ decides the dynamic of the step response. Whenever $\xi > 0$, the system converges at steady state. When $\xi > 1$, the system converges exponentially, and the system can be regarded as a series connection of two inertial elements with different time constants T_1 and T_2, $(T_1 > T_2)$. Thus, the system becomes :

$$H(s) = \frac{\omega_n^2(\tau s + 1)}{(T_1 s + 1)(T_2 s + 1)} \tag{3.32}$$

The two poles p_1 and p_2

$$\begin{aligned}
p_1 &= -\frac{1}{T_1} = -\omega_n\xi + \omega_n\sqrt{\xi^2 - 1} \\
p_2 &= -\frac{1}{T_2} = -\omega_n\xi - \omega_n\sqrt{\xi^2 - 1}
\end{aligned}$$

For a second order system without zero, the time response of a step input $f(t) = 1$ is :

$$h_0(t) = 1 - \frac{p_2}{p_2 - p_1}e^{p_1 t} + \frac{p_1}{p_2 - p_1}e^{p_2 t}$$

For a second order system with zero, the step response is :

$$h(t) = h_0(t) + \tau\dot{h}_0(t)$$

Therefore, the values of the poles and the zeros decide the speed of the response. When the damping ratio $\xi > 1$, the poles are on the real axis, and the system converges exponentially. The further the negative poles are from the imaginary axis, the faster the system responses. Moreover, the closer the zero is from the imaginary axis, the faster the system responses.

Thus, we may choose the coefficients according to these properties and the circuit inherent physical characteristics. For instance, $\tilde{x}_1$ which corresponds to the battery side current is related much more to the DC bus voltage which corresponds to $\tilde{x}_3$ than the ultracapacitor voltage which corresponds to $\tilde{x}_4$. This is to say, for the input-output $\tilde{x}_1 \mapsto \tilde{x}_3$ system, the poles could be negative and far away from the imaginary axis. While, for the input-output $\tilde{x}_4 \mapsto \tilde{x}_1$ system, the poles could be negative and very close to the imaginary axis. For instance, after some theoretical analysis and simulation tests, we may find the coefficients as follows :

$$\begin{array}{lll} j_1 = 3.25; & j_2 = 0.01; & j_3 = 1.18 \times 10^{-5}; \\ r_1 = 8.5; & r_2 = 0.18; & r_3 = 2.11; \\ c_1 = 1800; & c_2 = 50; & c_3 = 0; \\ c_4 = 2.12; & c_5 = 0; & c_6 = 0.3413; \end{array}$$

when the system parameters are chosen as :

$$L_1 = 10mH \quad L_2 = 10mH \quad C = 3.25F \quad C_{sc} = 3850\mu F$$

Thus, the determinant of $\mathcal{R}_d$ is $det(\mathcal{R}_d) = 0.056 > 0$. The closed-loop matrix A is :

$$\begin{pmatrix} -850 & 844.1 & 0,003 & -18000 & -12987 & 0 \\ -325 & -47 & 3.64 \times 10^{-6} & -5000 & -550 & 0 \\ -1 & -0,003 & -0.65 & 0 & 0 & -0.105 \\ 1 & 0 & 0 & 0 & 0 & 0 \\ 0 & 1 & 0 & 0 & 0 & 0 \\ 0 & 0 & 1 & 0 & 0 & 0 \end{pmatrix}$$

The eigenvalues of A are :

$$\{-439 \pm 534i, \quad -13.09, \quad -5.44, \quad -0.35, \quad -0.30\}$$

all on the left side of the complex plan, and thus guarantee the stability of the controlled closed-loop.

3.4.3 Internal model design

As shown in the control structure (Figure 3.2), the internal model is to calculate $\hat{x}_2$ so as to get the desired trajectory x_2^* for the inner fast loop. In order to realize the inner current control (3.15), it is necessary to have x_2^*. As v_2 tends towards $\bar{x}_2$ when $\tilde{\omega}_1 \rightarrow 0$, it remains to get $\hat{x}_2$.

For a Hamiltonian system (3.3), reprinted in a general form (3.33) :

$$\dot{x} = [\mathcal{J}(u) - \mathcal{R}] \nabla \mathcal{H}(x) + g(\omega) \tag{3.33a}$$

$$\mathcal{H}(x) = \frac{1}{2} x^\top Q x \tag{3.33b}$$

From (3.33a), we may obtain :

$$\begin{aligned} \nabla \mathcal{H}(x)^\top \dot{x} &= \nabla \mathcal{H}(x)^\top \{[\mathcal{J}(u) - \mathcal{R}] \nabla \mathcal{H}(x) + g(\omega)\} \\ &= -\nabla \mathcal{H}(x)^\top \mathcal{R} \nabla \mathcal{H}(x) + \nabla \mathcal{H}(x)^\top g(\omega) \end{aligned}$$

From (3.33b), we may obtain :

$$\nabla\mathcal{H}(x)^\top \dot{x} = 2Qx^\top \dot{x}$$

Thus, it is easy to get :

$$\begin{aligned} 2Qx^\top \dot{x} &= -\nabla\mathcal{H}(x)^\top \mathcal{R}\nabla\mathcal{H}(x) + \nabla\mathcal{H}(x)^\top g(\omega) \\ Q\frac{d}{dt}(x^\top x) &= -\nabla\mathcal{H}(x)^\top \mathcal{R}\nabla\mathcal{H}(x) + \nabla\mathcal{H}(x)^\top g(\omega) \end{aligned}$$

Integrating at both sides of the equation, we obtain :

$$Q(x^\top x) = -\int \nabla\mathcal{H}(x)^\top \mathcal{R}\nabla\mathcal{H}(x) + \int \nabla\mathcal{H}(x)^\top g(\omega) + cte \tag{3.34}$$

where, cte is a constant. It can be seen that (3.34) expresses the energy conservation law. The left side is the total energy stored in the system, the first term on the right side is the energy dissipation, the second term is the energy supplied by the exosystem, and thus the constant cte is the initial energy in the system :

$$\underbrace{Q(x^\top x)}_{\text{stored energy}} = \underbrace{-\int \nabla\mathcal{H}(x)^\top \mathcal{R}\nabla\mathcal{H}(x)}_{\text{dissipated energy}} + \underbrace{\int \nabla\mathcal{H}(x)^\top g(\omega)}_{\text{supplied energy}} + \underbrace{\mathcal{H}[x(0)]}_{\text{initial energy}} \tag{3.35}$$

Hence, the state references can be deduced based on the energy expression (3.35).

Back to our specific case, the control objective is to absorb the fast disturbance $\tilde{\omega}_1$ by the ultracapacitor side converter, this is to say that we want the current disturbance $\tilde{\omega}_1$ to go through the ultracapacitor side converter. This is equivalent to $\tilde{\omega}_1 = -u_2\frac{x_2}{L_2}$.

In order to get the desired trajectories of the system states, multiply $\frac{x_2}{L_2}$ at both sides of (3.2b), substitute with (3.2a) and (3.2c) and after some manipulations, we get, when $x_3 = \bar{x}_3$:

$$\frac{1}{L_2}x_2\dot{x}_2 + \frac{1}{C_{sc}}x_4\dot{x}_4 = \tilde{\omega}_1\frac{\bar{x}_3}{C} - \frac{x_4^2}{R_{sc}C_{sc}^2} \tag{3.36}$$

This is equivalent to :

$$\frac{d}{dt}(\frac{1}{2L_2}{x_2}^2) + \frac{d}{dt}(\frac{1}{2C_{sc}}{x_4}^2) = \tilde{\omega}_1\frac{\bar{x}_3}{C} - \frac{x_4^2}{R_{sc}C_{sc}^2} \tag{3.37}$$

Integrating both sides of the equation with respect to t, we get the following energy equation :

$$\underbrace{\frac{1}{2L_2}x_2^2 + \frac{1}{2C_{sc}}x_4^2 +}_{\text{stored energy in UC}} \underbrace{\int_0^t \frac{x_4^2}{R_{sc}C_{sc}^2}dt}_{\text{dissipated energy in UC}} = \underbrace{\mathcal{H}[x(0)]}_{\text{initial energy}} + \underbrace{\int_0^t \tilde{\omega}_1\frac{\bar{x}_3}{C}dt}_{\text{supplied energy}} \tag{3.38}$$

where, $\mathcal{H}[x(0)]$ is a constant which represents the initial energy stored in the ultracapacitor side converter. Notice that $\frac{1}{2L_2}x_2^2 + \frac{1}{2C_{sc}}x_4^2$ is actually the total stored energy in the ultracapacitor side converter (the sum of the “kinetic energy" stored in the inductor $\frac{1}{2L_2}x_2^2$ and the “potential energy" stored in the ultracapacitor $\frac{1}{2C_{sc}}x_4^2$). $\int_0^t \frac{x_4^2}{R_{sc}C_{sc}^2}dt$ is the dissipated energy consumed by the resistor, and $\int_0^t \tilde{\omega}_1\frac{\bar{x}_3}{C}dt$ can be explained as the disturbance energy in the DC bus.

$$\mathcal{H}[x(0)] = \frac{1}{2L_2}\bar{x}_2^2 + \frac{1}{2C_{sc}}\bar{x}_4^2 + \int_0^t \frac{\bar{x}_4^2}{R_{sc}C_{sc}^2}dt$$

Eliminating $\bar{x}_2$ by substituting with (3.13), we get :

$$\mathcal{H}[x(0)] = (\frac{L_2}{2R_{sc}^2C_{sc}^2} + \frac{1}{2C_{sc}})\bar{x}_4^2 + \int_0^t \frac{\bar{x}_4^2}{R_{sc}C_{sc}^2}dt$$

Substituting into (3.38), we get :

$$\frac{x_2^2}{2L_2} + \frac{x_4^2}{2C_{sc}} = (\frac{L_2}{2R_{sc}^2C_{sc}^2} + \frac{1}{2C_{sc}})\bar{x}_4^2 + \int_0^t \left(\tilde{\omega}_1\frac{\bar{x}_3}{C} - \frac{x_4^2 - \bar{x}_4^2}{R_{sc}C_{sc}^2}\right)dt \tag{3.39}$$

Consequently, the desired trajectory can be deduced from :

$$\begin{aligned}\frac{(x_2^*)^2}{2L_2} + \frac{(x_4^*)^2}{2C_{sc}} &= \underbrace{(\frac{L_2}{2R_{sc}^2C_{sc}^2} + \frac{1}{2C_{sc}})\bar{x}_4^2}_{\bar{H}} \\ &+ \underbrace{\int_0^t \left(\tilde{\omega}_1\frac{\bar{x}_3}{C} - \frac{(x_4^*)^2 - \bar{x}_4^2}{R_{sc}C_{sc}^2}\right)dt}_{\tilde{W}}\end{aligned} \tag{3.40}$$

It is not easy to write analytical forms of x_2^* and x_4^*. Herein, we propose a novel algorithm to obtain an approximation of the solution.

From physical point of view, $(\bar{H} + \tilde{W})$ is supposed to be positive, then we may obtain an ellipse expression as follow :

$$\frac{1}{2L_2(\bar{H} + \tilde{W})}(x_2^*)^2 + \frac{1}{2C_{sc}(\bar{H} + \tilde{W})}(x_4^*)^2 = 1 \tag{3.41}$$

Thus, the desired trajectory x_4^* is the trajectory along the axis :

$$\begin{aligned}x_4^* &= [2C_{sc}(\bar{H} + \tilde{W})]^{\frac{1}{2}} \\ &= (2C_{sc}\bar{H})^{\frac{1}{2}}(1 + \frac{\tilde{W}}{\bar{H}})^{\frac{1}{2}}\end{aligned} \tag{3.42}$$

Applying the binominal series [2] to get an approximation of the desired trajectory x_4^* as follow :

$$x_4^* = \sqrt{2C_{sc}\bar{H}}(1 + \frac{1}{2\bar{H}}\tilde{W} - \frac{1}{8\bar{H}^2}\tilde{W}^2) \tag{3.43}$$

the first derivative is :

$$\dot{x}_4^* = \sqrt{2C_{sc}\bar{H}}(\frac{1}{2d}\dot{\tilde{W}} - \frac{1}{4d^2}\tilde{W}\dot{\tilde{W}}) \tag{3.44}$$

2. The binomial series is explicitly written as :

$$(1+x)^p = \sum_{n=0}^{\infty} \binom{p}{n} x^n = 1 + px + \frac{p(p-1)}{2!}x^2 + \cdots$$

where, $\binom{p}{n} = \frac{p!}{n!(p-n)!}$. When $|x| < 1$, the series converges absolutely for any complex number p.

then, the desired trajectory x_2^* can be deduced from (3.2d) :

$$x_2^* = -L_2\dot{x}_4^* - \frac{L_2 x_4^*}{R_{sc}C_{sc}} \tag{3.45}$$

thus, we obtain $\hat{x}_2$ as follow :

$$\hat{x}_2 = x_2^* - \bar{x}_2 = -L_2\dot{x}_4^* - \frac{L_2\hat{x}_4}{R_{sc}C_{sc}} \tag{3.46}$$

Notice that when $R_{sc} \to \infty$, the expression of the desired trajectory can be simplified as an analytical form.

3.5 Simulation results

The effectiveness of the control algorithm is verified through simulation. The controller is applied to the system shown in Figure 3.1. The system parameters are given as follows :

$$\begin{array}{lllllllll} L_1 & = & 2.5mH\,; & R & = & 100\Omega\,; & C & = & 440\mu F\,; \\ L_2 & = & 2.5mH\,; & R_{sc} & = & 1K\Omega\,; & C_{sc} & = & 3.25F\,; \\ E & = & 100V\,; & \bar{V}_{dc} & = & 600V\,; & \bar{V}_{sc} & = & 400V\,; \end{array}$$

The exogenous disturbance is first set as a sinusoidal signal with fundamental frequency $7.5Hz$ (corresponds to a rotation speed $47.1rad/s$ on the crankshaft). Figure 3.3 gives the simulation results. In order to see clearly the effectiveness of the designed controller, an ordinary cascade control algorithm without considering disturbance rejection ($\hat{x}_2$ is set to zero) is first applied to the DC-DC converters, and then the control algorithm designed in this chapter is applied at time $t = 5s$. It can be seen from the figure that the external sinusoidal current leads to unwanted oscillations in the DC bus voltage and the battery current. When the designed controller is added, the amplitude of these oscillations are significantly reduced. On the contrary, the oscillations in the ultracapacitor side converter are increased, which implies that the disturbance is successfully absorbed by the ultracapacitor side converter. Moreover, the ultracapacitor voltage remains around it nominal state of charge ($400V$). Figure 3.4 gives the frequency spectrum analysis of the current in the ultracapacitor side converter. It is clear in the figure that the signal contains a harmonic of $7.5Hz$, and the amplitude of the harmonic obviously increases when the designed controller is added.

Similar comparison is presented in Figure 3.5. The exogenous disturbance is set as a persistent disturbance with three harmonics ($7.5Hz$,$15Hz$ and $22.5Hz$). Similar with the system responses with sinusoidal disturbance, when the designed disturbance rejection algorithm is switched on at $t = 5s$, the oscillations in the battery side converter obviously reduce, while the oscillations in the ultracapacitor side converter significantly increase. A frequency spectrum analysis of the current I_{L_2} is shown in Figure 3.6. The current effectively absorbs the three harmonics. Moreover, the DC bus voltage the ultracapacitor voltage remains around their nominal values.

The next step is to test the control algorithm when there are step variations in the external current. To achieve this, a step signal plus a sinusoidal harmonic is set as the exogenous current. In the control algorithm, $\tilde{\omega}_1$ and $\bar{\omega}_1$ are obtained by using a band-pass filter and a low-pass

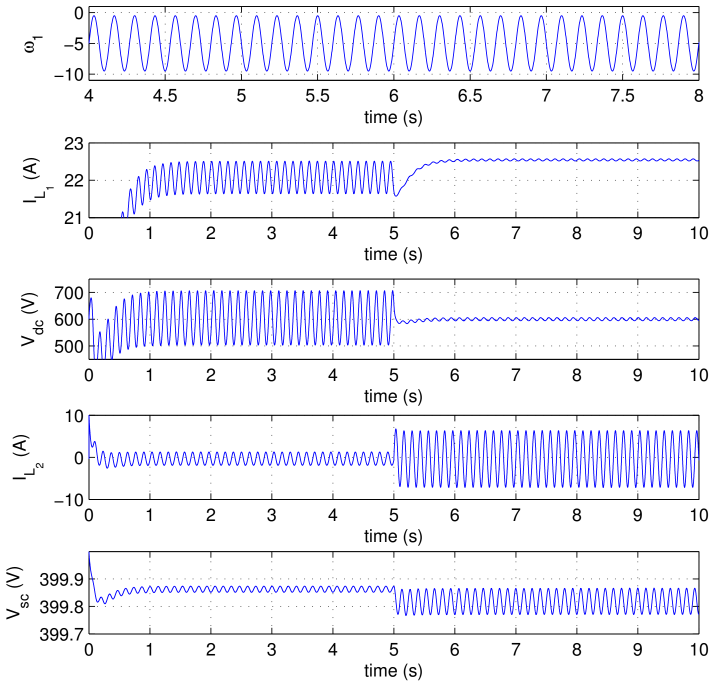

FIGURE 3.3 – Simulation results with sinusoidal current disturbance (From top to bottom : external current, current through L_1, voltage in the DC bus, current through L_2 and ultracapacitor voltage)

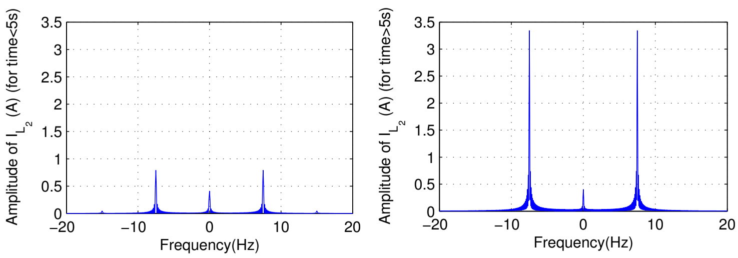

FIGURE 3.4 – Spectrum analysis of the current through L_2 with (right) and without (left) the control algorithm

filter shown in Figure 3.7. Choosing the cut-off frequency of the low-pass filter as $5rad/s$, and the cut-off frequency of the band-pass filter between $5rad/s$ and $1000rad/s$, the outputs of the filters, $\bar{\omega}_1$ and $\tilde{\omega}_1$, are given in Figure 3.8. Figure 3.9 shows the simulation results. Similarly, in order to see clearly the effectiveness of the designed controller, a contrast of the simulation results with and without the designed controller are presented in different colours. It can be seen from the figure that with the designed controller, the ultracapacitor side converter effectively absorbs the transient and sinusoidal disturbance, and more importantly, the battery current varies more smoothly. The DC bus voltage and the ultracapacitor voltage remains around their nominal

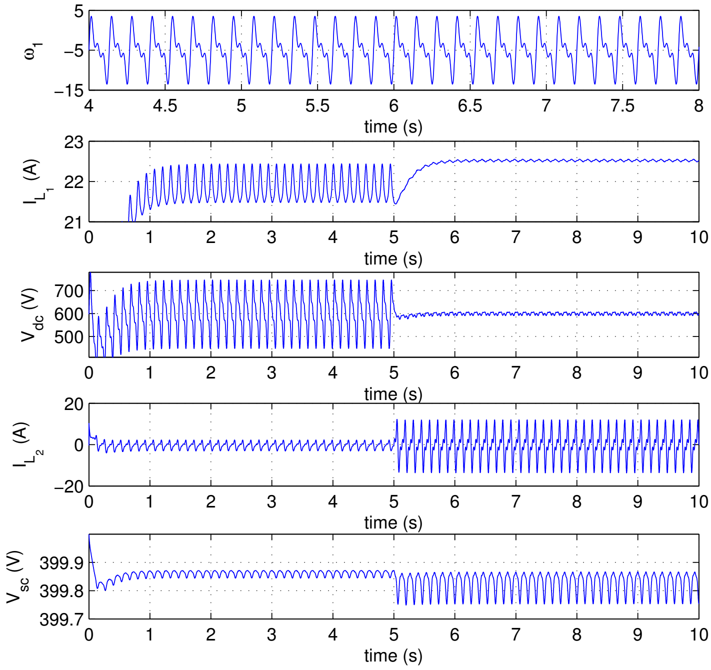

FIGURE 3.5 – Simulation results with three harmonic current disturbance (From top to bottom : external current, current through L_1, voltage in the DC bus, current through L_2 and ultracapacitor voltage)

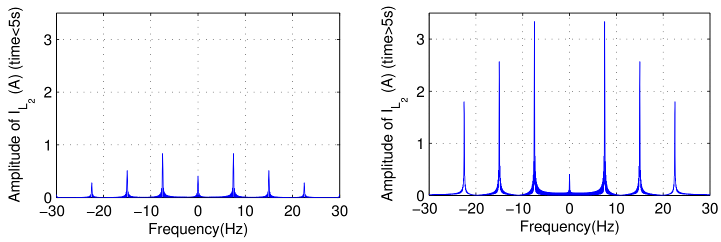

FIGURE 3.6 – Spectrum analysis of the current through L_2 with (right) and without (left) the control algorithm

values.

Now that we have tested the control performance of system under different exogenous disturbances. It can be seen clearly from the system responses that the trajectory of the states in the ultracapacitor side converter forms a limit cycle at steady state. It is based on this fact that we calculate the trajectory reference in section 3.4.3. Figure 3.10 shows the desired trajectories of (I_{L_2}, V_{sc}) under different exogenous disturbances. It can be seen that the limit cycle is a regular ellipse when the external current is a regular sinusoidal signal. When the number of harmonics increases, the shapes of the limit cycles become irregular but remain in the neighbourhood.

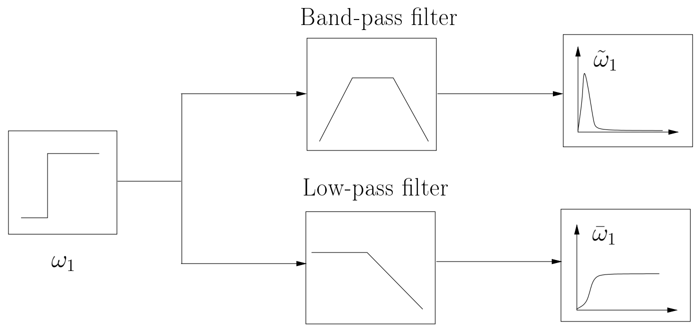

FIGURE 3.7 – Schematic diagram of filters

Moreover, when there is a transient disturbance, the trajectory skip from a limit cycle to another.

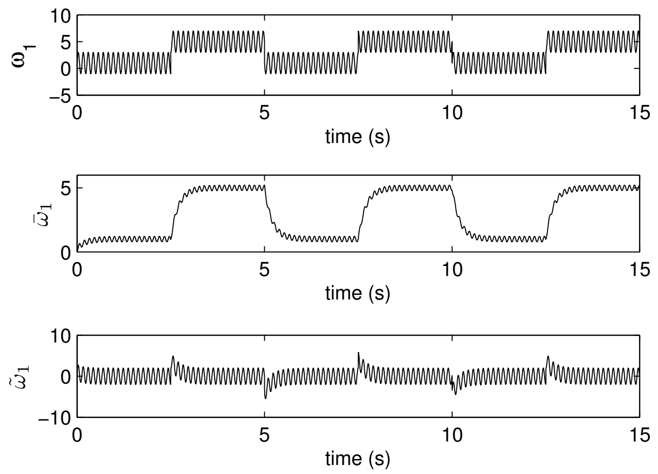

FIGURE 3.8 – External current and the outputs of the filters

3.6 Conclusions

In this chapter, we have presented our contributed controller for hybrid batteries/ultracapacitor energy storage system with exogenous disturbed current. The current disturbance may be sinusoidal or transient. The sinusoidal disturbance is due to the internal combustion engine torque ripples compensation, and the transient disturbance, which has been widely studied by researchers, is caused by the sudden exchange of power in the process of acceleration or braking. Our control objective is to protect the battery from the disturbances and capture the disturbances via the ultracapacitor. Meanwhile, we attempt to maintain a constant voltage in the DC bus, and maintain the average voltage of the ultracapacitor around a given value. Our control idea is based on a multi-timescale approach which separates the system into a fast model and a

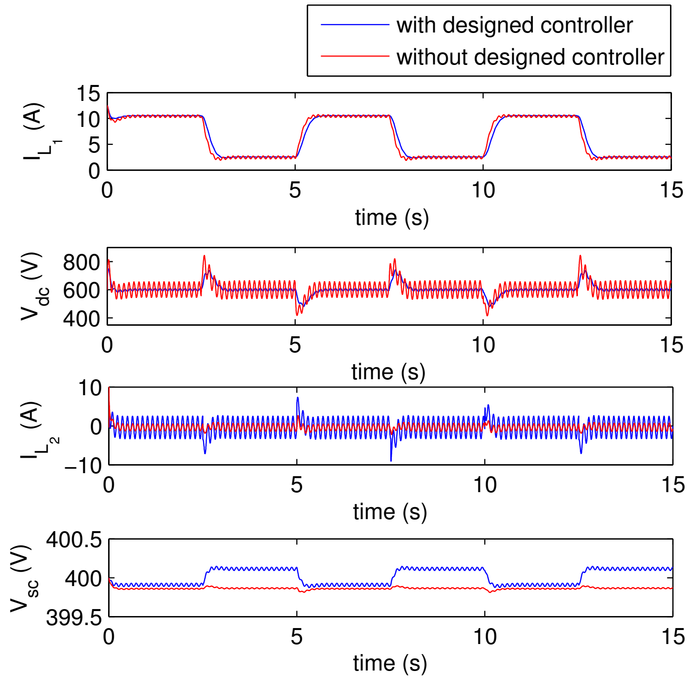

FIGURE 3.9 – Simulation results with sinusoidal and step current disturbance (From top to bottom : current through L_1, voltage in the DC bus, current through L_2 and ultracapacitor voltage)

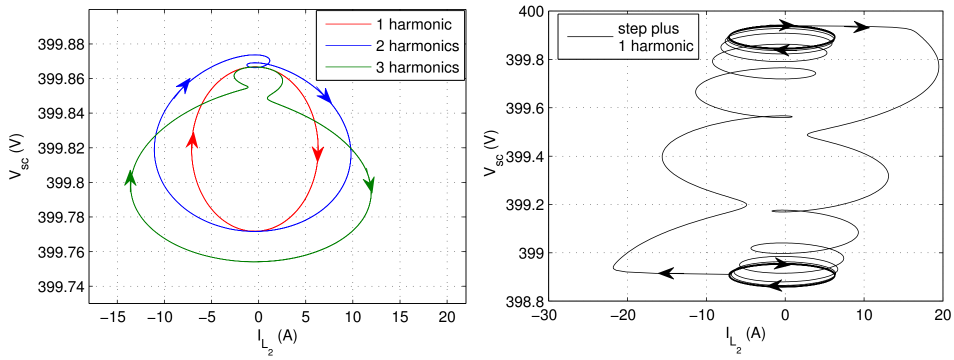

FIGURE 3.10 – Desired trajectories of ultracapacitor side converter (left : when the external disturbance ω_1 is persistent sinusoidal signal with different harmonics ; right : when ω_1 is transient signal plus a sinusoidal signal)

slow model. Furthermore, we consider the hybrid energy system alone without disturbances, and identify the solution of the problem as a static solution. And then, we define the solution of the system with disturbances as a dynamic solution. The fast model and the slow model are then connected through a cascade control structure with a fast inner loop and a slow outer loop. The control objective is achieved by driving the slow model to the static solution and forcing the fast model to reach the desired dynamic solution. The dynamic solution is deduced from the analysis of energy distribution and generated by an internal model. The controller aiming to drive the system to the static equilibrium is designed via interconnection and damping assignment. The effectiveness of the controller has been verified through simulations. In order to be more convincing, we attempt to apply the control algorithm in the experiments. The experiment results will be presented in the next chapter.

Chapitre 4

Experiment implement and results analysis

Sommaire

4.1 Introduction

In the last chapter, we have developed our disturbance rejection algorithm for battery/ultracapacitor hybrid energy system with exogenous current disturbance. In this chapter, we attempt to apply the control algorithm to experiments and test it in real-time. Thanks to dSPACE software and hardware, we are able to edit the algorithm under MATLAB/Simulink environment.

We have mentioned that, for our hybrid electric vehicle application, the exogenous current disturbance on the DC bus is transferred from the DC-AC converter electrically connected to the PMSM. The PMSM is mechanically connected to the ICE. Strictly speaking, to be more convincing, we should integrate the DC-AC converter, the PMSM, the ICE, and the active control algorithm developed in [Nje11] with our hybrid energy system and test our disturbance rejection algorithm for the DC-DC converters. However, due to the complexity of the whole system and the limit of time, we are not able to implement all these. Instead, we build an alternative exosystem utilizing a resistive load and an AC power source to emulate the behaviour of the real exosystem. The persistent disturbance generated by the real exosystem can be decomposed into several harmonics. Hence, herein we test one harmonic and the same control algorithm can be extended to other harmonics. The transient disturbance is caused by the sudden change of the power demand. This is reflected via the change of the resistive load. In this way, we might actually generalize our hybrid energy storage system and the disturbance rejection algorithm to a wider range of applications, not only hybrid electric vehicles but also pure electrical vehicles or even renewable energy generation system wherever a hybrid energy storage system is applied and exogenous current disturbances appear in the DC bus.

A comparison of the experimental results with and without the disturbance rejection algorithm under different exogenous disturbances will be presented to evaluate the controller performance. The system responses show that, with the designed control algorithm, the disturbances in the battery side converter are obviously rejected while the disturbances are effectively absorbed in the ultracapacitor side converter.

4.2 Experimental equipment

The experimental test bench is mainly composed of a Lithium-Ion battery system, an ultracapacitor pack, a boost converter, a bi-directional DC-DC converter, resistive loads and a sinusoidal voltage generator. The voltage generator is connected to the circuit to simulate sinusoidal current disturbances. Several strategies are applied to protect the circuit including protection resistors which limit the currents in the stage of start-up of the system. The overall test bench is shown in Figure 4.1. The circuit signals communicate with the control terminal through a dSPACE DS1104 board and the related dSPACE software. The dSPACE provides an interface for the communication of analog signals and numerical signals, and provides a powerful platform allowing to control and monitor the current and the voltage of the circuit in real time and to design the control program under MATLAB/simulink environment [DS204, Gha12]. In this section, we will present some details of each experimental module and the embedding of the control algorithm. The parameters of the experimental equipment and the control algorithm can be found in Table 4.1.

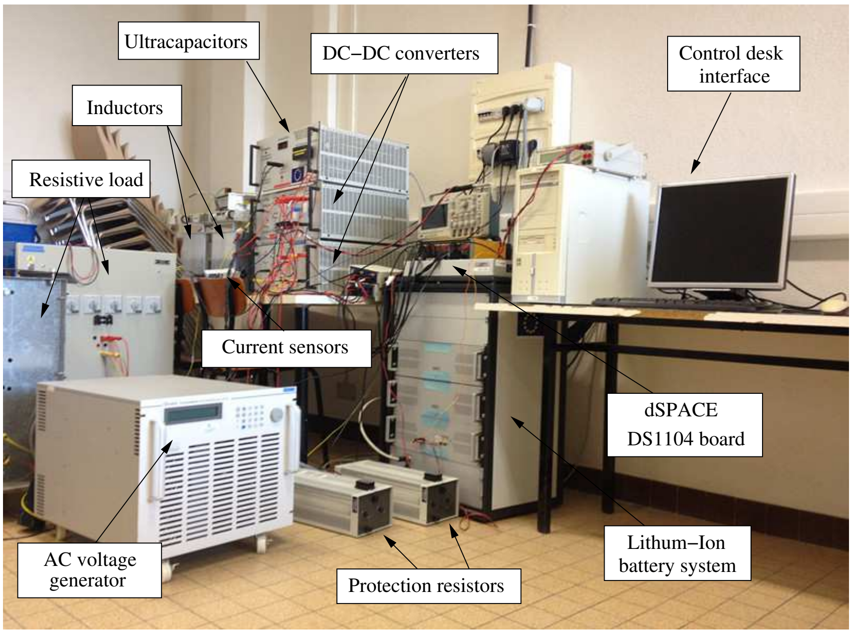

FIGURE 4.1 – Experimental test bench

4.2.1 Battery system

The battery we use is a SAFT Lithium-Ion battery system [MAH09]. It is composed of two battery modules MOD-VLM48-039 connected in series. Each module contains 14 VL41M cells (4V, 39Ah). The system comes with a battery management module. The module needs to be supplied by a $24V$ power source and enables to monitor the battery states and protect the battery. We may therefore monitor the state of charge (SOC) of the battery and charge or stop charging the battery according to the percentage of SOC. When the battery is connected to the boost converter, it imposes its nominal voltage (≈100V) on the DC bus due to the existence of the diode. Our desired voltage in the DC bus is 300V. The moment when the power converter stats up, there is a peak current through the inductor. For sake of security, we have integrated a fuse in the converter to limit the current flow to 5A. Consequently, it is necessary to avoid this transient current exceeding 5A. To achieve this, we utilize a sliding rheostat to connect the battery to the boost converter. This protection resistor is set to maximum at the moment when the control input is added, and then set to zero when the circuit is steady.

4.2.2 Ultracapacitor

Our laboratory possesses a pack of ultracapacitor having access to four various capacitances according to different connection modes. En mode solo, we have access to two capacitances : the maximum capacitance 52F, with the maximum voltage 15V, and a smaller capacitance 6.5F, with the maximum voltage 120V. In parallel mode, connecting in parallel two identical 6.5F capacitors, we may obtain a 13F capacitor with the same maximum voltage 120V. In series mode, connecting in series two 6.5F capacitors, we may obtain a 3.25F capacitor with the maximum voltage 240V. In our study, we use the series mode capacitor 3.25F/240V.

TABLE 4.1 – Electric parameters of the experimental system

Battery parameters	
Maximum voltage	112V
Minimum voltage	76V
Nominal voltage	100V
Maximum charge current @+20°C	30A
Maximum discharge current @+20°C	150A
Ultracapacitor parameters	
Capacitance	3.25F
Maximum voltage	240V
Nominal voltage	160V
Nominal current	10A
Estimated resistive loss	$R_{sc} = 8.7k\Omega$
Three-phase AC power source generator parameters	
Maximum power	4.5K VA
Maximum Power per Phase	1.5 K VA
Output voltage	0-150V
Frequency	15Hz-1.2kHz
Maximum current per Phase (r.m.s)	12A
DC-DC converter parameters	
Battery side inductance	L_1 = 10mH
Ultracapacitor side inductance	L_2 = 10mH
Maximum current through the inductances	5A
Capacitance on the DC bus	$C = 3850\mu$F
Maximum voltage on the DC bus	425V
Nominal voltage on the DC bus	300V
Estimated total resistive loss in the circuit	$R = 900\Omega$

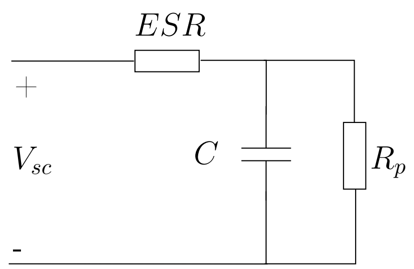

FIGURE 4.2 – Classical ultracapacitor model

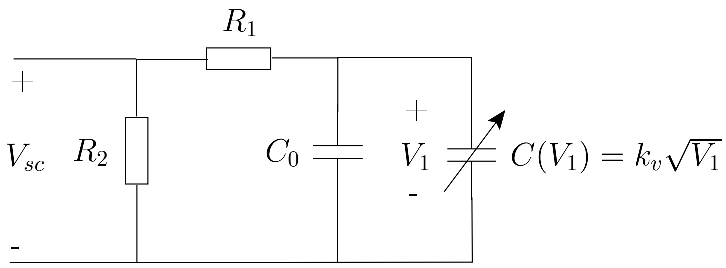

FIGURE 4.3 – An accuate ultracapacitor model

A classical physical model of ultracapacitor is shown in Figure 4.2. In this model, the ultracapacitor is considered as a conventional capacitor connecting in parallel and in series with a resistor respectively. The model have been accepted and utilized by most researches, and the series resistor is usually referred to as an equivalent series resistor (ESR).

Our colleagues in the electrical team of our laboratory have done a concentrated research of ultracapacitors and proposed a more accurate physical and mathematical model [BTCM13, HJDT12] shown in Figure 4.3. In the proposed model, they have taken into account the self-discharge of ultracapacitors and found out that the total capacitance is approximately linear to the square root of the terminal voltage. Thus, the total capacitance can be written as :

$$C_{sc} = C_0 + k_v\sqrt{V_1}$$

where, k_v is a parameter reflecting the effects of the diffused layer of a ultracapacitor, and can be calculated through experiments.

In our study, our aim is to capture the high-frequency current with the ultracapacitor. The current flow through the ultracapacitor is an important variable which is a varying manifold at steady state. A complicated physical model of ultracapacitor leads to a complicated variable derivative in state space representation and desired trajectory representation, and thus has no much positive effect on the control algorithm. Actually, we need only to take the ultracapacitor self-discharge into consideration and try to maintain its voltage around a certain value. Consequently, we choose a relative simply model of ultracapacitor with a parallel connection of a conventional capacitor and an internal resistor. Thus, a parallel internal resistor may sufficiently represent the self-discharge phenomenon, and the internal resistance R_{sc} can be easily estimated through experiments.

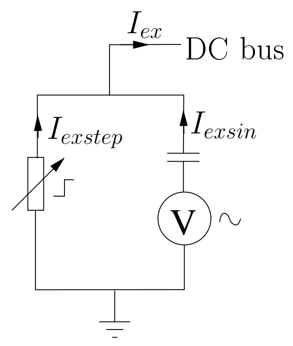

FIGURE 4.4 – Exosystem

4.2.3 Exosystem

As mentioned in the second chapter, the exogenous current disturbance consists of two kinds of disturbances, i.e., transient disturbance and persistent disturbance. The transient disturbance is caused by the load power sudden change during acceleration and deceleration. While, the persistent disturbance is due to the combustion engine torque ripple compensation, and can be decomposed into several sinusoidal disturbances with different frequencies. The torque ripple compensation is achieved through a PMSM torque control. The control algorithm has been applied to the DC-AC converter connecting the hybrid energy storage system. The battery and ultracapacitor energy storage devices are connected to the DC-AC converter through two DC-DC converters. The active control algorithm of the AC-DC converter leads to a sinusoidal current disturbance on the bus. In the theoretical analysis stage, we have regarded the hybrid energy storage system as an isolated plant and the impact on the DC bus as an exogenous disturbance. Similarly, in the experimental stage, we utilize an "exosystem" to simulate the impact of the current disturbance.

The hybrid energy system is connected to a resistive load and an AC source, as shown in Figure 4.4. Thus, the transient disturbance can be achieved through a step change of the resistive load. The sinusoidal disturbance can be achieved from the AC source. We have two candidate devices in our lab, an AC current generator and an AC voltage generator. However, the AC current generator is not amenable for the experiment because the rated voltage of the AC current generator is only around 120V, it cannot be connected directly to the DC bus. Therefore, we utilize the AC voltage generator connecting with a capacitor to generate a sinusoidal current disturbance in the DC bus.

The AC voltage generator is a Chroma model 61703 programmable AC power source [ACs02]. It delivers pure, 5-wire, 3-phase AC power. The output voltage may vary from 0 to 150V, and the frequency from 15Hz to 1.2kHz. We have shown in the second chapter that when the rotational speed of the vehicle is 900rpm (94.24rad/s), the harmonic disturbances correspond to a fundamental frequency of 7.5Hz. Since the available lowest frequency of the AC source is 15Hz, two times of the fundamental frequency, we may utilize a single-phase sinusoidal output with this frequency as the persistent disturbance. A capacitor (4700μF,450V) is utilized to connect the AC source to the DC bus. It is used to share the voltage on the DC bus, so as to protect the AC source. Furthermore, a sliding rheostat is also connected in series with the AC source to

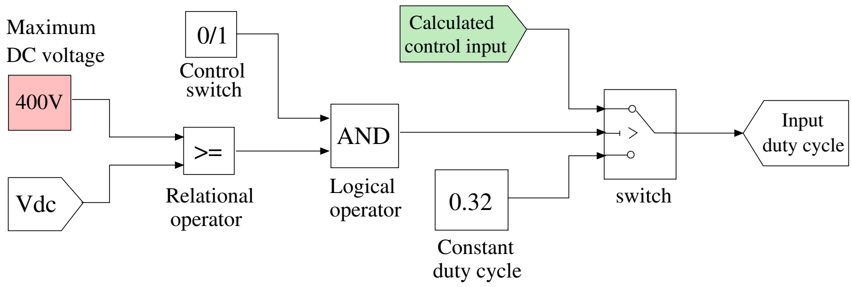

FIGURE 4.5 – Over voltage protection for the DC bus

avoid the over current. Therefore, it is referred to as a protection resistor.

4.2.4 Power converters

Our laboratory has researched and developed independently several boost converters and has developed recently a buck-boost bi-directional DC-DC converter especially for our application. Being different from the bi-directional DC-DC converter, the switch interfacing the inductor and the capacitor is replaced by a diode allowing only unidirectional current. Our experimental objective is to capture the high frequency disturbance by the ultracapacitor. Therefore, we connect the battery with a boost converter and connect the ultracapacitor with the bi-directional DC-DC converter.

The switches are IGBT. The two switches in the bi-directional DC-DC converter are conjugated. The control inputs are Pulse-width modulation (PWM) out of the dSPACE hardware. The frequency of the PWM is set at 4500Hz.

The maximum current through the inductors is set to 5A. We have mounted fuses in the converters to achieve over current protection. Therefore, two sliding rheostat (0-106Ω3.5A) are utilized. One is connected between the battery and the boost converter ; another is connected between the ultracapacitor and the bi-directional converter. The resistances are set to the maximum at the initial stage when the control signals are switched in, and set to zero when the system tends to be steady. Therefore, it is obvious that the protection resisters only work at the start up stage, and have no influence after the control signals switched in.

The maximum voltage in the DC bus is set to 425V, exceeding this voltage will ring the alarm. In order to limit the voltage in the DC bus, we design an over voltage protection in the control interface to avoid the DC bus voltage exceeding 400V. Figure 4.5 shows the over voltage protection structure. The constant duty cycle is a preset open-loop control input which drives the DC bus voltage to the nominal value. The value of the switch boost block decides to switch in or off our designed closed-loop controller. When its value is 0, the closed-loop controller is switched off, the system operates with the constant duty cycle. When its value is 1, the closed-loop controller is switched in. If the DC bus voltage remains below 400V, the system remains regulated by the closed-loop controller. If our designed closed-loop controller drives the DC voltage beyond the limit, then the over voltage protection cuts immediately the closed-loop controller and switches in the open-loop controller. Thus, we assure that the circuit always operates within the safety range in the debugging process of the closed-controller.

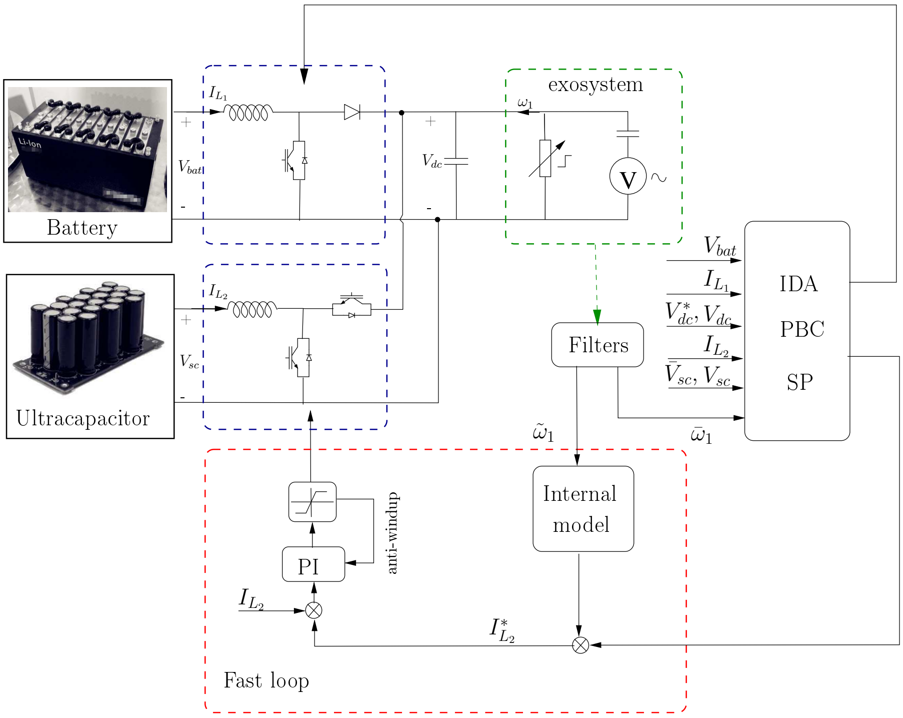

FIGURE 4.6 – Experimental control structure

4.3 Control algorithm embedding

The circuit voltage and current signals are transferred to the control computer through the dSPACE ADC module. The control PWM signals are exported from the dSPACE PWM module. The control algorithm is edited under MATLAB/Simulink environment. We embed the cascade control algorithm elaborated in the last chapter and verify its effectiveness in real time. The global structure is shown in Figure 4.6. The battery system is connected to a boost converter, and the ultracapacitor pack is connected to a bidirectional DC-DC converter. The PWM signals are applied to control the IGBTs. The exosystem emulating the exogenous disturbance can be switched in or off on the DC bus. The generated disturbances are extracted by digital filters. The internal model is to calculate the desired dynamic trajectory reference of the states. The fast inner current loop is to control the ultracapacitor side converter and to impose the current tracking the desired dynamic trajectory. The slow outer loop is to force the system operating around the desired equilibrium point. The fast loop is to impose the desired dynamic to the system and is achieved through a PI controller with anti-windup. The slow outer loop is designed via interconnect and damping assignment (IDA) and passivity-based control (PBC). The control parameters can be found in Table 4.2.

The output current ω_1 of the exosystem is to simulate the transient and persistent current disturbances. It is measured by a current sensor and transferred to the terminal computer. A low-pass filter and a band-pass filter are utilized to separate the constant component $\bar{\omega}_1$ and the high-frequency component $\tilde{\omega}_1$.

An anti-windup is added to avoid the integral saturation (windup). The structure anti-windup

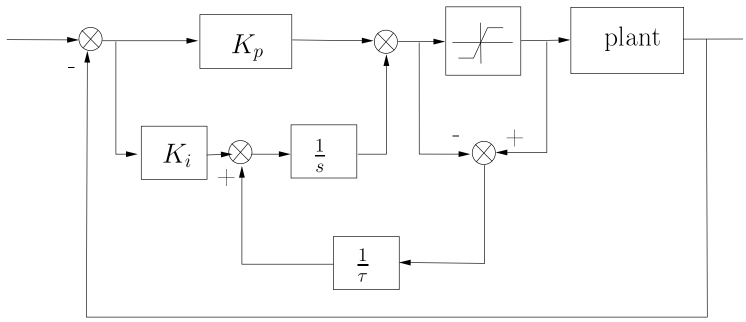

FIGURE 4.7 – Anti-windup

TABLE 4.2 – Control parameters of the disturbance rejection algorithm

Filters parameters			
Cut-off frequency of the low-pass filter			5rad/s
Cut-off frequency of the band-pass filter			5rad/s -1000rad/s
Control parameters			
Sampling frequency			F_s=10kHz
Switching frequency			4500Hz
Proportional term			k_p=5.6
Integral term			k_i=140
Interconnection structure			j_1=3.25 ;
			j_2=0.01 ;
			$j_3=1.18\times10^{-5}$.
Damping injection	r_1=8.5 ;	c_1=1800 ;	c_4=2.12 ;
	r_2=0.18 ;	c_2=50 ;	c_5=0 ;
	r_3=2.11 ;	c_3=0 ;	c_6=0.3413.

part is shown in Figure 4.7. When the error is in one direction, the integral action keeps accumulating and thus the output of the PI controller keeps increasing. When the actuators reach their extreme position, if the control command continues to increase, it will be beyond the limit range of the duty cycle $[0, 1]$. Thus, the actuator cannot follow the control command any more, and the system enters the saturation zone. Only when the error reverses, the system exits gradually from the saturation zone. In order to avoid the system entering the saturation zone where the actuators do not effectively work, the anti-windup part is added to adjust promptly the error input of the integrator.

4.4 Experimental results of battery/ultracapacitor hybrid system

The experiments are carried out in the following steps. Initially, the ultracapacitor is first charged to the nominal voltage with a DC source. Then, at the start up stage, the system is driven to the desired equilibrium point with an open-loop controller, i.e., two fixed duty cycle PWM signals.

Later, when the system operates steadily at the equilibrium point, we add the disturbances and the designed closed-loop controller to maintain the system around this operating point.

The experimental results will be presented in three sections according to different exogenous disturbances. First, we will show the system responses under sinusoidal current disturbances. Then, the system responses under step current disturbances will be presented. Finally, we will test the so-called general disturbances composed of the two kinds of the disturbances.

The objective of the experiment is to observe the disturbance absorption at the ultracapacitor side converter, so as to verify the effectiveness of the designed controller. Similar with the simulations in the last chapter, for each section, we will do contrast experiments with and without disturbance rejection algorithm. We apply first an ordinary cascade control algorithm without considering disturbance rejection. This is achieved via disconnecting the internal model which imposes the desired dynamic to the system. We may observe visually the influence of the disturbances to the system. Then, we reconnect the internal model to see the contrast results with disturbance rejection algorithm.

4.4.1 Sinusoidal disturbance

We first add the sinusoidal current disturbance to the DC bus. As mentioned before, the frequency of the sinusoidal disturbance is set at 15Hz, the available lowest frequency of the AC source generator. The nominal DC bus voltage is 300V and the nominal ultracapacitor voltage is 160V.

Figure 4.8 gives the experimental results. The figure shows the system responses without the designed controller during the first 20 seconds. The designed disturbance rejection algorithm is added afterwards. It can be observed from the figure that without the designed algorithm, the sinusoidal disturbance leads to substantial oscillations in the DC bus voltage and the battery current. These current oscillations do damage to the battery and need to be rejected. After the designed disturbance rejection algorithm is added, we may see clearly that the oscillations in the battery side converter are significantly reduced. On the contrary, the oscillations in the current and the voltage of the ultracapacitor increase. This implies that, with the designed algorithm, the ultracapacitor side converter successfully absorbs the sinusoidal disturbance. Moreover, the ultracapacitor voltage remains around its nominal value, which indicates that the self-discharging has been effectively compensated by the battery.

Figure 4.9 and Figure 4.10 show respectively the spectrum of the battery current and the ultracapacitor current. It can be seen from Figure 4.9 that during the first 20 seconds, the battery current contains a 15Hz harmonic caused by the exogenous current disturbance in the DC bus. When the designed algorithm is added, this harmonic disappears. On the contrary, it can be seen from Figure 4.10 that the 15Hz harmonic in the ultracapacitor current increases, which further verifies the absorption of the sinusoidal disturbance.

Figure 4.11 gives the output of the internal model imposing the desired dynamic component of the ultracapacitor current I_{L_2}. Since the desired constant component of I_{L_2} is zero. The desired trajectory $I_{L_2}^{ref}$ is entirely described by the output of the internal model. During the first 20 seconds, the internal model is disconnected, so $I_{L_2}^{ref} = 0$. It can be seen from the figure that, when the internal model is reconnected, the curves almost coincide. This shows that the fast inner loop effectively converges I_{L_2} to its reference.

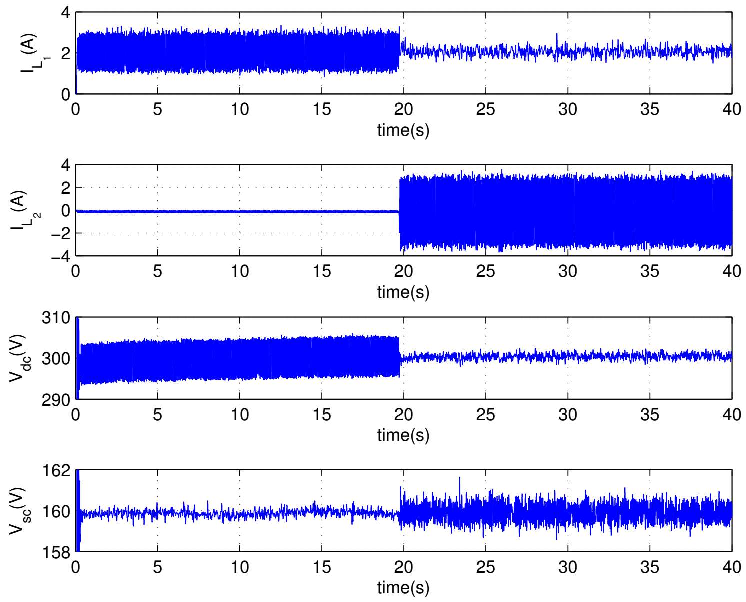

FIGURE 4.8 – System responses with and without disturbance rejection algorithm under sinusoidal disturbance

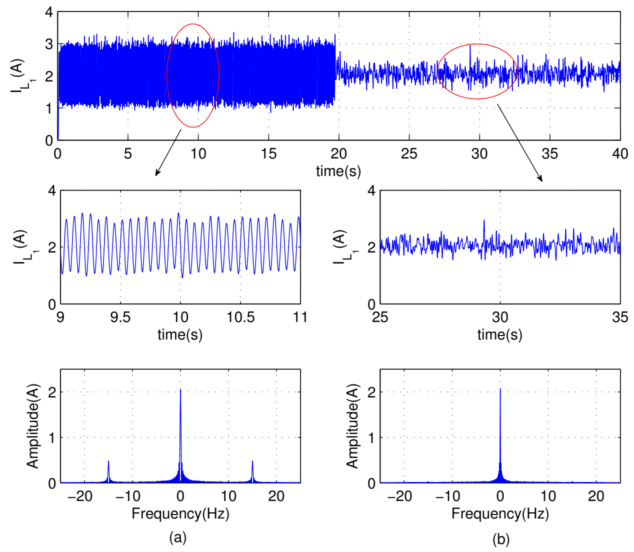

FIGURE 4.9 – Battery current static spectrum with and without disturbance rejection algorithm under sinusoidal disturbance

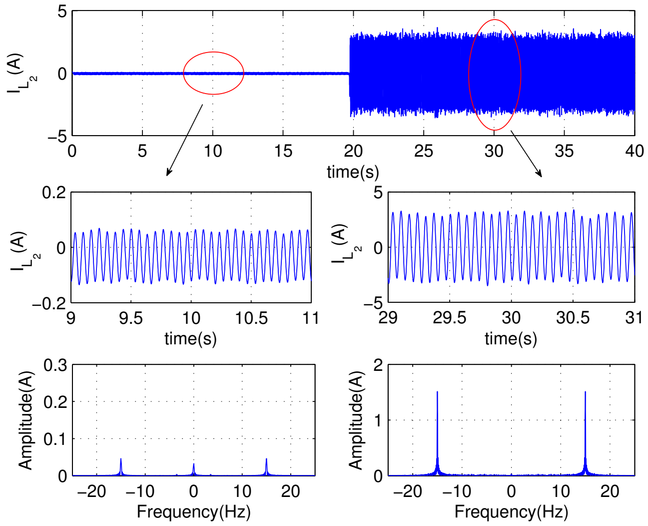

FIGURE 4.10 – Ultracapacitor current spectrum with and without disturbance rejection algorithm under sinusoidal disturbance

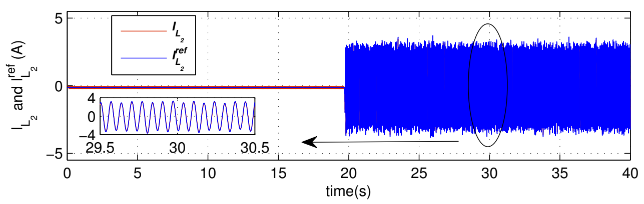

FIGURE 4.11 – Ultracapacitor current and its reference under sinusoidal disturbance

4.4.2 Transient disturbance

We have shown the control performance under sinusoidal current disturbance. In this section we test the system responses with step current disturbance. The step current variation in the DC bus is achieved by switching in and switching off an additional resistive load. During the transient, when the power demand suddenly increases, the battery current increases and vice versa. This corresponds exactly with the vehicle application. The sudden change of the power demand causes a rapid variation in the battery current which is harmful to the battery. Numerous researchers have studied this problem and proposed different control strategies to deal with the transient. Herein, we will show how our control algorithm forces the ultracapacitor to capture this transient and smooth the battery current.

Figure 4.12 and Figure 4.13 shows respectively the experimental results without and with the disturbance rejection algorithm. It can be seen from Figure 4.12 that, without the designed algorithm, each time when the addition resistor is switched in or switched off, there is a rapid step variation in the battery current. Figure 4.13 shows the system responses with the disturbance rejection algorithm. It can be seen clearly that there is a peak current each transient when the power demand changes. This implies that the ultracapacitor effectively absorbs the transient disturbance, and the current through the battery varies more smoothly.

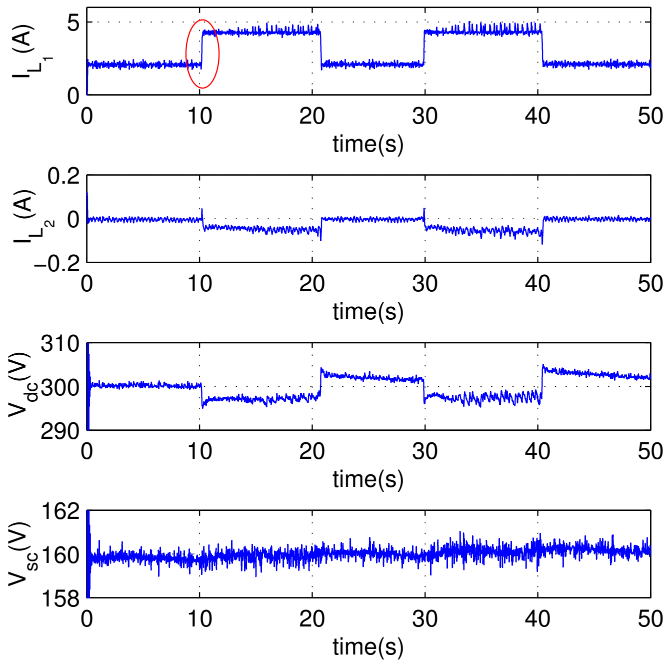

FIGURE 4.12 – System responses without disturbance rejection algorithm under transient disturbances

Figure 4.14 gives a contrast of the battery current and the ultracapacitor current with and without the designed algorithm. It can be seen from the contrast that, with the same power

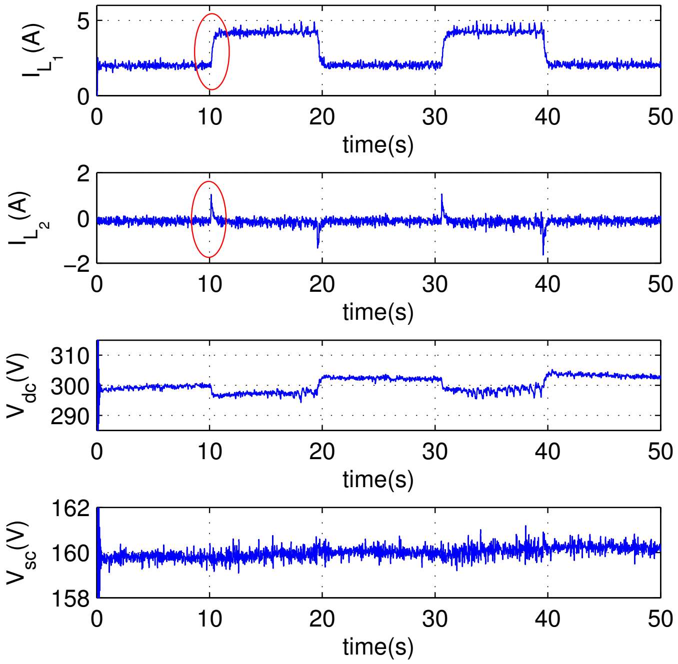

FIGURE 4.13 – System responses with disturbance rejection algorithm under transient disturbances

demand, the battery current varies more smoothly with our designed controller. The transient disturbance is successfully captured by the ultracapacitor.

It has been verified that the fast inner loop drives the ultracapacitor current to converge with its reference under sinusoidal disturbance. Herein, instead of printing two almost overlapping curves, we show the difference between the ultracapacitor current and its reference in Figure 4.15. It can be seen from the figure that the error is small enough (the order of magnitude 10^{-4}) to be neglected. This indicates that the fast inner is also effective under transient disturbances.

4.4.3 General disturbance

Now that we have tested the controller performance under sinusoidal disturbance and transient disturbance respectively, we will combine these two classes of disturbances together and observe the controller performance. Actually, these two kinds of disturbances almost cover all the disturbances in vehicle application. Through harmonic decomposition methods, other forms of disturbance can always be decomposed into several harmonics and be regarded as several sinusoidal disturbances with different frequencies. Consequently, we call the combination of the sinusoidal and transient disturbance a general disturbance.

Figure 4.16 shows the experimental results with and without the disturbance rejection algorithm. The algorithm is added at time t=25s. During the first 25 seconds, the high-amplitude oscillations and the rapid variations in the battery current can be observed. After the distur-

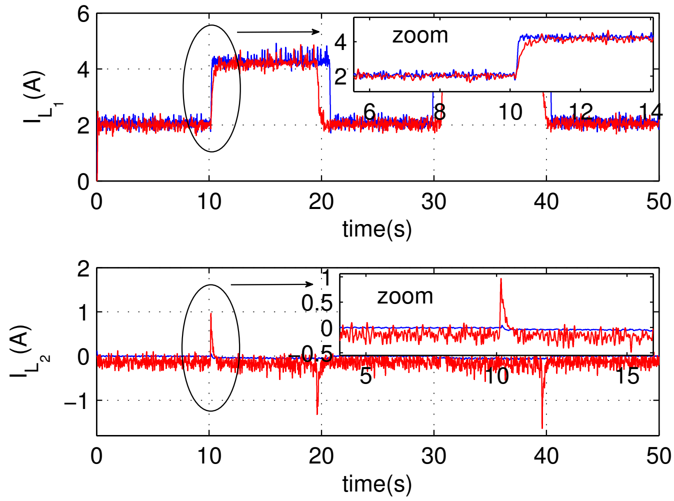

FIGURE 4.14 – Contrasts of battery and ultracapacitor current with and without disturbance rejection algorithm under transient disturbances

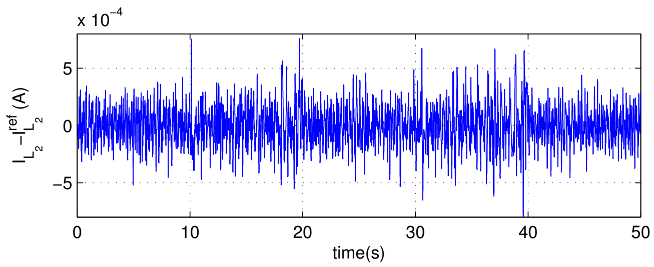

FIGURE 4.15 – The error between ultracapacitor current and its reference

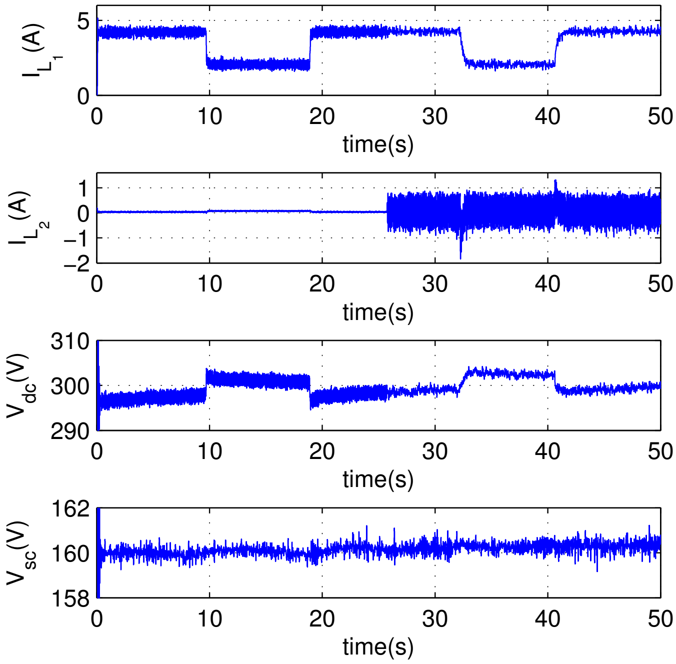

FIGURE 4.16 – System responses with and without disturbance rejection algorithm under both transient disturbances and sinusoidal disturbances

bance rejection algorithm is added, these oscillations obviously reduce, and the battery current varies smoothly when the power demand changes. On the contrary, the ultracapacitor current absorbs more oscillations and appears high-frequency peak current when the load power demand changes. Moreover, the DC bus voltage and ultracapacitor voltage remain around their nominal values. Herein, the reduction of the battery current oscillation is not that significant because we set a small exogenous sinusoidal current so as to limit the battery current. This is due to the aforementioned constraint that the inductor current in the power converters cannot exceed 5A.

4.5 Conclusions

In this chapter, we have completed our study with experiments. The real-time experiments are implemented with dSPACE hardware and software. A real battery/ultracapacitor hybrid energy storage system is built and connected to the DC bus with a boost converter and a bi-directional converter. An exosystem built with a resistive load and an AC power source is utilized to emulate the behavior of the real exosystem composed of AC-DC converter, PMSM, ICE and the torque ripples compensation active controller. The replaced exosystem generates transient and sinusoidal disturbances in the DC bus. We have defined the combination of these two class of disturbance as a general disturbance. Actually, general disturbances cover almost all general form of disturbances which can be decomposed into different harmonics. The disturbance rejection control algorithm developed in the last chapter is tested under each disturbance situation. We have analyzed the system responses with and without the designed controller. With the disturbance rejection control algorithm, the disturbance rejection target is successfully achieved in the battery side converter, and the disturbance absorption task is effectively completed. Moreover, the DC bus voltage and the ultracapacitor voltage remain around their nominal values. In summary, this chapter has verified the effectiveness of the disturbance rejection control algorithm and declares a cloture of our study.

General conclusions

In this thesis, we have studied and achieved an energy management in a battery/ultracapacitor hybrid energy storage system with exogenous disturbances. A disturbance rejection control algorithm based on a cascade control structure is proposed to absorb the disturbances causing battery wear via the ultracapacitor. We have taken two kinds of disturbances into consideration : transient disturbance results from the power demand sudden changes during vehicle accelerations and decelerations ; and harmonic persistent disturbances introduced from the process of torque ripples compensation in hybrid electric vehicles, an issue left over in the thesis of Mohamed NJEH.

In the state of the art, we have presented a contrast of three main energy storage devices : fuel cells, batteries and ultracapacitors ; and reviewed various configurations of the hybridization among them and several control strategies. The topology of our hybrid energy storage system is two DC-DC power converters interfacing the battery/ultracapacitor and the DC bus, which provides a large flexibility to manage the energy, and is adaptable in vehicular and other applications. The transient current disturbance in the DC bus has been widely studied in the literature. Therefore, we focus mainly on the sinusoidal disturbance based on the disturbance signal harmonic decomposition. The contributed disturbance rejection control algorithm is turned out to be capable of applying to both kinds of the disturbances.

The control objective is to allocate the energy in the hybrid energy storage system, especially, to capture the disturbance energy via the ultracapacitor, so as to achieve a steady energy output from the battery and maintain a constant DC voltage. Based on this idea, we have first simplified the problem by considering the battery side converter and the ultracapacitor side converter separately, and exploited the nonlinear error output regulation theories to solve the problem. Specifically, the harmonic disturbance is described with a linear exosystem. The error output is defined as the difference between the disturbance energy and the energy captured in the ultracapacitor. The error feedback regulator consists of two subcontrollers : an internal model providing the steady-state control input while the system states operating along their desired trajectories ; and a stabilizer controller stabilizing the interconnection of the original system and the internal model. Simulation results have verified the effectiveness of the regulator, yet several existing defaults hinder the regulator from testing in the experiments, including the strict stability and the neglect of the ultracapacitor self-discharge phenomenon and the battery/ultracapacitor interaction.

Thereafter, we consider the overall hybrid energy system as a whole, and take the ultracapacitor self-discharge in to account via adding an internal resistor. The new model is a multi-input multi-output (MIMO) four-dimensional nonlinear Hamiltonian system. Original method solving Hamiltonian system is to solve partial differential equations. However, it is too complex to find analytical solutions dealing with our MIMO four-dimensional model. Consequently, we exploit an alternative approach that analyzes the system in two timescales. Thus, referring to the singular perturbation theory, the system can be regulated through a cascade control structure. The ultracapacitor current, which is supposed to absorb the dynamic current disturbance, has the fastest motion ration and is chosen as the inner loop control. Besides, we define the desired system equilibrium point as the steady-state response disregarding the disturbance ; and the desired dynamic trajectory as the system response with the disturbance. Thus, the essence of the cascade control structure is to drive the system to the desired equilibrium through the outer slow loop, and impose the desired dynamic via the inner fast loop. The regulator of the inner fast loop is a simple PI controller, while the regulator for the outer slow loop is designed via Hamiltonian system interconnection and damping assignment.

The task of the ultracapacitor is to absorb the transient and the sinusoidal disturbance. For this tracking problem, a key point is to determinate the expression of the desired dynamic trajectories Consider a harmonic sinusoidal disturbance, then the desired trajectories of the ultracapacitor current and voltage are supposed to be limit cycles. An approximation based on energy allocation principle is applied to calculate the reference trajectories. This algorithm is embedded in an internal model, from where the reference is generated.

Simulations under MATLAB/Simulink environment and experiments with dSPACE hardware and software have been carried out to verify the effectiveness of the disturbance rejection cascade control algorithm. A contrast of the system responses with and without the algorithm has been presented under transient disturbance, sinusoidal disturbance, and the combination of both respectively. The contrast results show evidently that the disturbances causing battery wear are successfully absorbed by the ultracapacitor. Moreover, the oscillations in the DC bus voltage are also reduced ; the ultracapacitor self-discharge is compensated, and it maintains at the nominal state of charge.

Other than the works we have done, the study of the hybrid energy storage system could be further developed in the following aspects :

- Replace the filters in the control algorithm with a harmonic decomposition method and test the control performance with a real ripple signal.
- Build a real connection between the battery/ultracapacitor system and the propulsion system (the electric machine and the engine) to further evaluate the control performance.
- Take the vehicle start-up phase into consideration, and integrate the limitation of the over current and the charge of the ultracapacitor into the control algorithm, so as to further complete the energy management of the hybrid energy storage system.
- Develop a battery supervision algorithm to monitor in real-time the state of charge of the battery and to manage the change and discharge cycles while the electric machine working at generator mode and motor mode.
- Extend the disturbance rejection control algorithm to other applications such as pure electric vehicles and renewable energy generation systems where exogenous disturbances exist and cause battery wear.

Bibliographie

[ABDM07] M.-Y. Ayad, M. Becherif, A. Djerdir, and A. Miraoui. Sliding mode control for energy management of dc hybrid power sources using fuel cell, batteries and supercapacitors. In *Clean Electrical Power, 2007. ICCEP '07. International Conference on*, pages 500–505, May 2007.

[ABH+10] M.Y. Ayad, M. Becherif, A. Henni, A. Aboubou, M. Wack, and S. Laghrouche. Passivity-based control applied to dc hybrid power source using fuel cell and supercapacitors. *Energy Conversion and Management*, 51 :1468–1475, 2010.

[ABH11] MY Ayad, M Becherif, and A Henni. Vehicle hybridization with fuel cell, supercapacitors and batteries by sliding mode control. *Renewable Energy*, 36(10) :2627–2634, 2011.

[ACs02] Programmable ac power source 61701/61702/61703/61704 user's manual, November 2002.

[AS10] J.J. Awerbuch and C.R. Sullivan. Filter-based power splitting in ultracapacitor-battery hybrids for vehicular applications. In *Control and Modeling for Power Electronics (COMPEL), 2010 IEEE 12th Workshop on*, pages 1–8, June 2010.

[AW10] Zahra Amjadi and Sheldon S. Williamson. A novel control technique for a switched-capacitor-converter-based hybrid electric vehicle energy storage system. *IEEE transactions on industrial electronics*, 57 :926–934, 2010.

[Bat96] S. Battilotti. Global output regulation and disturbance attenuation with global stability via measurement feedback for a class of nonlinear systems. *Automatic Control, IEEE Transactions on*, 41(3) :315–327, Mar 1996.

[BDB+14] N Benyahia, H Denoun, A Badji, M Zaouia, T Rekioua, N Benamrouche, and D Rekioua. Mppt controller for an interleaved boost dc–dc converter used in fuel cell electric vehicles. *International Journal of Hydrogen Energy*, 2014.

[BGFC04] D. Biel, F. Guinjoan, E. Fossas, and J. Chavarria. Sliding-mode control design of a boost-buck switching converter for ac signal generation. *Circuits and Systems I : Regular Papers, IEEE Transactions on*, 51(8) :1539–1551, Aug 2004.

[BK08] J. Bauman and M. Kazerani. A comparative study of fuel-cell-battery, fuel-cell-ultracapacitor, and fuel-cell-battery-ultracapacitor vehicles. *Vehicular Technology, IEEE Transactions on*, 57(2) :760–769, March 2008.

[BPI97] Christopher I Byrnes, Francesco Delli Priscoli, and Alberto Isidori. *Output regulation of uncertain nonlinear systems*. Springer, 1997.

[BPIK97] C.I. Byrnes, F.Delli Priscoli, A. Isidori, and W. Kang. Structurally stable output regulation of nonlinear systems. *Automatica*, 33 :369 – 385, 1997.

[BTCM13] F. Bensmaine, S. Tnani, G. Champenois, and E. Mouni. Modeling and parameter identification of supercapacitors using a bidirectional dc-ac converter. In *Industrial Electronics Society, IECON 2013 - 39th Annual Conference of the IEEE*, pages 1019–1024, Nov 2013.

[CCM+03] Jonathan Chauvin, Gille Corde, Philippe Moulin, Michel Castagné, Nicolas Petit, and Pierre Rouchon. Time-varying linear observer for torque balancing on a di engine. In *Modeling and Control of Economic Systems 2001 :(SME 2001) : a Proceedings Volume from the 10th IFAC Symposium, Klagenfurt, Austria, 6-8 September 2001*. Pergamon, Elsevier Science, 2003.

[CDG12] M Camara, Brayma Dakyo, and Hamid Gualous. Polynomial control method of dc/dc converters for dc-bus voltage and currents management–battery and supercapacitors. *Power Electronics, IEEE Transactions on*, 27(3) :1455–1467, 2012.

[CE09] J. Cao and A. Emadi. A new battery/ultra-capacitor hybrid energy storage system for electric, hybrid and plug-in hybrid electric vehicles. In *Vehicle Power and Propulsion Conference, 2009. VPPC '09. IEEE*, pages 941–946, Sept 2009.

[CGG+10] Mamadou Baïlo Camara, Hamid Gualous, Frederic Gustin, Alain Berthon, and Brayima Dakyo. Dc/dc converter design for supercapacitor and battery power management in hybrid vehicle applications–polynomial control strategy. *Industrial Electronics, IEEE Transactions on*, 57(2) :587–597, 2010.

[Cha08] Chok-You Chan. Simplified parallel-damped passivity-based controllers for dc-dc power converters. *Automatica*, pages 2977–2980, 2008.

[CKS12] Mid-Eum Choi, Seong-Woo Kim, and Seung-Woo Seo. Energy management optimization in a battery/supercapacitor hybrid energy storage system. *Smart Grid, IEEE Transactions on*, 3(1) :463–472, March 2012.

[CRO13] Lila CROCI. *Gestion de l'énergie dans un système multi-sources photovoltaïque et éolien avec stockage hybride Batteries/Supercondensateurs*. PhD thesis, Univercité de Poitiers, 2013.

[CW02] K.T. Chau and Y.S. Wong. Overview of power management in hybrid electric vehicles. *Energy Conversion and Management*, 43 :1953–1968, 2002.

[DC03] B.G. Dobbs and P.L. Chapman. A multiple-input dc-dc converter topology. *Power Electronics Letters, IEEE*, 1(1) :6–9, March 2003.

[DCC] Ping Dai, S. Cauet, and P. Coirault. Disturbance rejection of hybrid battery/ultracapacitor energy storage system applied in hybrid electric vehicles. *Control Engineering Practice (submitted)*.

[DCC13a] Ping Dai, S. Cauet, and P. Coirault. Gestion multi-sources dans le cadre d'un volant d'inertie actif pour une propulsion hybride diesel/électrique. In *Journées Automatique et Automobile*, oct 2013.

[DCC13b] Ping Dai, S. Cauet, and P. Coirault. Passivity-based control and sliding mode control of hybrid dc power source applied to hybrid electric vehicles. In *Systems and Control (ICSC), 2013 3rd International Conference on*, pages 691–696, Oct 2013.

[DCC14] Ping Dai, S. Cauet, and P. Coirault. Perturbation rejection control strategy of batteries/supercapacitors hybrid power sources for hybrid electric vehicles. In *2014 40th International Conference of the IEEE Industrial Electronics Society (IECON)*, Oct 2014.

[Din06] Zhengtao Ding. Output regulation of uncertain nonlinear systems with nonlinear exosystems. *Automatic Control, IEEE Transactions on*, 51(3) :498–503, March 2006.

[DL03] R.I. Davis and R.D. Lorenz. Engine torque ripple cancellation with an integrated starter alternator in a hybrid electric vehicle. implementation and control. *IEEE Transactions on Industry Applications*, 39 :1765–1774, 2003.

[DS204] Ds1104 r&d controller board rti reference, March 2004.

[EAN10] A.H. Eghbali, B. Asaei, and P. Nader. Fuel efficient control strategy, based on battery-ultracapacitor energy storage system, in parallel hybrid electric vehicles. In *Vehicle Power and Propulsion Conference (VPPC), 2010 IEEE*, pages 1–5, Sept 2010.

[EFGGT14] H. El Fadil, F. Giri, J.M. Guerrero, and A. Tahri. Modeling and nonlinear control of a fuel cell/supercapacitor hybrid energy storage system for electric vehicles. *Vehicular Technology, IEEE Transactions on*, 63(7) :3011–3018, Sept 2014.

[FCv] Fuel cell vehicles. `http://www.fueleconomy.gov/feg/fuelcell.shtml`.

[FH00] H. Fujimoto and Y. Hori. Vibration suppression and optimal repetitive disturbance rejection control in semi-nyquist frequency region using multirate sampling control. In *Decision and Control, 2000. Proceedings of the 39th IEEE Conference on*, volume 4, pages 3745–3750 vol.4, 2000.

[FSW74] B Francis, OA Sebakhy, and WM Wonham. Synthesis of multivariable regulators : the internal model principle. *Applied Mathematics and Optimization*, 1(1) :64–86, 1974.

[FW76] Bruce A Francis and W Murray Wonham. The internal model principle of control theory. *Automatica*, 12(5) :457–465, 1976.

[Gao05] Wenzhong Gao. Performance comparison of a fuel cell-battery hybrid powertrain and a fuel cell-ultracapacitor hybrid powertrain. *Vehicular Technology, IEEE Transactions on*, 54(3) :846–855, May 2005.

[GFGJ10] Pablo Garcia, Luis M Fernandez, Carlos Andres Garcia, and Francisco Jurado. Energy management system of fuel-cell-battery hybrid tramway. *Industrial Electronics, IEEE Transactions on*, 57(12) :4013–4023, 2010.

[Gha12] Azad Ghaffari. dspace and real-time interface in simulink, December 2012.

[GJM97] S.V. Gusev, W. Johnson, and J. Miller. Active flywheel control based on the method of moment restrictions. In *American Control Conference, 1997. Proceedings of the 1997*, volume 5, pages 3426–3430, 1997.

[GS05] Lino Guzzella and Antonio Sciarretta. *Vehicle propulsion systems*, volume 2. Springer, 2005.

[Gul11] Hanifi Guldemir. Study of sliding mode control of dc-dc buck converter. *Energy and Power Engineering*, 3 :401–406, 2011.

[GvdS03] Luca Gentili and Arjan van der Schaft. Regulation and input disturbance suppression. for port-controlled hamiltonian systems. In *2nd IFAC Workshop on Lagrangian and Hamiltonian Methods for Nonlinear Control*, April 3-5, 2003.

[HCSW07] J. Hao, C. Chen, L. Shi, and J. Wang. Nonlinear decentralized disturbance attenuation excitation control for power systems with nonlinear loads based on the hamiltonian theory. *Energy Conversion, IEEE Transactions on*, 22(2) :316–324, June 2007.

[HD08] Sangtaek Han and D. Divan. Bi-directional dc/dc converters for plug-in hybrid electric vehicle (phev) applications. In *Applied Power Electronics Conference and Exposition, 2008. APEC 2008. Twenty-Third Annual IEEE*, pages 784–789, Feb 2008.

[HGB+13] M Hilairet, Malek Ghanes, O Béthoux, V Tanasa, JP Barbot, and D Normand-Cyrot. A passivity-based controller for coordination of converters in a fuel cell system. *Control Engineering Practice*, 21(8) :1097–1109, 2013.

[HJDT12] Kanoun Houcem, Gabano Jean-Denis, and Poinot Thierry. Ultracapacitor identification using continuous lpv fractional modeling. In *IFAC Symposium on System Identification*, 2012.

[HJS14] Cui Hongyu, Yang Jun, and Li Shihua. Nonlinear disturbance rejection control for a buck-boost converter with load uncertainties. In *Control Conference (CCC), 2014 33rd Chinese*, pages 3788–3793, July 2014.

[HL93] Jie Huang and C-F Lin. Internal model principle and robust control of nonlinear systems. In *Decision and Control, 1993., Proceedings of the 32nd IEEE Conference on*, pages 1501–1506. IEEE, 1993.

[HSWC05] J. Hao, L. Shi, J. Wang, and C. Chen. Nonlinear disturbance attenuation excitation control of structure preserving power systems based on hamiltonian theory. In *Power Engineering Society General Meeting, 2005. IEEE*, pages 1665–1670 Vol. 2, June 2005.

[Hua01] Jie Huang. Remarks on the robust output regulation problem for nonlinear systems. *Automatic Control, IEEE Transactions on*, 46(12) :2028–2031, 2001.

[IB90] Alberto Isidori and Christopher I Byrnes. Output regulation of nonlinear systems. *Automatic Control, IEEE Transactions on*, 35(2) :131–140, 1990.

[JH07] S. Boggs J. Ho, T. R. Jow. Historical introduction to capacitor technology. *Batteries and energy storage technology*, pages 61–78, 2007.

[JLBT08] Xing Jian Jing, Zi Qiang Lang, Stephen A. Billings, and Geofrey R. Tomlinson. Frequency domain analysis for suppression of output vibration from periodic disturbance using nonlinearities. *Journal of Sound and Vibration*, 314 :536 – 557, 2008.

[KA13] G.C. Konstantopoulos and A.T. Alexandridis. Generalized nonlinear stabilizing controllers for hamiltonian-passive systems with switching devices. *Control Systems Technology, IEEE Transactions on*, 21(4) :1479–1488, July 2013.

[KG02] Hassan K Khalil and JW Grizzle. *Nonlinear systems*, volume 3. Prentice hall Upper Saddle River, 2002.

[KK08] J.W. Kimball and P.T. Krein. Singular perturbation theory for dc-dc converters and application to pfc converters. *Power Electronics, IEEE Transactions on*, 23(6) :2970–2981, Nov 2008.

[KL10] A. Khaligh and Zhihao Li. Battery, ultracapacitor, fuel cell, and hybrid energy storage systems for electric, hybrid electric, fuel cell, and plug-in hybrid electric vehicles : State of the art. *Vehicular Technology, IEEE Transactions on*, 59(6) :2806–2814, July 2010.

[KP07] Min-Joong Kim and Huei Peng. Power management and design optimization of fuel cell/battery hybrid vehicles. *Journal of Power Sources*, 165(2) :819 – 832, 2007.

[KZ03] Y. Kishinevsky and S. Zelingher. Coming clean with fuel cells. *IEEE Power & Energy Magazine*, 1 :20–25, 2003.

[LdVC+04] M. Lopez, L.G. de Vicuna, M. Castilla, P. Gaya, and O. Lopez. Current distribution control design for paralleled dc/dc converters using sliding-mode control. *Industrial Electronics, IEEE Transactions on*, 51(2) :419–428, April 2004.

[Lei11] Guo Lei. Composite hierarchical anti-disturbance control (chadc) for systems with multiple disturbances : Survey and overview. In *Control Conference (CCC), 2011 30th Chinese*, pages 6193–6198, July 2011.

[LFBASRCO12] J. Linares-Flores, J.L. Barahona-Avalos, H. Sira-Ramirez, and M.A. Contreras-Ordaz. Robust passivity-based control of a buck-boost-converter/dc-motor system : An active disturbance rejection approach. *Industry Applications, IEEE Transactions on*, 48(6) :2362–2371, Nov 2012.

[LJL+09] K. Lee, T.M. Jahns, T.A. Lipo, V. Blasko, and R.D. Lorenz. Observer-based control methods for combined source-voltage harmonics and unbalance disturbances in pwm voltage-source converters. *Industry Applications, IEEE Transactions on*, 45(6) :2010–2021, Nov 2009.

[LMT13] O. Laldin, M. Moshirvaziri, and O. Trescases. Predictive algorithm for optimizing power flow in hybrid ultracapacitor/battery storage systems for light electric vehicles. *Power Electronics, IEEE Transactions on*, 28(8) :3882–3895, Aug 2013.

[LSMSG+15] O. Lopez-Santos, L. Martinez-Salamero, G. Garcia, H. Valderrama-Blavi, and T. Sierra-Polanco. Robust sliding-mode control design for a voltage regulated quadratic boost converter. *Power Electronics, IEEE Transactions on*, 30(4) :2313–2327, April 2015.

[MAB10] Sebastien Mariethoz, Stefan Almer, and Mihai Baja. Comparison of hybrid control techniques for buck and boost dc-dc converters. *IEEE transactions on control systems technology*, 18 :1126– 1145, 2010.

[MAH09] Pierre MAHAULT. User's manual lithium-ion battery system, December 2009.

[Mil04] J.M. Miller. *Propulsion Systems for Hybrid Vehicles*. IEE power and energy series. Institution of Electrical Engineers, 2004.

[MT10] F.L. Mapelli and D. Tarsitano. Energy control for plug-in hev with ultracapacitors lithium-ion batteries storage system for fia alternative energy cup race. In *Vehicle Power and Propulsion Conference (VPPC), 2010 IEEE*, pages 1–6, Sept 2010.

[NCCM11] Mohamed Njeh, Sébastien Cauet, Patrick Coirault, and Pascal Martin. $\mathcal{H}_\infty$ control strategy of motor torque ripple in hybrid electric vehicles : an experimental study. *IET - Control Theory and Applications*, 5 :131–144, 2011.

[Nfc] National fuel cell research center. `http://www.nfcrc.uci.edu/3/FUEL-CELL-INFORMATION/FCexplained/FC-Types.aspx`.

[Nje11] Mohamed Njeh. *Contribution au controle des pulsations de couple d'une propulsion hybride.* PhD thesis, Univercité de Poitiers, 2011.

[NUOK00a] Y. Nakajima, M. Uchida, H. Ogane, and Y. Kitajima. A study on the reduction of crankshaft rotational vibration velocity by using a motor-generator. *JSAE Review*, 5 :335–341, 2000.

[NUOK00b] Yuki Nakajima, Masaaki Uchida, Hiroaki Ogane, and Yasuhiko Kitajima. A study on the reduction of crankshaft rotational vibration velocity by using a motor-generator. *JSAE Review*, 21 :335–341, 2000.

[OGC04] Romeo Ortega and Eloisa Garcia-Canseco. Interconnection and damping assignment passivity-based control : A survey. *European Journal of Control*, 10(5) :432–450, 2004.

[OIRA11] C. Olalla, I.Queinnec, R.Leyva, and A.ElAroudi. Robust optimal control of bilinear dc-dc converters. *Control Engineering Practice*, 19 :688–699, 2011.

[OK12] O.C. Onar and A. Khaligh. A novel integrated magnetic structure based dc/dc converter for hybrid battery/ultracapacitor energy storage systems. *Smart Grid, IEEE Transactions on*, 3(1) :296–307, March 2012.

[OPNSR98] Romeo Ortega, Julio Antonio Loria Perez, Per Johan Nicklasson, and Hebertt J. Sira-Ramirez. *Passivity-based Control of Euler-lagrange Systems : Mechanical, Electrical and Electromechanical Applications.* Springer London Ltd, 1998.

[OvdSME02] Romeo Ortega, Arjan van der Schaft, Bernhard Maschke, and Gerardo Escobar. Interconnection and damping assignment passivity-based control of port-controlled hamiltonian systems. *Automatica*, 38 :585 – 596, 2002.

[Pen08] F.Z. Peng. Z-source networks for power conversion. In *Applied Power Electronics Conference and Exposition, 2008. APEC 2008. Twenty-Third Annual IEEE*, pages 1258–1265, Feb 2008.

[PMC12] O. Pelan, N. Muntean, and O. Cornea. Comparative evaluation of buck and switched-capacitor hybrid buck dc-dc converters. In *Power Electronics, Electrical Drives, Automation and Motion (SPEEDAM), 2012 International Symposium on*, pages 1330–1335, June 2012.

[POE04] M. Perez, R. Ortega, and J.R. Espinoza. Passivity-based pi control of switched power converters. *Control Systems Technology, IEEE Transactions on*, 12(6) :881–890, Nov 2004.

[PPMT08] Alireza Payman, Serge Pierfederici, and Farid Meibody-Tabar. Energy control of supercapacitor/fuel cell hybrid power source. *Energy Conversion and Management*, 49(6) :1637 – 1644, 2008.

[PPMTD11] A. Payman, S. Pierfederici, F. Meibody-Tabar, and B. Davat. An adapted control strategy to minimize dc-bus capacitors of a parallel fuel cell/ultracapacitor hybrid system. *Power Electronics, IEEE Transactions on*, 26(12) :3843–3852, Dec 2011.

[PR07] P. Pisu and G. Rizzoni. A comparative study of supervisory control strategies for hybrid electric vehicles. *Control Systems Technology, IEEE Transactions on*, 15(3) :506–518, May 2007.

[Rec] What are rechargeable batteries ? `http://rechargeablebatteryinfo.com/what-are-rechargeable-batteries.php`.

[RS14] A. Riccobono and E. Santi. Comprehensive review of stability criteria for dc power distribution systems. *Industry Applications, IEEE Transactions on*, 50(5) :3525–3535, Sept 2014.

[SB03] R.M. Schupbach and J.C. Balda. Comparing dc-dc converters for power management in hybrid electric vehicles. In *Electric Machines and Drives Conference, 2003. IEMDC'03. IEEE International*, volume 3, pages 1369–1374 vol.3, June 2003.

[SJ08] G.R. Sangeetha and J. Jacob. Repetitive controller for periodic disturbance rejection in motor-gear transmission system. In *India Conference, 2008. INDICON 2008. Annual IEEE*, volume 2, pages 559–564, Dec 2008.

[SJK03] Jacquelien M.A. Scherpen, Dimitri Jeltsema, and J. Ben Klaassens. Lagrangian modeling of switching electrical networks. *Systems & Control Letters*, 48 :365–374, 2003.

[SOY14] Balaji Sampathnarayanan, Simona Onori, and Stephen Yurkovich. An optimal regulation strategy with disturbance rejection for energy management of hybrid electric vehicles. *Automatica*, 50(1) :128 – 140, 2014.

[SRd96] H. Sira-Ramirez and M.D. deNieto. A lagrangian approach to average modeling of pulsewidth-modulation controlled dc-to-dc power converters. *Circuits and Systems I : Fundamental Theory and Applications, IEEE Transactions on*, 43(5) :427–, May 1996.

[SRO95] Hebertt Sira-Ramirez and Romeo Ortega. Passivity-based controllers for the stabilization of dc-to-dc power converters. In *Decision and Control, 1995., Proceedings of the 34th IEEE Conference on*, volume 4, pages 3471–3476. IEEE, 1995.

[SS99] Arjan van der Schaft and A. J. Schaft. *L2-Gain and Passivity in Nonlinear Control*. Springer-Verlag New York, Inc., Secaucus, NJ, USA, 2nd edition, 1999.

[SSL14] Alberto Santucci, Aldo Sorniotti, and Constantina Lekakou. Power split strategies for hybrid energy storage systems for vehicular applications. *Journal of Power Sources*, 258(0) :395 – 407, 2014.

[SSS03] Ali Saberi, Anton A Stoorvogel, and Peddapullaiah Sannuti. Control of linear systems with regulation and input constraints. *Communications and Control Engineering. London, UK : Springer*, 2003.

[SVP+91] Supramaniam Srinivasan, Omourtag A Velev, Arvind Parthasarathy, David J Manko, and A John Appleby. High energy efficiency and high power density proton exchange membrane fuel cells¡ªelectrode kinetics and mass transport. *Journal of Power Sources*, 36(3) :299–320, 1991.

[TK11] Ali Tofighi and Mohsen Kalantar. Adaptive passivity-based control of pem fuel cell/battery hybrid power source. *Electrical Review*, 87 :164–171, 2011.

[TRD09] Phatiphat Thounthong, Stephane Raël, and Bernard Davat. Energy management of fuel cell/battery/supercapacitor hybrid power source for vehicle applications. *Journal of Power Sources*, 193(1) :376 – 385, 2009. Scientific Advances in Fuel Cell Systems.

[TT13] Siang Fui Tie and Chee Wei Tan. A review of energy sources and energy management system in electric vehicles. *Renewable and Sustainable Energy Reviews*, 20 :82–102, 2013.

[TV99] B. Tomescu and H.F. VanLandinham. Disturbance rejection and robustness considerations in dc/dc converters. In *Power Electronics Specialists Conference, 1999. PESC 99. 30th Annual IEEE*, volume 2, pages 1204–1209 vol.2, 1999.

[UA08] M. Uzunoglu and M.S. Alam. Modeling and analysis of an fc/uc hybrid vehicular power system using a novel-wavelet-based load sharing algorithm. *Energy Conversion, IEEE Transactions on*, 23(1) :263–272, March 2008.

[UGS99] V.I. Utkin, J. Guldner, and J. Shi. *Sliding Mode Control in Electromechanical Systems*. Taylor & Francis, 1999.

[WB04] Martin Winter and Ralph J Brodd. What are batteries, fuel cells, and supercapacitors ? *Chemical reviews*, 104(10) :4245–4270, 2004.

[WIAT11] JennHwa Wong, NRN Idris, Makbul Anwari, and Taufik Taufik. A parallel energy-sharing control for fuel cell-battery-ultracapacitor hybrid vehicle. In *Energy Conversion Congress and Exposition (ECCE), 2011 IEEE*, pages 2923–2929. IEEE, 2011.

[WPXY08] X. Wu, S.K. Panda, Jianxin Xu, and V.D. Yurkevich. Dual frame cascaded controller design for three phase pwm boost rectifier under generalized supply voltage conditions using singular perturbation method. In *Power Electronics Specialists Conference, 2008. PESC 2008. IEEE*, pages 731–737, June 2008.

[YSPJ08] H. Yoo, Seung-Ki Sul, Yongho Park, and Jongchan Jeong. System integration and power-flow management for a series hybrid electric vehicle using supercapacitors and batteries. *Industry Applications, IEEE Transactions on*, 44(1) :108–114, Jan 2008.

[YZB11] Zhihong Yua, Donald Zinger, and Anima Bose. An innovative optimal power allocation strategy for fuel cell, battery and supercapacitor hybrid electric vehicle. *Journal of Power Sources*, 196 :2351–2359, 2011.

[YZG11] V.D. Yurkevich, G.S. Zinoviev, and A.A. Gordeev. Pwm current controller design for multi-level dc-dc converter via singular perturbation technique. In *Micro/Nanotechnologies and Electron Devices (EDM), 2011 International Conference and Seminar of Young Specialists on*, pages 390–398, June 2011.

[ZBT+11] Haihua Zhou, T. Bhattacharya, Duong Tran, T.S.T. Siew, and A.M. Khambadkone. Composite energy storage system involving battery and ultracapacitor with dynamic energy management in microgrid applications. *Power Electronics, IEEE Transactions on*, 26(3) :923–930, March 2011.

[Zho06] Chongfu Zhou. Carbon nanotube based electrochemical supercapacitors. 2006.

[ZPM+11] M. Zandi, A. Payman, J.-P. Martin, S. Pierfederici, B. Davat, and F. Meibody-Tabar. Energy management of a fuel cell/supercapacitor/battery power source for electric vehicular applications. *Vehicular Technology, IEEE Transactions on*, 60(2) :433–443, Feb 2011.

[ZZQ14] Jianwu Zeng, Zhe Zhang, and Wei Qiao. An interconnection and damping assignment passivity-based controller for a dc-dc boost converter with a constant power load. *Industry Applications, IEEE Transactions on*, 50(4) :2314–2322, July 2014.

Résumé

Ce mémoire porte sur l'étude d'un système de gestion d'énergie électrique dans un système multi-sources soumis à des perturbations exogènes. L'application visée est l'alimentation d'une propulsion hybride diesel/électrique équipée d'un système d'absorption des pulsations de couple. Les perturbations exogènes considérées peuvent être transitoires ou persistantes. Une perturbation transitoire correspond à une variation rapide du couple de charge, due par exemple à une accélération ou une décélération du véhicule. Une perturbation persistante provient du système de compensation des pulsations de couple générées par le moteur thermique. Le premier objectif du contrôle est de maintenir constante la tension du bus continu. Le deuxième objectif est d'absorber dans un système de stockage rapide constitué de super condensateur ces perturbations qui peuvent à terme provoquer une usure prématurée de la batterie. Le troisième objectif est de compenser l'auto-décharge dans le super condensateur en maintenant constante sa tension nominale. Les deux sources (batterie et super condensateur) sont reliées au bus continu par l'intermédiaire de deux convertisseurs boost DC/DC. La commande consiste à piloter les rapports cycliques de chaque convertisseur. C'est un système non linéaire où la commande est multiplicative de l'état. L'approche classique consistant à résoudre les équations Francis-Byrnes-Isidori ne s'applique pas directement dans ce cas où la sortie et la matrice d'interconnection dépendent de la commande. De plus, si cette approche est bien adaptée au rejet de perturbations persistantes, elle montre ces limites pour le rejet de perturbations non persistantes combiné à des objectifs de régulation. Notre approche a consisté à écrire le système sous un formalisme *Port-Controlled Hamiltonian* et à s'affranchir de la contrainte de la dépendance de la matrice d'interconnection avec la commande en utilisant la théorie des perturbations singulières. La commande du système dégénéré peut ensuite être calculée par une approche passive. Les performances de cette commande ont été testées en simulation et à l'aide d'un banc d'essai expérimental. Les résultats montrent l'efficacité du système d'absorption des différents types de perturbation tout en respectant les deux objectifs de régulation.

Mots-clés : véhicules hybrides électriques, système multi-source, gestion d'énergie, rejet perturbations persistantes, régulation de sortie, formalisme Port-Controlled Hamiltonian, perturbations singulières.

Abstract

This thesis presents the research of energy management in a battery/ultracapacitor hybrid energy storage system with exogenous disturbance in hybrid electric vehicular application. Transient and harmonic persistent disturbances are the two kinds of disturbances considered in this thesis. The former is due to the transient load power demand during acceleration and deceleration, and the latter is introduced from the process of the internal combustion engine torque ripples compensation. Our control objective is to absorb the disturbances causing battery wear via the ultracapacitor, and meanwhile, to maintain a constant DC voltage and to compensate the self-discharge in the ultracapacitor to maintain it operating at the nominal state of charge. The object system is nonlinear due to the multiplicative relation between the input and the state. The traditional approach to solve Francis-Byrnes-Isidori equations cannot be directly applied in this case since the interconnect matrix depends on the control input. Besides, even if this approach is well suited to the rejection of persistent disturbances, it shows the limits for the case of non-persistent disturbances which is also our object. Our contributed control method is realized through a cascade control structure based on the singular perturbation theory. The ultracapacitor current with the fastest motion rate is controlled in the inner fast loop through which we impose the desired dynamic to the system. The reduced system controlled in the outer slow loop is a Hamiltonian system and the controller is designed via interconnection and damping assignment. Simulations and experiments have been carried out to evaluate the control performance. A contrast of the system responses with and without the control algorithm shows that, with the control algorithm, the ultracapacitor effectively absorbs the disturbances; and verifies the effectiveness of the control algorithm.

Keywords : hybrid electric vehicles, hybrid energy storage system, energy management, persistent disturbance rejection, output regulation, Port-Controlled Hamiltonian system, singular perturbation theory.